

**The spatial organization of chloroplast protein synthesis
and the Calvin Benson Cycle in *Chlamydomonas reinhardtii***

Shiva Bakhtiari Koohsorkhi

A Thesis
in
The Department
of
Biology

Presented in Partial Fulfillment of the Requirements
For the Degree of Doctor of Philosophy at
Concordia University
Montreal, Quebec, Canada

December 2021

© Shiva Bakhtiari, 2021

CONCORDIA UNIVERSITY

School of Graduate Studies

This is to certify that the thesis prepared

By: Shiva Bakhtiari Koohsorkhi

Entitled: The spatial organization of chloroplast protein synthesis and the Calvin Benson Cycle in *Chlamydomonas reinhardtii*

and submitted in partial fulfillment of the requirements for the degree of

Doctor of Philosophy (Biology)

Complies with the regulations of the University and meets the accepted standards with respect to originality and quality.

Signed by the final Examining Committee:

_____ Chair
Dr. David Mumby

_____ External Examiner
Dr. Jean Rivoal

_____ External Examiner
Dr. Andreas Bergdahl

_____ Examiner
Dr. Alisa Piekny

_____ Examiner
Dr. Malcolm Whiteway

_____ Supervisor
Dr. William Zerges

Approved by

Dr. Robert Weladji, Graduate Program Director

_____ 2021 _____
Dr. Pascale Sicotte - Dean of Faculty

Abstract

The spatial organization of chloroplast protein synthesis and the Calvin Benson Cycle in

Chlamydomonas reinhardtii

Shiva Bakhtiari Koohsorkhi, Ph.D.

Concordia University, 2021

Chloroplasts are the characteristic organelle in cells of plants and algae. They host numerous essential metabolic pathways, including photosynthesis. Many processes are required for the biogenesis and homeostasis of the chloroplast. This thesis will look at the spatial organization of some of these processes in the chloroplast of *Chlamydomonas reinhardtii*. This unicellular alga is a model organism for chloroplast biology. The diverse functions of chloroplasts depend on the translation of thousands of different proteins. Most of these proteins are encoded in the nucleus, translated in the cytoplasm, and imported into the organelle post-translationally. Translation by organelle-bound ribosomes and co-translational import have been described for the ER and mitochondria, but not for the chloroplast. Chapter 2 describes evidence of localized translation at the chloroplast in *Chlamydomonas* and addresses the questions of ribosome docking on the chloroplast and co-translational import of chloroplast proteins. The results reveal a domain of the chloroplast envelope which is bound by translating cytoplasmic ribosomes and is a specialized location of co-translational protein import. These ribosomes are retained by chloroplasts, during their purification from other cellular organelles, can be visualized on the outer chloroplast envelope with immunofluorescence microscopy (IF) and high-resolution electron tomography, and are translationally active. Co-translational protein import is supported by results

of fluorescence *in situ* hybridization (FISH) showing that mRNAs encoding chloroplast proteins, but not an mRNA encoding a non-chloroplast protein, are retained by this domain during chloroplast purification. This envelope domain is spatially aligned with regions of envelope that were shown previously to be enriched in the protein translocons of the inner and outer membrane of the chloroplast envelope (TIC and TOC) and presumed to be specialized locations of protein import. Inside the chloroplast and adjacent to the envelope domain with translating cytoplasmic ribosomes is the chloroplast translation zone (T-zone). This intraorganellar compartment is where plastid ribosomes translate subunits of photosystem I (PSI) and photosystem II (PSII) of the photosynthetic electron transport chain. Together, these results reveal a complex spatial coordination of translation by cytoplasmic and chloroplast ribosomes for protein targeting and biogenesis of photosynthesis complexes in this semi-autonomous organelle.

Chapter 3 describes new insights into the spatial organization of the Calvin Benson Cycle, the pathway that converts CO₂ to carbohydrates in photosynthesis. Using fluorescence microscopy, I show that, under certain conditions, enzymes and related proteins in this pathway are localized to a specific compartment in the chloroplast. This compartment is different from the widely accepted locations of these enzymes and suggest some intriguing possibilities and resolutions to current problems in the field. Together, these findings support the highly compartmentalized nature of chloroplasts in *Chlamydomonas reinhardtii* and highlight the potentials of this model organism for studying chloroplast biogenesis and addressing fundamental cell biology questions. Moreover, they raise the possibility that similar organizations can occur in more complex photosynthetic organism such as higher plants.

ACKNOWLEDGMENTS

I would like to thank my colleague Dr. Yi Sun who initiated the project described in chapter two of this thesis and who I have collaborated with closely during this time.

I also like to thank the Centre for Microscopy and Cellular Imaging at Concordia University and in particular Dr. Chris Law for all his training, technical guidance and for designing specific macros to fit our research needs.

In addition, I would like to thank Dr. Hui Bui for his guidance in making the 3D reconstructions for the electron tomography images.

I would also like to thank my fellow lab members, especially Dr. James Dhaliwal for his help and support throughout our years together and Melissa Valente-Paterno for designing the synchronized cell system which was used in many of my experiments.

I also thank my committee members, Dr. Alisa Piekny and Dr. Malcolm Whiteway, for their helpful advice and constructive comments during my committee meetings.

Lastly, I would like to especially thank my supervisor, Dr. William Zerges, for giving me the opportunity to conduct research and complete my PhD, and for being a valuable mentor throughout my time in the lab.

CONTRIBUTION OF AUTHORS

Chapter 2:

The results presented in chapter two of this thesis are part of a co-authored work, which has been submitted for publication. Dr. Yi Sun, Dr. William Zerges and I all contributed to the development of ideas and project. Except for the contributions described below, I performed all other experimental work, data collection and analysis related to this chapter.

Figure 2.1: Yi Sun and I both contributed to the immunoblot analysis shown in Panel B.

Yi Sun performed the co-staining of CyL4 and LCIA shown in panel C. Dr. Chris Law wrote the Fiji macro used to measure average signal intensity in Panel D. I performed all macro analysis presented throughout this thesis.

Figure 2.2: Dr. Hui Bui and his student, Daniel Dai, acquired the tomograph images. I generated the 3-D reconstructions.

Figure 2.3: Yi Sun performed the PMY- KCl wash assays in Panel D.

Figure 2.5: Yi Sun prepared the sucrose gradients shown in panel A and B. I performed the immunoblot analyses on the fractions.

Chapter 3

Chapter 3 is a manuscript in preparation on which I am the primary author. Dr. William Zerges and I were both involved in the conception and design of experiments. Except for the contributions described below, I conducted all experiments, data collection and data analyses.

Figure 3.6: Melissa Valente Paterno acquired the TEM images shown in Panel A.

Figure 3.7: Yi Sun prepared the sucrose gradients shown in Panels A and B. I performed the immunoblot analysis on the fractions.

TABLE OF CONTENTS

LIST OF ABBREVIATIONS	xi
LIST OF FIGURES.....	xiii
LIST OF SUPPLEMENTAL DATA	xiv
CHAPTER 1: INTRODUCTION.....	1
1.1 Cellular Compartmentalization	1
1.1.1 Compartmentalization of Chloroplasts	2
1.1.2 Mitochondrial Compartmentalization.....	4
1.1.3 Compartmentalization of Protein Synthesis.....	5
1.1.4 Chloroplast and Mitochondrial Protein Targeting	6
1.2 <i>Chlamydomonas reinhardtii</i> as a Model Organism	9
1.3 The Calvin Benson Cycle.....	14
1.3.1 Rubisco and Photorespiration	16
1.3.2 Carbon Concentrating Mechanism	16
1.3.4 CCM in Land Plants.....	17
1.3.4 CCM in Cyanobacteria and Algae	18
1.3.5 CCM in <i>Chlamydomonas reinhardtii</i>	19
1.4 Thesis Overview.....	22
CHAPTER 2: CHLOROPLAST-LOCALIZED TRANSLATION FOR PROTEIN TARGETTING IN <i>CHLAMYDOMONAS REINHARDTII</i>	24
ABSTRACT	24
2.1 INTRODUCTION.....	25
2.2 MATERIALS AND METHODS.....	27
2.2.1 Strains and culture conditions.....	27
2.2.2 Chloroplast isolation	28
2.2.3 Immunoblot analysis.....	28
2.2.4 IF-staining and microscopy.....	29

2.2.5	Probe design and preparation.....	30
2.2.6	FISH.....	30
2.2.7	Image analysis of distributions of average fluorescence signals <i>in situ</i>	32
2.2.8	High resolution electron tomography	33
2.2.9	RiboPuromycylation and puromycin-release assays	33
2.2.10	Preparation of low-density membranes	34
2.3	RESULTS.....	35
2.3.1	Cyto-ribosomes associate with a domain of the chloroplast envelope	35
2.3.2	Cyto-ribosomes on the chloroplast envelope domain imaged by high-resolution electron tomography	39
2.3.3	Chloroplast-bound cyto-ribosomes are active	41
2.3.4	mRNAs encoding chloroplast proteins localize at the cyto-ribosomes on the chloroplast envelope.....	45
2.3.5	Biochemical evidence of the import envelope domain.....	50
2.4	DISCUSSION	54

CHAPTER 3: SPATIAL ORGANIZATION OF THE CALVIN BENSON CYCLE IN *CHLAMYDOMONAS REINHARDTII* 56

ABSTRACT.....	56
3.1 INTRODUCTION.....	57
3.2 MATERIALS AND METHODS	61
3.2.1 Culture conditions.....	61
3.2.2 Immunofluorescence staining	62
3.2.3 Probe design and preparation.....	62
3.2.4 FISH.....	63
3.2.5 Microscopy	64
3.2.6 Image analysis of distributions of average fluorescence signals <i>in situ</i>	64
3.2.7 Immunoblot analysis.....	65
3.2.8 Subcellular fractionation.....	65
3.2.9 Transmission electron microscopy	66
3.3 RESULTS.....	67
3.3.1 Localization of Calvin-Benson Cycle enzymes in the chloroplast	67

3.3.2	Re-localization of phosphoribulokinase during the light phase of the diel cycle ...	69
3.3.3	Localization of PRK across the diel cycle under 0.5% CO ₂	73
3.3.4	RBCL localizes to chloroplast lobes in early to mid-light phase.....	75
3.3.5	Localization of a bicarbonate transporter in <i>Chlamydomonas</i>	78
3.3.6	Transmission electron microscopy images reveal constrictions at the base of chloroplast lobes.....	80
3.3.7	PRK is associated with thylakoid membranes	82
3.4	DISCUSSION	84
CHAPTER 4: CONCLUSION.....		87
4.1	Overview	87
4.2	Future directions	91
REFERENCES.....		94
SUPPLEMENTAL DATA		109
APPENDIX I: Photosystem Biogenesis Is Localized to the Translation Zone in the Chloroplast of <i>Chlamydomonas</i> (Sun et al., 2019).....		123

LIST OF ABBREVIATIONS

CCM	Carbon concentrating mechanism
ER	Endoplasmic reticulum
FISH	Fluorescent <i>in situ</i> hybridization
HCO ₃ ⁻	Bicarbonate ions
HSM	High-salt minimal medium
IF	Immunofluorescence
LHCII	Light-harvesting complex II
RBCL	Large subunit of Rubisco
RBCS	Small subunit of Rubisco
Rubisco	Ribulose-1,5-bisphosphate carboxylase/oxygenase
RuBP	Ribulose-1,5-bisphosphate
PET	Photosynthetic electron transport chain
PSI	Photosystem I
PSII	Photosystem II
SRP	Signal recognition particle
TAP	Tris-acetate phosphate
TIC	Translocon at the inner chloroplast envelope
TOC	Translocon at the outer chloroplast envelope
PGK	Phosphoglycerate kinase
TPI	Triosphosphate isomerase
FBP	Fructose biphosphatase
RPE	Riboluse 5-phosphate epimarase

PRK	Phosphoribulokinase
RPI	Ribose 5-phosphate isomerase
SBP	Sedoheptulose 1,7 biphosphatase
TEM	Transmission electron microscopy
PMY	Puromycin
RPM	RiboPuromycylation assay
T-zone	Translation zone
3PGA	3-phosphoglycerate

LIST OF FIGURES

- Figure 1.1 Cytological organization of *Chlamydomonas* cells
- Figure 1.2 The carbon concentrating mechanism in *Chlamydomonas reinhardtii*
- Figure 2.1 Cyto-ribosomes are bound to a domain of the chloroplast envelope
- Figure 2.2 Electron Tomography images show cyto-ribosomes on the chloroplast outer envelope membrane
- Figure 2.3 The cyto-ribosomes on the chloroplast are translationally active
- Figure 2.4 FISH results reveal that mRNAs encoding specifically chloroplast-localized proteins are bound to isolated chloroplasts
- Figure 2.5 Isolation and analyses of low-density membrane
- Figure 3.1 Distribution of Calvin Benson Cycle enzymes in the chloroplasts
- Figure 3.2 Growing chloroplasts during the light phase of the diel cycle show spatiotemporal patterning of PRK
- Figure 3.3 Spatiotemporal patterning of PRK in the light phase under 0.5% CO₂
- Figure 3.4 Localization of RBCL in early-mid light phase of diel cycle
- Figure 3.5 LCIA localizes to chloroplast lobes in photo-autotrophically grown cells
- Figure 3.6 TEM ultrastructure of diurnally entrained cells
- Figure 3.7 PRK is associated with thylakoid membranes
- Figure 4.1 Our model

LIST OF SUPPLEMENTAL DATA

Figure S 2.1. Localization patterns reported previously

Figure S 2.2. Experimental controls

Figure S 2.3. Isolated chloroplasts retain their normal morphology

Figure S 2. 4. Biological replicate for WB experiments

Movie S 2.1. 3D reconstruction of ribosome-bound domain in the chloroplast

Movie S 2.2. 3D reconstruction of lobe region in the chloroplast

Table S 2.1. Sequences of FISH probes used in chapter 2

Table S 3.1. Sequences of FISH probes used in chapter 3

CHAPTER 1: INTRODUCTION

1.1 Cellular Compartmentalization

Eukaryotic cells are highly organized units. One of their defining features is the presence of subcellular compartments called organelles. Each organelle has specialized functions (Gabaldón & Pittis, 2015). The organelles found in a typical eukaryotic cell are the nucleus, the Golgi apparatus, the endoplasmic reticulum (ER), the mitochondrion, lysosomes, and peroxisomes (Alberts et al., 2002b). Each of these organelles is bound by either a single or double membrane, which physically separates it from the cytoplasm (Gould, 2018; Mullock & Luzio, 2013). The membrane also carries out selective import of proteins and transport of metabolites to establish the organellar composition and can have roles in specialized organellar functions (Béthune et al., 2019; Gould, 2018). Compartmentalization by organelles increases efficiency as multiple pathways and incompatible reactions can take place within a cell simultaneously (Martin, 2010; Wellen & Snyder, 2019). It can also prevent deleterious side reactions, such as the action of pathways on inappropriate substrates (Flechsler et al., 2021; Gabaldón & Pittis, 2015; Martin, 2010).

Many organelles are themselves partitioned into microcompartments that fine-scale compartmentalization of biochemical pathways (Martin, 2010; Wellen & Snyder, 2019). Together, these compartments and microcompartments regulate cellular processes by concentrating the required components to a specific space inside the cell (Flechsler et al., 2021; Martin, 2010). For example, the mitochondria is an energy-producing organelle that has several well known compartments. These include the outer and inner membranes, the intermembrane space and the matrix (Bowsher & Tobin, 2001; Shimizu, 2019). New imaging techniques have revealed that these compartments are further subdivided into specific regions or zones, each responsible for a

specific function. One example of these zones is the apoptosis zone which is an area on the mitochondrial outer membrane, where the proapoptotic factor Bak has been found to localize and drive the mitochondrial apoptosis pathway. (Shimizu, 2019). We use the term “zone” for a subcellular region that is defined by the localization of marker proteins for particular processes but for which the ultrastructure is still unknown.

Meanwhile the ER is composed of rough and smooth membrane domains. In addition to this, it has contact sites that enable the exchange of material with different organelles, including mitochondria, endosomes, and the plasma membrane (English & Voeltz, 2013; Hoffman et al., 2019). An example of this is the contact site between the ER and mitochondria which is called the mitochondria-associated membrane. These specialized domains have their own multiprotein assemblies that accommodate their function (Hoffman et al., 2019).

Bacterial cells also have microcompartments which are analogues to the lipid-bound organelles found in eukaryotes. These microcompartments enclose chemical reactions that benefit from being separated from the cytosol. Carboxysomes are an example of a bacterial microcompartment that is involved in CO₂-fixation (Kerfeld et al., 2018).

1.1.1 Compartmentalization of Chloroplasts

Chloroplasts are found only in plants and algae. They have long been known as the organelle responsible for carrying out photosynthesis (Alberts et al., 2002a; Cooper, 2000). They also perform several other critical functions such as the synthesis of amino acids and lipids (Hernández & Cejudo, 2021). Additionally, they play a role in the assimilation of sulfur, phosphorus and nitrogen (Armbruster & Strand, 2020; Giordano & Raven, 2014).

Chloroplasts consist of six known compartments. On the outside, they are surrounded by an envelope, composed of the outer and inner membranes. These two membranes are separated by a narrow intermembrane space (Engel et al., 2015). On the inside, they contain a matrix called the stroma and an elaborate network of flattened membranous vesicles called the thylakoids (Chua & Gillham, 1977). The fluid-filled space within the thylakoids is called the lumen (Engel et al., 2015; Kirchhoff, 2014).

Each area is associated with its own function. For example, the chloroplast envelope, is involved in the transport of photosynthetic metabolites, protein translocation, lipid transfer, and exchange of ions (Jarvis & Soll, 2002; Thomson et al., 2020; Ullmann, 2001). The stroma contains a variety of metabolic enzymes, multiple copies of the chloroplast's circular DNA and all components of the chloroplast translation machinery (Ullmann, 2001; Wallace, 1982).

The thylakoids are responsible for the light dependent reactions of photosynthesis. These reactions are carried out by several multi-subunit complexes which include photosystem I (PSI), photosystem II (PSII), their associated light-harvesting systems, chlorophyll a and b and carotenoids (Schottkowski et al., 2012; Vothknecht & Westhoff, 2001). PSI, PSII and the cytochromes b6/f are the major complexes of the photosynthetic electron transport chain (PET) (Kirchhoff, 2019; Vothknecht & Westhoff, 2001). PET oxidizes water to provide electrons for the reduction of NADP, and the generation of an electrochemical proton gradient, which is used for the synthesis of ATP (Brudvig, 2008; Harris, 1989). The LHCI (light harvesting complex I) associated with photosystem I and LHCII (light harvesting complex II) associated with photosystem II collect light for photosynthesis and determine how much light energy is transferred to the photosystems (Sun et al., 2019a; Uniacke & Zerges, 2007).

Another compartment found in the chloroplasts of most green algae is the pyrenoid (Freeman Rosenzweig et al., 2017; Zhan et al., 2018). This is a non-membrane bound spherical structure that is in the basal region of the chloroplast and is involved in the assimilation of CO₂ during the Calvin Benson Cycle (Freeman Rosenzweig et al., 2017; Moroney & Ynalvez, 2007). The pyrenoid matrix contains most of the pool of Ribulose-1, 5- biphosphate carboxylase/oxygenase (Rubisco), which is a key enzyme in CO₂ fixation (Mackinder et al., 2016).

1.1.2 Mitochondrial Compartmentalization

The mitochondria are in many respects similar to chloroplasts. Both organelles originated through endosymbiosis and therefore have their own DNA and translation machinery (Keeling, 2010; Rose, 2019). The mitochondria are best known for their role in energy metabolism, notably cellular respiration and ATP synthesis (Kühlbrandt, 2015). In fact, in non-photosynthetic eukaryotes, mitochondria are the main source of ATP (Bowsher & Tobin, 2001). The mitochondria are also involved in other essential functions. These include the production of NADH and GTP in the citric acid cycle, the biosynthesis of amino acids, heme groups and iron-sulfur clusters or the synthesis of phospholipids for membrane biogenesis. They are also involved in calcium signaling and responses to stress (Avendaño-Monsalve et al., 2020; Kühlbrandt, 2015).

Like the chloroplast, mitochondria are separated from the cytoplasm by an outer and inner mitochondrial membrane. These membranes divide the organelle into three compartments, each with its distinct role and protein composition (Kühlbrandt, 2015; Rose, 2019). The innermost compartment, which is surrounded by the inner mitochondrial membrane, is known as the matrix. This is the equivalent of the chloroplast stroma. The matrix contains the mitochondrial DNA, ribosomes

and enzymes of the citric acid cycle (Avendaño-Monsalve et al., 2020; Kühlbrandt, 2015; Rose, 2019).

The second compartment is the space between the inner and outer mitochondrial membranes, known as the intermembrane space. All matrix proteins imported into the mitochondria from the cytoplasm must pass through the intermembrane space. This is done through the translocon of the outer (TOM) and inner (TIM) membrane (Grevel et al., 2020a; Vogel, Bornhovd, et al., 2006).

However, the inner membrane of the mitochondria is much more elaborate in comparison with the chloroplast. This membrane forms multiple folds and invaginations into the matrix which are called cristae (Rabl et al., 2009; Vogel, Bornhovd, et al., 2006). The space within the cristae is known as the crista lumen. These cristae are where the proteins involved in the respiratory electron transport and ATP synthesis are located (Kühlbrandt, 2015; Rabl et al., 2009) and are analogous to the thylakoid membranes in chloroplasts (Grevel et al., 2020a; Rabl et al., 2009). Furthermore, the connection between each cristae and inner mitochondrial membrane is known as crista junctions. The TIM/TOM supercomplexes are also localized at cristae junctions (Kühlbrandt, 2015), analogous to the chloroplast TIC/TOC complexes which will be discussed further in Chapter 2 (Gold et al., 2017a; Schottkowski et al., 2012b; Vogel, Bornhovd, et al., 2006).

1.1.3 Compartmentalization of Protein Synthesis

Translation is an example of an essential cellular processes that is compartmentalized in eukaryotic cells (Hovland et al., 1996; Sommer & Schleiff, 2014). Except for a small minority of proteins which are synthesized within the mitochondria and the chloroplasts, protein synthesis is

partitioned between the cytoplasm and the outer surface of the ER (Avendaño-Monsalve et al., 2020; Jan et al., 2014; Sommer & Schleiff, 2014). Many proteins are translated by free ribosomes at random locations in the cytoplasm (Campbell, 1989). These proteins are later targeted to specific organelles via the recognition of an N-terminal transit peptide on the protein by targeting factors and the import translocon in the organellar membrane(s). This mechanism, where the protein is fully translated prior to import, is known as the post-translational import pathway (Avendaño-Monsalve et al., 2020; Kim & Hwang, 2013).

In contrast, proteins destined for secretion, the Golgi, lysosomes or the plasma membrane are synthesized by ribosomes that are bound to the ER (Kim & Hwang, 2013). These proteins often have an N-terminal signal sequence which is recognized by a protein complex called the signal-recognition particle (SRP) which directs them to the translocon in the ER membrane (Aviram & Schuldiner, 2017). Once there, translation is activated, and the nascent polypeptide is translocated across the ER membrane or, for integral membrane proteins, into it through a mechanism known as the co-translational import pathway (Aviram & Schuldiner, 2017; Sommer & Schleiff, 2014). Co-translational protein targeting reduces the risk of protein aggregation in the cytoplasm, which would prevent or impede their post-translational import (Grevel et al., 2020a).

1.1.4 Chloroplast and Mitochondrial Protein Targeting

Both chloroplasts and mitochondria originated from photosynthetic bacteria that underwent endosymbiosis with their respective host cells approximately 1-2 billion years ago (Keeling, 2010; Kim & Hwang, 2013). Since then, many of the genes of the endosymbiotic bacteria have been transferred to the nucleus, and the organelle genomes have been left with less than one

hundred protein-coding genes only (Kim & Hwang, 2013; Peeters & Small, 2001). Today, most mitochondrial and chloroplast proteins are encoded by the nuclear genome and synthesized by cytoplasmic ribosomes. These proteins are subsequently imported into the organelles through a complex protein translocation machinery (Keeling, 2010).

A total of 3000 proteins are thought to be present in the chloroplast. For the mitochondria, this number is believed to be 2000 (Peeters & Small, 2001). These proteins are found in the membranes, intermembrane spaces or stroma and matrix of each of these organelles (Avendaño-Monsalve et al., 2020; Peeters & Small, 2001). Therefore, to get to their proper location, many of these proteins have to cross a double membrane through the import translocons (Sommer & Schleiff, 2014; Thomson et al., 2020).

In the case of chloroplasts, the widely accepted import mechanism is a post-translational one (Weis et al., 2013b; Zerges, 2000). This means the protein is fully translated by free ribosomes at random locations in the cytoplasm. The resulting pre-protein generally has a cleavable N-terminal extension, called a transit peptide (Weis et al., 2013b; Zerges, 2000) which is recognized by the translocon at the outer chloroplast envelope, also known as the TOC complex and initiates the translocation of the pre-protein into the chloroplast (Andrès et al., 2010; Jarvis & Soll, 2002). This acts in coordination with the translocon at the inner chloroplast envelope, also known as the TIC complex, to fully import the pre-proteins into the chloroplast stroma (Soll & Schleiff, 2004; Thomson et al., 2020). After import, the N-terminal transit peptides are cleaved by proteases, to create proteins that can be either folded, assembled into a functional complex, or targeted to one of the many chloroplast compartments (Jarvis & López-Juez, 2013; Zerges, 2000). In addition to transit peptides, there are molecular chaperons on both the cytoplasmic and stromal sides of the

chloroplast envelope that use ATP and facilitate the post-translational import of the nuclear encoded pre-proteins into the chloroplast (Shi & Theg, 2013; Strittmatter et al., 2010).

The predominant view of protein import into the mitochondria is also through a similar post-translational mechanism (Gold et al., 2017b; Kellems et al., 1974). However, recent studies have demonstrated that this may be limited to a certain class of proteins only (Garcia et al., 2007; Williams et al., 2014). For example, all studied matrix proteins or transporters such as the ATP/ADP carrier (Aac2 or AAC), have been shown to be imported after full synthesis *in vitro* (Avendaño-Monsalve et al., 2020). However, in recent decades, evidence has been found in support of localized protein synthesis at the mitochondrial outer membrane, thereby suggesting a co-translational import mechanism for this organelle (Gold et al., 2017b; Kellems et al., 1974). Indeed, it was demonstrated 30 years ago that a subclass of cytoplasmic polysomes is bound to the surface of mitochondria (Avendaño-Monsalve et al., 2020; Garcia et al., 2007; Kellems et al., 1974). More recently, electron microscopy images have shown cytoplasmic ribosomes in discrete clusters near the cristae junctions (Gold et al., 2017). These ribosomes have also been shown to interact specifically with the translocon of the outer mitochondrial membrane, known as the TOM complex, and nascent chain binding has been found to be crucial for ribosome recruitment and stabilization to this region (Gold et al., 2017b; Vogel, Bornhövd, et al., 2006; Williams et al., 2014a). This interaction highlights how protein synthesis may be coupled with transport (Gold et al., 2017). Furthermore, numerous mRNAs encoding mitochondrial proteins have been found, either on the mitochondrial surface or in close proximity, both in yeast and human cells, consistent with a role for cotranslational protein insertion (Avendaño-Monsalve et al., 2020; Gold et al., 2017; Kellems et al., 1974). Meanwhile, other studies have found that the proteins that are translated in the vicinity of the mitochondria, are almost exclusively of prokaryotic origin and are key elements

of the core molecular complexes (Garcia et al., 2007; Gold et al., 2017). Accessory proteins on the other hand were translated on free cytoplasmic polysomes (Garcia et al., 2007). Additionally, proximity-specific ribosome profiling has shown that in yeast, most inner-membrane proteins are co-translationally targeted to the mitochondria, reminiscent of proteins entering the endoplasmic reticulum (ER) (Lesnik et al., 2014; Williams et al., 2014a). As for the chloroplast, evidence for localized ribosomes on the envelope and the possibility of a co-translational import mechanism had not been found until now. However, the results presented in Chapter 2 reveal the first examples of such a mechanism in the chloroplast of the green algae *Chlamydomonas reinhardtii*.

1.2 *Chlamydomonas reinhardtii* as a Model Organism

The development of *Chlamydomonas* as a model organism dates to the 1950s when its first mutants were generated (Harris et al., 2009). This unicellular green alga is ideal for classic genetic studies because of its haploid genome which allows for mutations to be immediately expressed and produce an observable phenotypes (Harris et al., 2009; Merchant et al., 2007). Furthermore, different *Chlamydomonas* strains can be crossed in the laboratory to introduce multiple traits into a single haploid strain, for example to generate double or triple mutants (Merchant et al., 2007; Sasso et al., 2018).

Chlamydomonas also has a fully sequenced and annotated chloroplast and nuclear genomes which are amenable to manipulation (Merchant et al., 2007; Shin et al., 2016). It also has a growing array of tools and techniques for molecular genetic studies (Mussnug, 2015) including a genome-wide library of mapped, indexed insertional mutants (Li et al., 2016; Sasso et al., 2018) and

CRISPR-mediated targeted gene disruptions (Ferenczi et al., 2017; Sasso et al., 2018; Shin et al., 2016).

Today, this alga is widely used to study diverse cellular and metabolic processes such as photosynthesis (Rochaix, 2001), chloroplast biology (Sun et al., 2019), cilia structure and function (Wingfield & Lechtreck, 2018), nutrient homeostasis (Grossman, 2000; Merchant et al., 2006), cell cycle control (Goodenough et al., 2007) and more. Among the features that make *Chlamydomonas* an excellent laboratory species is its ease of use. This alga only requires water, salts, air, and light and very little space to grow. In terms of studies on photosynthesis and chloroplast biology, this alga has several advantages over plants. First, it has a short generation time and cultures can be ready within days for experiments. In fact, under optimal conditions, *Chlamydomonas* cultures can grow so rapidly that they can double in cell numbers approximately every 8 hours (Harris et al., 2009). Additionally, *Chlamydomonas* can grow in the dark, on media that has been supplemented with acetate, while retaining a functional photosynthetic apparatus. This has allowed for light-sensitive photosynthesis mutants to be isolated and remain fully viable (Harris et al., 2009; Salomé & Merchant, 2019). The existence and viability of such mutants has greatly advanced our understanding of photosynthesis, particularly the order of electron carriers in the photosynthetic electron transport chain (Gorman & Levine, 1965; Sasso et al., 2018). For examples two core proteins of photosystem II (D1 and D2) were first identified in *Chlamydomonas* (Chua & Gillham, 1977; Sasso et al., 2018) and later proposed to be key components of the reaction center in this photosystem (Sasso et al., 2018; Satoh, 2003).

Chlamydomonas cells and their chloroplasts also have a highly stereotypical organization which make it well suited for studies of intracellular organization and the localization of specific proteins and mRNAs. A typical wild-type cell has an oblong shape that is between 8-10 μm in

length (Harris et al., 2009) and is surrounded by a cell wall. Each cell has a central cytosolic region which contains contractile vacuoles, Golgi vesicles and several mitochondria (Atteia et al., 2009) (Fig 1.1 A).

The anterior pole of each cell contains two flagella which are 10–12 μm in length (Wingfield & Lechtreck, 2018). Each cell also has a prominent cup-shaped chloroplast which makes up approximately 40% of the cell volume (Harris et al., 2009; Pröschold et al., 2005). This single chloroplast is surrounded by a double membrane called the chloroplast envelope. Inside the chloroplast, are the thylakoid membranes as well as a non-membrane bound compartment called the pyrenoid as well as starch granules. Also located between the inner and outer membranes of the chloroplast envelope and the plasma membrane is the light sensing eyespot which forms part of the vision apparatus that directs phototactic responses in *Chlamydomonas* (Engel et al., 2015; Sasso et al., 2018).

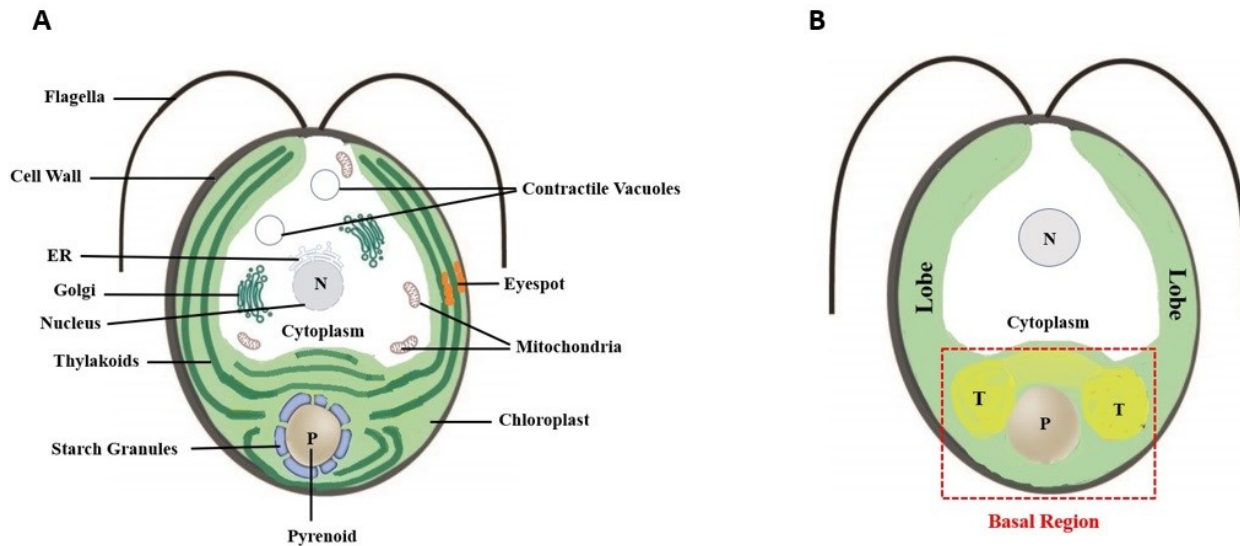


Fig 1.1- Cytological organization of *Chlamydomonas reinhardtii* cells. A) The alga is encased in a cell wall (in black). Each cell has two anterior flagella. The cytoplasm is shown in white. The typical compartments found in the cytoplasmic region of a *Chlamydomonas* cell include the nucleus, mitochondria, the Golgi and contractile vacuoles. B) The single cup-shaped chloroplast (in green) occupies a large portion of the cell's volume. The basal region of the chloroplast contains the pyrenoid (P). Extending out from the basal region are two chloroplast lobes. Also located in the basal region is the T-zone (T) which is the primary location for the synthesis and assembly of photosystem II.

The stereotypic morphology of this algal system has allowed us to identify even greater organization in the chloroplast. Among these organized regions is a T-zone, located in the basal region of the chloroplast (Fig 1.1 B). This T-zone is the location for the *de novo* synthesis and assembly of photosystem II and possibly photosystem I (Sun et al., 2019; Uniacke & Zerges, 2007). This domain is enriched in chloroplast ribosomes, photosystem II-specific translation factors and unassembled photosystem II proteins (see Appendix I). Meanwhile, subunits of the chloroplast import translocon (TIC and TOC) have been found to localize within the region that connect the chloroplast lobes to the basal region (Uniacke & Zerges, 2009) . The proximity of this import domain to the T-zone, allows for the trafficking of nuclear encoded photosystem subunits. Also in the basal region, we have found cytoplasmic ribosomes localized on the chloroplast envelope. These ribosomes are specifically enriched in the area between the two chloroplast lobes (see Chapter 2). This spatial organization highlights the coordination of protein synthesis on and within the chloroplast by its two genomes. Meanwhile in the lobes there is a domain that has some of the markers for the Calvin Benson Cycle (see Chapter 3). This region works in concert with the pyrenoid in the basal region, which as mentioned earlier is packed with Rubisco. The pyrenoid also houses the thylakoid tubules which are connected to the thylakoids (He et al., 2020; Zhan et al., 2018). These tubules are used to transport the required molecules such as CO₂, ATP, and the intermediates of the Calvin-Benson Cycle to the enzyme Rubisco.

1.3 The Calvin Benson Cycle

As mentioned, chloroplasts are mainly known for their role in photosynthesis. This is the process by which plants, algae and cyanobacteria convert light energy into chemical energy (Harris, 1989). Photosynthesis provides the oxygen we breath and the food we eat and is essentially the foundation for all life (Harris, 1989; Johnson, 2016). This process can be broken down into two major stages: the light-dependent reactions and the light-independent reactions, also known as the Calvin Benson Cycle (Rochaix, 2001). These stages are highly compartmentalized.

The light-dependent reactions take place within the thylakoid membranes. They are carried out by several multisubunit complexes which include photosystem I, photosystem II and their associated light-harvesting systems, as well as chlorophyll a and b and carotenoids (Harris, 1989; Rochaix, 2001). These two photosystems work together with cytochrome b6/f complex to form the photosynthetic electron transport (PET) chain (Johnson, 2016; Rochaix, 2001).

The PET reactions begin with photosystem II using energy from the sun to split water into oxygen, protons, and electrons (Brudvig, 2008). The released O₂ is used for aerobic respiration while the released electrons start to move down an electron transport chain that works in concert with a series of electron acceptors and carriers, such as plastoquinone, plastocyanin, ferredoxin and ferredoxin NADP⁺ reductase (Gorman & Levine, 1965; Ullmann, 2001; Uniacke & Zerges, 2007). This flow of electrons ultimately leads to the reduction of NADP to NADPH while at the same time, creating a proton gradient across the thylakoid membranes. This proton gradient is then used by ATP synthase to make ATP from ADP (Brudvig, 2008; Wollman et al., 1999).

The NADPH and ATP produced by the light reactions are utilized by the Calvin-Benson Cycle to fix CO₂ into carbohydrates (Biel & Fomina, 2015; Gurrieri et al., 2021). The Calvin Benson Cycle can be found in all photosynthetic eukaryotes as well as many photosynthetic bacteria (Biel & Fomina, 2015; Meyer et al., 2020). The full cycle involves 13 reactions that are catalyzed by 11 different enzymes. These reactions take place in the chloroplast stroma and are often divided into the following 3 steps: carbon fixation, reduction, and regeneration (Janasch et al., 2019). The enzyme that initiates this pathway is ribulose-1,5-bisphosphate carboxylase oxygenase (Rubisco). Rubisco takes gaseous carbon dioxide (CO₂) and uses it to carboxylate a 5-carbon molecule called ribulose-1,5-bisphosphate (RuBP) (Erb & Zarzycki, 2018; Raines, 2003). RuBP reacts with CO₂ and H₂O to produce two 3-phosphoglycerate (3PGA) molecules, each a 3-carbon carboxylic acid (Raines, 2003). The two triose phosphate sugars resulting from this reaction are then reduced and modified using NADPH and ATP from the light reactions and ATP synthase (Biel & Fomina, 2015; Erb & Zarzycki, 2018). The regenerative phase of the cycle involves a series of reactions that convert triose phosphates into the CO₂ acceptor molecule, RuBP (Biel & Fomina, 2015; Heldt & Piechulla, 2011; Raines, 2003). One in every six 3-carbon sugars can leave the cycle and five in every six reduced 3-carbon sugars are required to regenerate RuBP (Biel & Fomina, 2015; He et al., 2020).

Rubisco and phosphoribulokinase (PRK), the enzyme that phosphorylates the substrate for Rubisco, are the only enzymes that are unique to the Calvin cycle. All other enzymes in this pathway can also be found in other processes such as the oxidative pentose phosphate pathway and glycolysis (Agarwal et al., 2009; Rumpho et al., 2009).

1.3.1 Rubisco and Photorespiration

Rubisco is the most abundant enzyme on earth (Iñiguez et al., 2020). As previously discussed, Rubisco incorporates CO₂ into an organic molecule during the first stage of the Calvin Benson Cycle and therefore is the key enzyme in carbon fixation (Erb & Zarzycki, 2018; Jungnick et al., 2014). However, in addition to its carboxylase activity, Rubisco also has an oxygenase activity and when it is in the presence of O₂, it initiates the process of photorespiration (Eisenhut et al., 2019). Photorespiration is a wasteful pathway in that it uses ATP and NADPH to recover a carbon from the 2-carbon product, phosphoglycolate (Busch, 2020; Jungnick et al., 2014).

The emergence of oxygenic photosynthesis led to drastic increases in atmospheric O₂ levels (Keeling, 2010; Nelson & Ben-Shem, 2004). Under these conditions, the chance that oxygen will compete with CO₂ for the active site of Rubisco and lead to inefficient CO₂ fixation is high (Küken et al., 2018). This inefficiency is thought to be the reason for the high abundance of Rubisco in photosynthetic organisms (Busch, 2020).

1.3.2 Carbon Concentrating Mechanism

Atmospheric CO₂ concentration is a major factor contributing to plant growth and photosynthesis rate. Therefore, increasing the efficiency of carbon fixation can directly increase crop yields (Singh et al., 2014). The carbon concentrating mechanism (CCM) is a biological adaptation to low carbon dioxide concentrations in the environment. It is a mechanism that evolved in cyanobacteria and eukaryotic microalgae but is now found in nearly all photosynthetic organisms (Cummins, 2021; Goudet et al., 2020). The CCM concentrates carbon dioxide around

Rubisco so it can operate more efficiently while minimizing the wasteful process of photorespiration (Goudet et al., 2020) .

Photosynthetic organisms have a variety of ways to concentrate CO₂ and minimize photorespiration and favor the carboxylase activity of Rubisco. These include biochemical mechanisms which are found in plants with C₄ photosynthesis and crassulaceous acid metabolism (CAM) (Keeley & Rundel, 2003). It could also include the active transport of bicarbonate across membranes and processes that involve localized enhancement of the CO₂ concentration by acidification of a particular cellular compartment like those found in the green algae *Chlamydomonas* (Moroney & Ynalvez, 2007; Wang et al., 2015).

1.3.4 CCM in Land Plants

Land plants are often divided into three categories. The first category includes about 85% of plant species on Earth and are known as C₃ plants (Busch et al., 2013). These plants have no special features to deal with photorespiration. In C₃ plants, atmospheric CO₂ is absorbed through the leaf stomata and fixed by the enzyme Rubisco during the first step of the Calvin Benson Cycle (Busch et al., 2013; Cummins, 2021). However, C₃ plants are not adapted to non-optimal conditions and in hot dry environments, they close their stomata to prevent excessive water loss. This closing of the stomata, prevents O₂ from diffusing out of the leaf, thus increasing its concentration relative to CO₂. Because these plants have no carbon concentrating mechanism, their photosynthetic efficiency suffers through the process of photorespiration (Goudet et al., 2020).

The second and third category of plants are known as C₄ plants, and CAM plants. Both of these plant types have special coping mechanisms that allow them to survive in varying environmental conditions, such as hot dry habitats where water is not readily available. Both of

these plant types also have a two-stage process for concentrating carbon dioxide near the enzyme Rubisco (Keeley & Rundel, 2003). This means that atmospheric CO₂ is first fixed into an intermediate 4-carbon organic acid called oxaloacetate. This step is carried out by a non-rubisco enzyme called phosphoenolpyruvate (PEP) carboxylase that has no affinity for O₂. Oxaloacetate is then converted to another 4-carbon compound called malate which is decarboxylated and the released CO₂ is fixed by Rubisco via the Calvin Benson Cycle, exactly as in C₃ plants (Gowik & Westhoff, 2011; Keeley & Rundel, 2003). C₄ plants separate the initial CO₂ absorption and the Calvin Benson Cycle between different cell types (i.e, mesophyll and bundle-sheath cells) (Goudet et al., 2020). Meanwhile CAM plants separate these steps between night and day (Keeley & Rundel, 2003). This means at night, they open their stomata, allowing CO₂ to diffuse into the leaves. This CO₂ is then converted into oxaloacetate and malate through the same process as described for C₄ plants. Malate is stored in vacuoles and the next day, during daylight, it is broken down and the released CO₂ is fixed through the Calvin Benson Cycle (Bräutigam et al., 2017; Singh et al., 2014). This controlled release increases the concentration of CO₂ near Rubisco and prevents photorespiration (Busch et al., 2013 ; Gowik & Westhoff, 2011).

1.3.4 CCM in Cyanobacteria and Algae

Photosynthetic organisms like cyanobacteria and eukaryotic algae account for almost 50% of the world's photosynthesis (Giordano et al., 2005). However, living in aquatic ecosystems they often face many challenges in acquiring CO₂. Some of these obstacles include the slow diffusion of CO₂ in aqueous environments. CO₂ diffuses 10,000 times slower in water than in air (Goudet et al., 2020; Hagemann et al., 2016). Also, most CO₂ in water, which is near pH 7, is converted to bicarbonate ions (HCO₃⁻). Unlike CO₂, bicarbonate ions cannot cross membranes and enter cells

and organelles by simple diffusion (Fei et al., 2021). To overcome these challenges, they have developed a biophysical carbon concentrating mechanism. These CCMs involve a set of transport proteins and enzymes that deliver the appropriate inorganic carbon species, like CO₂ and bicarbonate HCO₃⁻ into cells and concentrate it in a compartment that is packed with Rubisco (Fei et al., 2021; Wang et al., 2015).

In cyanobacteria, for example, inorganic carbon in the form of HCO₃⁻ is pumped into the cytosol to a high concentration (Hagemann et al., 2016). This HCO₃⁻ is then converted into CO₂ in specialized compartments called carboxysomes which are filled with Rubisco (Cummins, 2021). Analogous to cyanobacterial CCMs, green algae concentrate HCO₃⁻ in a microcompartment that is found in the chloroplast called the pyrenoid (Moroney & Ynalvez, 2007). The pyrenoid matrix is packed with Rubisco. Also found in the pyrenoid are membrane tubules that are connected to the surrounding photosynthetic thylakoid membranes (Freeman Rosenzweig et al., 2017; He et al., 2020). Associated with the pyrenoid tubules is a carbonic anhydrase that converts HCO₃⁻ to CO₂ for fixation by Rubisco (Badger & Price, 1994; Moroney et al., 2011).

1.3.5 CCM in *Chlamydomonas reinhardtii*

The carbon concentrating mechanism in the model green alga *Chlamydomonas* involves three key elements: 1) inorganic carbon transporters at the plasma membrane and chloroplast envelope, 2) carbonic anhydrases (CA) which convert the accumulated HCO₃⁻ in the cell to CO₂ and 3) the pyrenoid which is tightly packed with the carbon fixing enzyme Rubisco (Giordano et al., 2005; Jungnick et al., 2014). CCM in *Chlamydomonas* is inducible under low CO₂ concentrations and can be divided into two phases. In the first phase, inorganic carbon is taken up

from the environment and delivered to the chloroplast, while the second part involves the generation of high levels of HCO_3^- in the chloroplast stroma, using the pH gradient across the thylakoid membrane (Jungnick et al., 2014; Spalding, 2008).

The carbonic anhydrase proteins in *Chlamydomonas*, include CAH1, CAH4 and CAH5 which are up-regulated under low CO_2 conditions (Moroney et al., 2011; Rai et al., 2021). CAH1 is found in the periplasmic space and generates HCO_3^- in for transport to the cytoplasm. CAH4 and CAH5 are localized to the mitochondria to convert CO_2 from respiration to HCO_3^- for transport to the chloroplast (Jungnick et al., 2014; Moroney et al., 2011). CAH3 carbonic is associated with photosystem II and is localized within the thylakoid lumen (Moroney et al., 2011; Wang et al., 2015). Its function is to convert the accumulated HCO_3^- in the chloroplast to CO_2 for fixation by Rubisco within the pyrenoid (Badger & Price, 1994; Jungnick et al., 2014; Wang et al., 2015). Another important component of the *Chlamydomonas* CCM is the inorganic carbon transporter system. These include the membrane proteins LCI1, LCIA and HLA3 (Spalding, 2008).

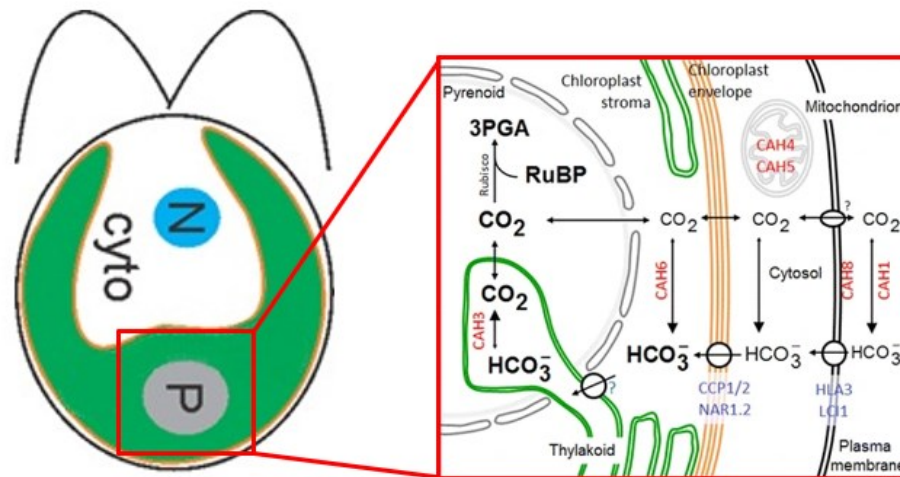


Fig. 1 .2- The Carbon Concentrating Mechanism in *Chlamydomonas*. On the left, a *Chlamydomonas* cell is seen with the cup-shaped chloroplast in green, enclosing the nucleus (N) and cytoplasmic region (cyto). The pyrenoid (P) is in the basal region of the chloroplast. The box on the right shows the carbon concentrating mechanism in *Chlamydomonas*. Bicarbonate (HCO_3^-) is transported from outside the chloroplast into the stroma by plasma membrane transporters HLA3 and LCI1, and envelope transporter LCIA (also called NAR1.2. in the figure above). CAH1, CAH3, CAH4/5, CAH6 and CAH8 are carbonic anhydrases that convert the accumulated bicarbonate (HCO_3^-) to CO_2 . The CO_2 is then delivered to the pyrenoid and is used as the substrate for Rubisco. (Adapted from (Jungnick et al., 2014)).

1.4 Thesis Overview

Despite our detailed knowledge of the composition, cytology, biogenesis and functions of chloroplasts, the cytological organization of the pathways that converge for the biogenesis of the photosynthesis complexes and the Calvin Benson Cycle is incompletely understood. To better comprehend the spatial organization of these processes, this thesis addresses several key questions. In Chapter 2, I address the long-standing question of protein import into chloroplasts. I show evidence that protein translocation into the organelle involves a co-translational pathway, as established for the endoplasmic reticulum and the mitochondria. For nuclear genome-encoded proteins that are localized to chloroplasts, the field has largely favored a post-translational import mechanism (Chua & Schmidt, 1979; Nakai, 2018; Soll & Schleiff, 2004; Thomson et al., 2020). Such has also been case for the mitochondria (Chua & Schmidt, 1979; Grevel et al., 2020). However, in recent years, there has been growing evidence for ribosome association and mRNA localization to the mitochondrial outer membrane thereby supporting a co-translational import model of a subset of mitochondrial proteins (Claros et al., 1995; Gold et al., 2017; Grevel et al., 2020a; Ott & Herrmann, 2010).

Using different biochemical and microscopy approaches, we reveal a spatially defined pool of cytoplasmic ribosomes on the chloroplast of *Chlamydomonas reinhardtii*. We show evidence that these ribosomes are associated with the outer chloroplast envelope and present the first example of localized translation on the chloroplast. I also present examples of mRNAs that encode chloroplast proteins, enriched in this same region further supporting the localized translation of chloroplast proteins.

Our results further support the possibility of a co-translational import mechanism for chloroplast-localized proteins since the localized mRNAs encode for chloroplast proteins and

because previous findings in our lab, found a specialized domain within the chloroplast that is the platform for the biogenesis of photosystems I and II (Sun et al., 2019; Uniacke & Zerges, 2007). Together these findings reveal a spatially aligned translation zone on and within the chloroplast, thereby supporting the idea of co-translational import.

In Chapter 3, I provide evidence for a new compartment in the chloroplast of *Chlamydomonas* that may be involved in the Calvin Benson Cycle during the early stages of the diel cycle. This is a finding that I made. I also show an initial characterization of how the enzymes involved in the various steps of this pathway are spatially organized. Chapter 4 presents a summary of the major findings, discusses how they advance these fields of chloroplast biogenesis and photosynthesis, and propose the future directions for these projects. Overall, I show that the chloroplast of *Chlamydomonas* is highly compartmentalized and much more complex than it is currently believed to be.

CHAPTER 2: CHLOROPLAST-LOCALIZED TRANSLATION FOR PROTEIN TARGETTING IN *CHLAMYDOMONAS REINHARDTII*

Adapted from: Sun Y., Bakhtiari S., Valente-Paterno M., Wu Y., Law C., Dai D., Dhaliwal J., Bui KH., and Zerges W. (2021). Chloroplast-localized translation for protein targeting in *Chlamydomonas reinhardtii*. *BioRxiv*. doi: <https://doi.org/10.1101/2021.12.27.474283>

ABSTRACT

Translation is localized within cells to ensure that the protein products arrive at the proper compartments, integrate into membranes and assemble to form multi-subunit complexes. The ER and mitochondria are bound by translating ribosomes for these functions. However, chloroplasts are believed to import only fully synthesized proteins. The following results revise this view by showing that translating cytoplasmic ribosomes are bound to a domain of the chloroplast envelope in *Chlamydomonas reinhardtii*. Ribosomes are retained by isolated chloroplasts and seen on the envelope by electron tomography. Chloroplast-bound ribosomes are active, based on results of the RiboPuromylation assay method and the puromycin-release assays. These ribosomes synthesize chloroplast proteins, based on their colocalization specifically with mRNAs encoding chloroplast proteins, seen by fluorescence *in situ* hybridization. Co-translational import of these proteins is supported by nascent polypeptide dependency of the ribosome-chloroplast associations. This ribosome-bound envelope domain aligns with the translation zone within the chloroplast, where chloroplast ribosomes synthesize proteins encoded by the plastid genome. We propose that translation on and within this semiautonomous organelle is spatially coordinated to facilitate the convergence of the nuclear-cytoplasmic and organellar genetic systems for chloroplast biogenesis and proteostasis.

2.1 INTRODUCTION

Translation is localized within cells to ensure the protein products are targeted to the proper compartments, integrated into membranes or assembled to form complexes (Das et al., 2021). For example, cytoplasmic ribosomes (cyto-ribosomes) bound to the ER synthesize nascent polypeptides undergoing co-translational import to the lumen or insertion into the organellar membrane. Peroxisomes and basal bodies are associated with mRNAs encoding their proteins, suggesting these organelles are sites of localized translation for protein targeting (Fingerhut & Yamashita, 2020; Haimovich et al., 2016; Zipor et al., 2009). RNA granules compartmentalize the translation of specific mRNAs for co-translational assembly of the proteasome and other yet unknown functions (Lui et al., 2014; Panasenکو et al., 2019). Mitochondria of *Saccharomyces cerevisiae* and the chloroplast of the unicellular green alga *Chlamydomonas reinhardtii* contain bacteria-type ribosomes, “mito-ribosomes” and “chloro-ribosomes”, respectively, for the synthesis of proteins encoded by the small genomes in these semiautonomous organelles. A substantial proportion of these ribosomes translate on membranes within the respective organelles for protein targeting and membrane insertion (Weis et al., 2013). On the outer membrane of mitochondria, in yeast and human cells, cyto-ribosomes synthesize proteins encoded by the nuclear genome, many of which undergo cotranslational import (Claros et al., 1995; Williams et al., 2014).

Chloroplast proteins encoded by nuclear genes are widely believed to be synthesized at random cytoplasmic locations and undergo posttranslational import (Jarvis & Lopez-Juez, 2014; Weis et al., 2013). This belief is based on the ability of isolated chloroplasts to import *in vitro* synthesized chloroplast pre-proteins (i.e. still having their N-terminal localization sequence) and EM images of chloroplasts lacking the arrays of bound cyto-ribosomes seen on the rough ER and mitochondria (Weis et al., 2013). The possibility that translation is localized on or near the

chloroplast in the unicellular green alga *Chlamydomonas reinhardtii* was raised by images from TEM and fluorescence microscopy showing that the cytoplasm adjacent to the chloroplast is enriched in cyto-ribosomes and the mRNA encoding a chloroplast-localized protein (Colon-Ramos et al., 2003; Uniacke & Zerges, 2009). Immediately within the chloroplast, localized chloro-ribosomes translate subunits of photosystem I (PSI) and photosystem II (PSII) into membranes of the T-zone, an intraorganellar compartment where these complexes of the photosynthetic electron transport system are assembled and then routed to thylakoid membranes throughout the chloroplast to carry out the light-driven reactions in photosynthesis (Schottkowski et al., 2012; Sun et al., 2019; Uniacke & Zerges, 2007, 2009). These results suggest a spatial coordination of protein synthesis by cyto-ribosomes on the chloroplast and chloro-ribosomes within for protein targeting and complex assembly. Yet it remains to be determined whether cyto-ribosomes translate on the chloroplast outer envelope membrane.

Here, we show that cyto-ribosomes translate on a domain of the chloroplast envelope in *Chlamydomonas*. These associations are demonstrated by two types of experimental evidence. First, the retention of cyto-ribosomes by chloroplasts during their isolation from free cyto-ribosomes and organelles known to bind them, i.e. ER and mitochondria. Second, immunofluorescence (IF) microscopy images of a marker cyto-ribosomal protein (cyL4) on the chloroplast surface and high-resolution electron tomography images showing ribosome clusters on the outer envelope membrane. Translational activity of these chloroplast-bound cyto-ribosomes is demonstrated by results of the RiboPuromycylation method and the puromycin-release assays (Kellems et al., 1974; Redman & Sabatini, 1966; Schmidt et al., 2009). A proportion of these chloroplast-bound cyto-ribosomes were tethered by their nascent polypeptides, which were likely undergoing cotranslational import *in vivo*. Synthesis of chloroplast proteins on the cyto-ribosome-

bound domain of the chloroplast envelope is supported by results of FISH showing that isolated chloroplasts retain on this domain mRNAs encoding chloroplast proteins but not an mRNA encoding a non-chloroplast protein. Finally, the cyto-ribosome-bound domain of the envelope is spatially aligned with two chloroplast features related to protein import: domains of the envelope enriched in the protein translocons of the inner/outer membrane of the chloroplast envelope (TIC and TOC) and the T-zone (Figure 1A) (Schottkowski et al., 2012; Sun et al., 2019; Uniacke & Zerges, 2007).

2.2 MATERIALS AND METHODS

2.2.1 Strains and culture conditions

Chlamydomonas reinhardtii strain used for most experiments has a cell-wall deficiency (CW15, to allow for the breakage of cells of isolation of chloroplasts) (cc-400 MT+). For the results in Figure 2, wild-type strain cc-125 was used. Strains were cultured to 1×10^5 cells·ml⁻¹ in high salt minimal (HSM) medium, with aeration, illuminated by five banks of red and blue LEDs, each at $150 \mu\text{E} \cdot \text{m}^{-2} \cdot \text{s}^{-1}$ at 23 °C with orbital shaking (120 rpm). cc-400 was cultured in HSM containing 1.0% (w/v) sorbitol. Cultures were entrained under alternating cycles of 12 h light:12 h dark for 3 days to a density of $\sim 4 \times 10^6$ cells·ml⁻¹. Culture samples were harvested at the fourth hour (ZT4) of final light cycle by centrifugation (3,000 x g, 5 min at RT).

2.2.2 Chloroplast isolation

Chloroplast isolation was performed as described previously (Mason et al., 2006) with the following modifications. Cell pellets were resuspended to 1×10^8 cells·ml⁻¹ in isolation buffer (IB) [300 mM Sorbitol, 50 mM HEPES-KOH pH 7.5, 25 mM MgCl₂, 0.1% (w/v) BSA]. Saponin (Sigma, # 47036) 10% (w/v) freshly dissolved in isolation buffer was added to 0.4% (w/v), followed by incubation at 22 °C for 10 min with occasional gentle agitation. The resuspension was passed twice through a 27-gauge needle at 0.1 ml·s⁻¹. Cells and chloroplasts were collected by centrifugation at 750 g for 2 min at 4 °C. The pellet was resuspended in isolation buffer and overlaid on a Percoll gradient as described in Mason et al., 2006. The gradient was centrifuged for 25 min at 3,200 g. The material at the 45-65% interface was collected. This was diluted by the addition of 4 volumes of isolation buffer. Chloroplasts were pelleted by centrifugation (670 g, 1 min, 4 °C), resuspended in buffer according to the downstream use.

2.2.3 Immunoblot analysis

For the immunoblots in Fig 2.1E, an equal number of isolated chloroplasts were resuspended in SDS-PAGE loading buffer and resolved by SDS-PAGE (12% acrylamide) (Sambrook & Russell, 2006). Proteins were transferred to a membrane of PVDF (BIO-RAD) or, for AOX1 detection, nitrocellulose (BIO-RAD) and reacted with primary and secondary antibodies as described previously (Sambrook & Russell, 2006). The primary antibodies were: α -BIP (Santa Cruz sc-33757) (1:150), α -AOX1 (Agrisera AS06 152, 1:150,000), α -cyL4 (1:6,000) and α -AtpB (1:6,000). The secondary antibody was horseradish peroxidase-conjugated goat anti-rabbit IgG antibody (KPL). Signals were detected using an ECL substrate (Thermo-Fisher) with an Imager

600 (Amersham/GE) according to the manufacturer's protocols. Signal quantification was conducted with Imager 600 Analysis Software (Amersham).

2.2.4 IF-staining and microscopy

IF-staining was performed as described previously (Uniacke, Colon-Ramos, et al., 2011). The primary antibodies and the dilutions were: α cyL4 (1:1000) 5, α AOX1 (1:1,200), and α BIP (1:100). The secondary antibody was AlexaFluor568 conjugated to goat anti-rabbit IgG (Thermo Fisher). For dual IF-staining (Figure 2.1C), chloroplasts were first reacted with α -LCIA (1:700) and then indirectly IF-labelled by AffiniPure Fab Fragment Donkey Anti-Rabbit IgG (H+L) conjugated to AlexaFluor488 (Jackson ImmunoResearch Inc). Chloroplasts were reacted with α cyL4 (1:1000) and then indirectly IF-labelled by goat anti-rabbit IgG conjugated to AlexaFluor568 (Thermo Fisher). For consistency, the cyL4 IF signal is presented in magenta and other signals in green. Microscopy was carried out with a Leica DMI6000B inverted epifluorescence microscope with a 63x Plan Apo objective (NA 1.4) and further magnified by a 1.6x tube lens. Images were acquired on a Hamamatsu Orca R2 C10600-10B camera controlled by Volocity software (Improvision). Filters: Texas Red (562/40nm excitation: 624/40nm emission) for AlexaFluor568 and GFP (472/30nm excitation: 520/35nm emission) for AlexaFluor488. Acquired images were taken using Z plane stacks with a spacing of 0.2 μ m per section; exposure settings, gain, and excitation intensity were kept constant where comparisons between intensities was required. For deconvolution, Z-stacks were taken by series capture at a thickness of 0.2 μ m per section and were deconvoluted with AutoQuant X3 (Media Cybernetics Inc).

2.2.5 Probe design and preparation

Complementary 31 nt probes were designed against each mRNA sequence using Benchling (12-24 probes for each mRNA). All probe sequences are provided in Table 1. The following sequence was added to the 5' end of each 31 nt probe: 5' CCTCCTAAGTTTCGAGCTGGACTCAGTG 3'. This is the reverse complement of the X FLAP sequence used in Tsanov et al. (Tsanov et al., 2016a). Oligos were ordered from Integrated DNA Technologies (IDT), in lyophilized format, using 25 nmol synthesis scale, standard desalting. Each probe was resuspended in TE buffer to a final concentration of 100 μ M. Equal volumes of each probe was combined together to generate an equimolar probe mix, at 20 μ M (mixed probe concentration). The X FLAP sequence itself 5' CACTGAGTCCAGCTCGAACTTAGGAGG 3' was 5' and 3' end labelled with Cy3. The equimolar probe mix was annealed to the fluorophore-labelled FLAP sequence in a heat block according to Tsanov et al. Annealed probes were stored at -20° C.

2.2.6 FISH

Slides were first boiled in 1.0 N HCL for 15 min to reduce autofluorescence and air dried overnight. On the following day, a 10 μ l drop of 0.1% Poly-L-lysine (Sigma) was dispensed at one end of the slide and smeared across with another slide. The Poly-L-lysine coated slides were kept in a slide rack covered with aluminum foil and left to dry for three to seven days. On the day of the experiment, approximately 1×10^6 cells were aliquoted onto the center of each slide. Cells were allowed to adhere to the slide for c.a. 5 min. Cell fixation was performed using 4% paraformaldehyde (w/v) freshly diluted in 1X PBS (phosphate buffered saline) for 10 minutes. The slides were then incubated twice, 10 minutes each, in methanol at -20° C. The next steps were

performed on an orbital shaker at low speed. Slides were washed twice, 10 minutes each in PBS-Mg at RT. Permeabilization was done by incubating the slides in freshly prepared 2.0% (v/v) Triton X-100 in 1X PBS for 10 min. This was followed by two 10 minutes washes in 1X PBS-Mg at RT and a 20-minute wash in 15% formamide freshly prepared in 1X SSC (3 M NaCl and 300 mM Sodium Citrate adjusted to pH 7.0 with HCl). The hybridization mix was made according to Tsanov et al. except for the BSA concentration which was 4.5 mg/ml in the hybridization mix. A 50 μ l aliquot of the hybridization mix was placed on a cover slip. Each slide was gently blotted with a kimwipe and placed cell side down onto the hybridization solution on the coverslip. The slides were incubated overnight at 37°C in a slide hybridization oven. A piece of moist paper towel was included to maintain humidity. Post hybridization buffer containing 1 \times SSC, 15% formamide was made fresh the next day. Slides were incubated in post hybridization buffer twice for 30 minutes each at 37°C. The slides were then washed twice with 1X PBS-Mg at RT, 10 minutes each. Slides were blotted dry with a KimWipe. 15 μ l of Anti-fade was added to the cell side of each slide. A coverslip was placed on top of the Anti-fade reagent and sealed with nail polish. All solutions were made with diethyl pyrocarbonate (DEPC)-treated water. For the results in Figure 2-4A, the average FISH signal intensity from the probe with random sequence obtained for cells or chloroplasts in each trial was subtracted from the average intensities of the mRNA FISH probes. p-values are from 2-tailed Student's t-tests comparing, $n \geq 3$ biological replicates using independent cultures. The images in Figure 2-4B-D were adjusted to best show distributions of each mRNA signal using Photoshop (Adobe). The TUB2 mRNA FISH signal was seen previously throughout the cytoplasm in deflagellated cells, as we observed here, possibly because the strain that we used lacks flagella (Supplemental Figure 1D, Figure 2.4D). Specificities of the FISH signals of the RBCS1/RBCS2 and LHCBM2/7 mRNAs were demonstrated previously. To

determine the average distribution of fluorescent signals in cells or chloroplasts of a data set, we used a macro which operates within ImageJ, described previously (<https://github.com/Zergeslab/cellHarvester>).

2.2.7 Image analysis of distributions of average fluorescence signals *in situ*

The average signal intensity heatmaps representing the *in-situ* pattern of our microscopy images were acquired using an automated Fiji macro called “Cell Harvester”. All images were deconvolved and the acquisitions were compiled into their respective maximum z projections. The first part of the protocol uses the macro to identify and outline chloroplasts in bright field images. The outlined shape is then superimposed onto the corresponding fluorescent channel. The outlined chloroplasts within the acquisition are then cropped to individual files and, based on bright field images only, oriented manually to make horizontal their longitudinal axis with the anterior (lobes) on the left and the basal region (pyrenoid) on the right, as is shown in the figures. It should be noted that in isolated chloroplasts the lobes are seen as poorly resolved material connected to one side of the chloroplast whereas the pyrenoid marks the posterior/basal region. Each chloroplast image is subsequently saved in an output folder. All cropped and orientated chloroplasts within each output folder in the data set were compiled into a single folder. This library was inputted into the second part of the macro which compiled all given chloroplasts into an ‘average representative cell’, while ensuring that they all contributed equally to the average. X and Y values were assigned to make sure all chloroplasts in the data set are set to the same scale. The output file was displayed as a heatmap in Fiji.

2.2.8 High resolution electron tomography

Sections of 300 nm thickness from the resin-embedded cells above were collected on Formvar support slot grids and stained. The dual-axis tilt series were collected using the FEI Tecnai G2 F20 200 kV TEM equipped with a Gatan Ultrascan 4000 4k x 4k CCD Camera System Model 895 and a single tilt holder. Tilt series were then acquired at 2° increment from -60° to 60°, at 19000x magnification, 5.91 Å pixel size using SerialEM. For the second axis tilt series acquisition, the slot grid was rotated 90° manually and the same area of interest was searched manually. The dual-axis tomograms were reconstructed from the tilt series using IMOD software package (Kremer et al., 1996). The modelling and visualization of the membrane and cyto-ribosomes were done also by IMOD.

2.2.9 RiboPuromycylation and puromycin-release assays

For the RiboPuromycylation method, isolated chloroplasts (1×10^8 ml⁻¹ in isolation buffer were treated with 1.0 mM puromycin (Bioshop) for 10 min at RT and then IF-stained with a mouse monoclonal antibody against puromycin (DSHB Hybridoma Product PMY-2A4, deposited by J. Yewdell). The IF signal was specific (Supplemental Figure 2C). The puromycin-release assay followed protocols that were used to show ribosome association to ER, mitochondria and thylakoid membranes (Redman & Sabatini, 1966; Schottkowski et al., 2012). cc-400 cells (9×10^8) were pelleted by centrifugation at 3,000 x g, 5 min at RT. Cell density was adjusted with HSM containing 1.0% (w/v) sorbitol to 1.2×10^7 . Cells were treated with 10 µg·mL⁻¹ of cycloheximide for 10 min, then pelleted by centrifugation at 3,000 x g for 5 min at RT and resuspended in 9.0 ml of isolation buffer with 0.4% (w/v) saponin and 10 µg·mL⁻¹ of cycloheximide. Chloroplasts were

isolated as previously described (Mason et al., 2006) and resuspended with 1.0 ml isolation buffer (150 μ l), pelleted at 1,000 x g for 3 min at RT, resuspended with 1.0 mL of one of the following four conditions: 1) isolation buffer + 5 mM DTT, 2) isolation buffer + 5 mM DTT + 750 mM KCl, 3) isolation buffer+ 5 mM DTT+ 1 mM puromycin + 750 mM KCl and 4) isolation buffer + 5 mM DTT + 1 mM puromycin. Samples were incubated at RT for 20 min. Chloroplast were pelleted by centrifugation (1,000 x g for 3 min at RT) for immune-blot analyses. Results are from three concurrent biological replicate experiments (i.e. from independent cultures, Supplemental Figure 4).

2.2.10 Preparation of low-density membranes

Chlamydomonas reinhardtii cc-400 strains were cultured in Tris-Acetate-Phosphate medium (TAP) (Harris, 1989) supplemented with 1% (w/v) sorbitol under continuous white light (approximately 50 μ E \cdot m⁻² \cdot s⁻¹) at 24 °C with gentle stirring to 2.5x10⁶ - 5x10⁶ cells \cdot ml⁻¹. Sequential sucrose density gradients were used to fractionate membranes (Zerges and Rochaix, 1998). Chloroplasts were isolated as described above except that the concentration of saponin was 0.25% (w/v), and the cell lysate was subjected to four passages through a syringe with a rate of 0.5 ml/s⁻¹. Chloroplasts isolated from 2.5x10⁹ cells were osmotically lysed in 1.4 ml of +Mg²⁺ hypotonic buffer [10 mM Tricine, pH 7.8, 5 mM MgCl₂, 5 mM β -mercaptoethanol] containing protease inhibitor cocktail for plants (BioShop) by pipetting 50 times with a 1.0 ml pipette. Membranes were fractionated based on buoyant density by centrifugation at 100, 000 x g (in a Beckman SW41Ti rotor) for 16 h at 4 °C on a continuous (0.3-1.8 M) sucrose gradient [prepared in +Mg²⁺ hypotonic buffer]. The dark green band (representing the thylakoid membranes) was collected and diluted with 3 volumes of +Mg²⁺ hypotonic buffer. Membranes were concentrated by

centrifugation at 30,000 rpm for 2 h (SW41Ti). The resulting pellet was fully resuspended by pipetting with a 1.0 ml pipette followed with intense vortex (30s x 3) in 1.5 ml of $-Mg^{2+}$ hypotonic buffer [10 mM Tricine, pH 7.8, 10 mM EDTA] containing protease inhibitor cocktail for plants (BioShop). Membranes were fractionated based on buoyant density by centrifugation at 100, 000 X g for 16 h at 4 °C on a continuous (0.3-1.8 M) sucrose gradient [prepared in $-Mg^{2+}$ hypotonic buffer containing 5 mM β -mercaptoethanol]. The fractions were collected (800 – 1000 μ l each) from the top with a 1.0 ml pipette with the disposable tip with its end cut to make a bore size of 3 mm.

2.3 RESULTS

2.3.1 Cyto-ribosomes associate with a domain of the chloroplast envelope

To explore the possibility that translation is localized to the outer envelope membrane of the chloroplast in *Chlamydomonas*, we asked first whether cyto-ribosomes and chloroplasts copurify away from cyto-ribosomes that are free or bound to contaminating ER and mitochondria. The chloroplast fraction retained more cyto-ribosomes than can be explained by contamination by mitochondria and ER (Figure 2.1B). To determine whether these retained cyto-ribosomes were bound to the isolated chloroplasts, we imaged the ribosomal protein cyL4 by IF microscopy. In whole cells, the cyL4 IF signal was in a pattern consistent with the cytoplasm, with enriched signal near the chloroplast, as was reported previously (Figure 2.1D, Supplemental Figure 2.1A) (Uniacke & Zerges, 2009b). On isolated chloroplasts, cyL4 IF-signal was seen on the chloroplast envelope, which was co-IF-stained for the envelope marker protein LCIA (Yamano et al., 2015a). The cyL4 signal was dramatically enriched along the envelope specifically bordering the central

nuclear-cytosolic region (Figure 2.1A and C). This localization pattern can be seen in both a representative chloroplast and the average signal distribution in all chloroplasts of the data set (Figure 2.1C and D). This localized cyL4 IF signal on the chloroplast envelope was not from cyto-ribosomes on ER or mitochondria bound to the isolated chloroplasts because the localization pattern of cyL4 was not seen for marker proteins for these organelles (Supplemental Figure 2.2A and B). These results support associations of cyto-ribosomes with a domain of the chloroplast envelope which aligns with the T-zone within the chloroplast (Figure 2.1A).

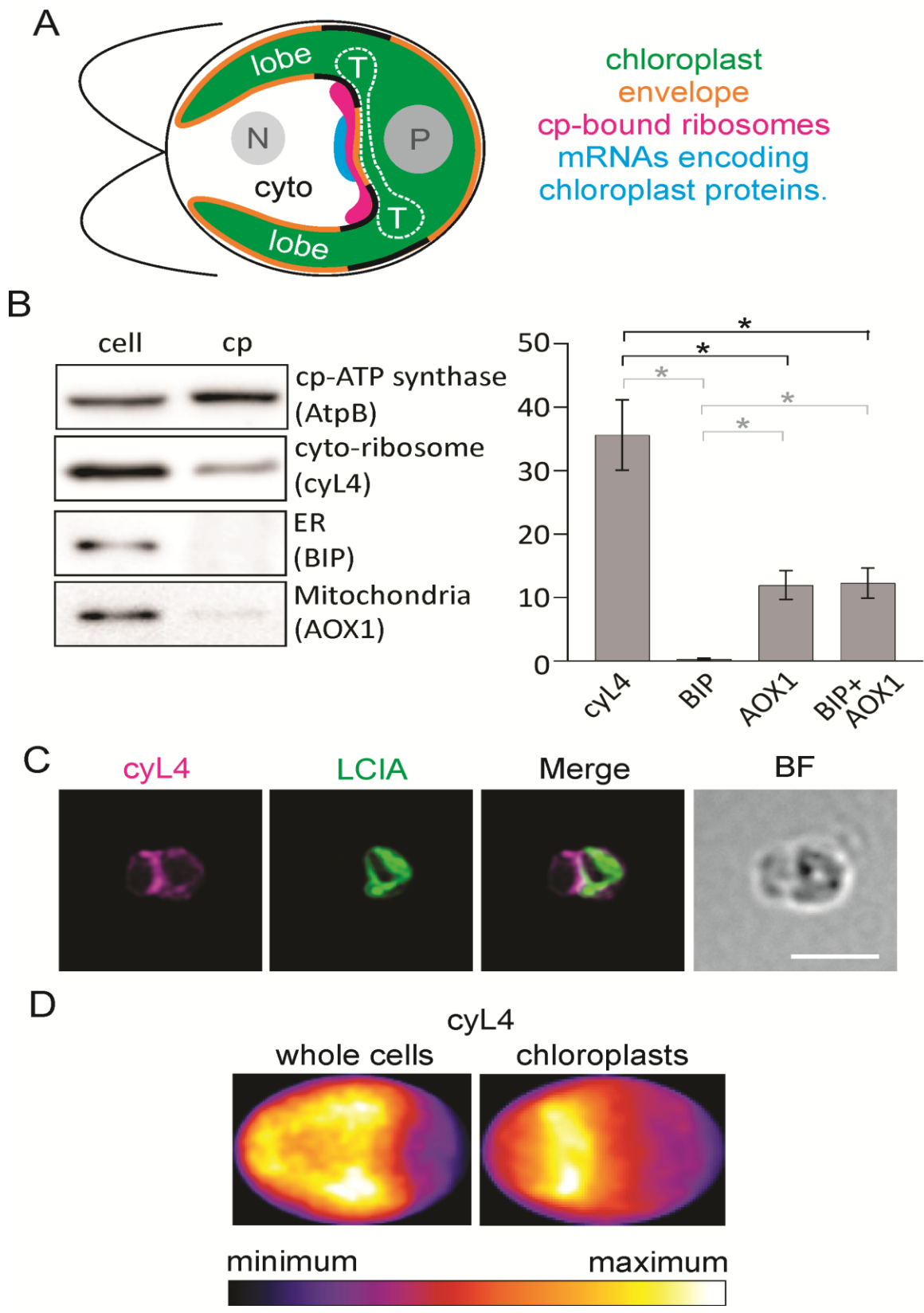


Figure 2.1. Cyto-ribosomes are bound to a domain of the chloroplast envelope.

(A) *Chlamydomonas* is used as a model organism for analyses of the cytological organization of chloroplastic processes because it has a single chloroplast with a stereotypic morphology and prominent cytological landmarks (A) (Uniacke, Colon-Ramos, et al., 2011). An illustration shows the cilia pair at the anterior cell pole, the nucleus (N), cytosol (cyto), and the chloroplast (green). The chloroplast (green) has lobes which enclose the nuclear-cytosolic region (cyto), the pyrenoid (P), the translation zone (T) and is surrounded by a dual membrane envelope (orange). The cyto-ribosome-bound domain of the envelope (magenta) includes the mRNA enriched region (cyan) and overlaps envelope domains enriched in the TOC/TIC protein import translocons (black)(Uniacke & Zerges, 2009b). (B) Results of immunoblot analyses of marker proteins in extracts of whole cells versus isolated chloroplasts reveal that cyto-ribosomes (cyL4) preferentially copurify with chloroplasts (AtpB) relative to cyto-ribosome-bound organelles; ER (BIP) and mitochondria (AOX1). (Immunoblot results represented by this graph are presented in Supplemental Figure 4. Error bars= 1.0 SEM, n=3 biological replicates from independent cultures). (C) IF-microscopy images of isolated chloroplasts show cyL4 localized to a domain of the chloroplast envelope, as seen relative to the envelope marker LCIA. The absence of LCIA signal from the lobes of the chloroplast does not reflect a change in chloroplast morphology during isolation (Supplemental Figure 3) (Mason et al., 2006a). (D) A heat map shows the average cyL4 IF signal of a maximal intensity projection from all cells or chloroplasts in these data sets (n= 32 chloroplasts, n= 102 cells). (BF, bright field; size bar, 5.0 μ m).

2.3.2 Cyto-ribosomes on the chloroplast envelope domain imaged by high-resolution electron tomography

The evidence cited against chloroplast-localized protein synthesis includes EM images of chloroplast envelope devoid of bound ribosomes and of chloroplasts of spinach leaves surrounded by a cyto-ribosome-free zone (Carde et al., 1982; Chepko et al., 1979; Chua & Schmidt, 1979). Therefore, to determine whether cyto-ribosomes can be seen on the chloroplast envelope, and to validate the cyL4 IF signal as a marker for them, we imaged cells with three-dimensional high-resolution electron tomography (Figure 2.2). We focused on the envelope domain that was seen to be enriched for cyto-ribosomes by IF microscopy (Figure 2.1C) in cells undergoing high rates of photosystem biogenesis (Sun et al., 2019). For reference, we imaged the envelope of chloroplast lobes, which did not strongly IF-stain for cyL4. The results show the presence of ribosome clusters on the chloroplast envelope domain where we observed the localized cyL4 IF signal (Compare Figures 2.1C and 2.2 C-F) (Supplemental Movie S2.1). Cyto-ribosome density was lower on other regions of the chloroplast envelope, e.g. of the chloroplast lobe (Figure 2.2F and G) (Supplemental Movie S2.2). This illustrates that, cyto-ribosomes are on the chloroplast envelope, thereby corroborating the results of IF microscopy.

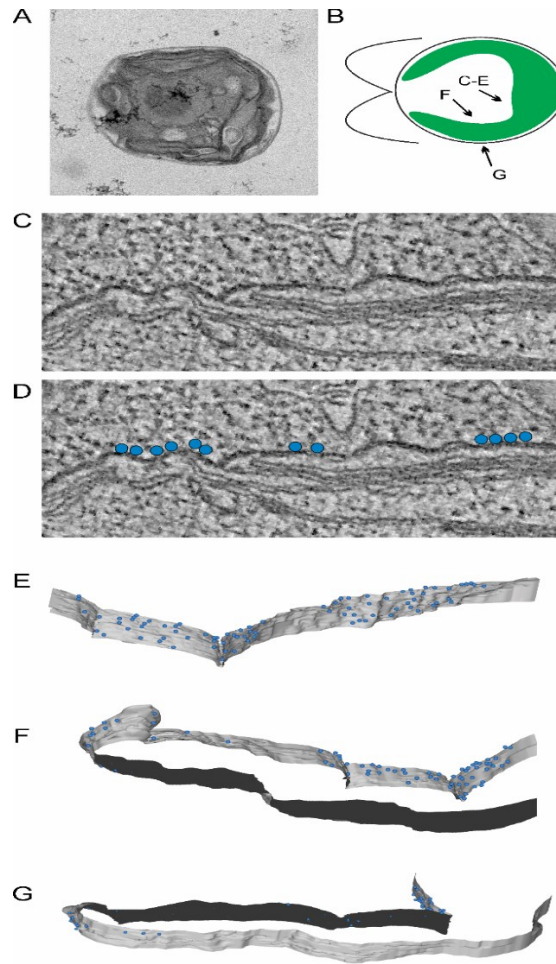


Fig. 2.2. Electron Tomography images show cyto-ribosomes on the chloroplast outer envelope membrane. (A) An EM image of the cell that was imaged. (B) The illustration shows the regions where the tomographs were acquired. (C) A tomographic slice showing the region of chloroplast envelope bound by cyto-ribosomes as seen by IF microscopy (Fig. 1C). (D) The image in C with the cyto-ribosomes on the envelope marked with blue spheres. Ribosomes were scored based on their distance from the envelope, with only those that were in close contact being selected. (E-G) Models of chloroplast envelope (grey, cytoplasmic face of the outer membrane; black, stromal face of the inner membrane) and bound cyto-ribosomes (blue dots) as seen from the angles shown in Panel B.

2.3.3 Chloroplast-bound cyto-ribosomes are active

We used two assays to determine whether the chloroplast-bound cyto-ribosomes are translationally active. The RiboPuromycylation method takes advantage of the conjugation of puromycin to the nascent polypeptide when it terminates translation and releases it from a ribosome. This method used the IF signal from puromycin-conjugated nascent polypeptides as a marker for locations of translation *in vivo* (Schmidt et al., 2009). Chloroplasts were isolated, treated with puromycin and then IF-stained with an antibody specific to puromycin (Schmidt et al., 2009). These chloroplasts showed the strongest IF-signal of puromycin-conjugated nascent polypeptides at the envelope domain that had the localized cyL4 IF-signal (Figure 2.3A). Localization of most of the puromycin signal to the cytoplasmic side of the chloroplast envelope (LCIA) demonstrates that these nascent polypeptides were from cyto-ribosomes and not chloro-ribosomes (Figure 2.3B). Moreover, this puromycin-nascent polypeptide localization pattern was consistently seen in the chloroplasts imaged, as revealed by the average puromycin IF signal distribution of maximal intensity projection of all chloroplasts in the data set (Figure 2.3C). These results support translational activity by the chloroplast-bound cyto-ribosomes *in vivo*.

The puromycin-release assay tests for organelle-localized translation by exploiting the specificity of puromycin for releasing translating ribosomes from their nascent polypeptides (Redman & Sabatini, 1966). Puromycin-induced cyto-ribosome release is evidence that the ribosomes were translating and tethered to the organelle by their nascent polypeptides that were undergoing cotranslational passage via the protein translocons in the organellar membrane (Gold et al., 2017a; Redman & Sabatini, 1966). In addition, ribosomes on the ER, mitochondria and thylakoid membranes required high-ionic strength (300-750 mM KCl) to be released, because they are bound to ribosome receptors on the organelle surface (Adelman et al., 1973; Chua et al., 1973;

Kellems et al., 1974). When chloroplasts were incubated in the high ionic strength condition (750 mM KCl), a significant proportion were released (32%, $p= 0.037$) (Figure 2.3D). Therefore, this proportion of retained cyto-ribosomes were bound to the chloroplast by non-covalent bonds alone. Treatments with both puromycin and high ionic strength released 49% of the ribosomes ($p= 0.012$), a significantly higher proportion (by 17%, $p= 0.023$) than were released during treatment with high ionic strength alone. Therefore, these cyto-ribosomes were bound to the chloroplasts by both non-covalent bonds and their nascent polypeptides. This result confirms that some of the chloroplast-bound cyto-ribosomes were translationally active *in vivo* and it reveals a dependency of these associations on tethering of cyto-ribosomes by their nascent polypeptides. This is considered evidence that nascent polypeptides undergo cotranslational import into an organelle (Adelman et al., 1973; Chua et al., 1973; Kellems et al., 1974). Moreover, the retention of the puromycin-conjugated nascent polypeptides by the chloroplast is consistent with their being anchored in the translocons for cotranslational import (Figure 2.3A-C). Finally, treatment of chloroplasts with puromycin alone did not release a significant proportion of their bound cyto-ribosomes ($p= 0.603$), revealing that few, if any, cyto-ribosomes were associated with the chloroplasts by nascent polypeptides alone. Together, these results reveal the chloroplast bound cyto-ribosomes are active and bound to the chloroplast by non-covalent bonds and tethering by their nascent polypeptides.

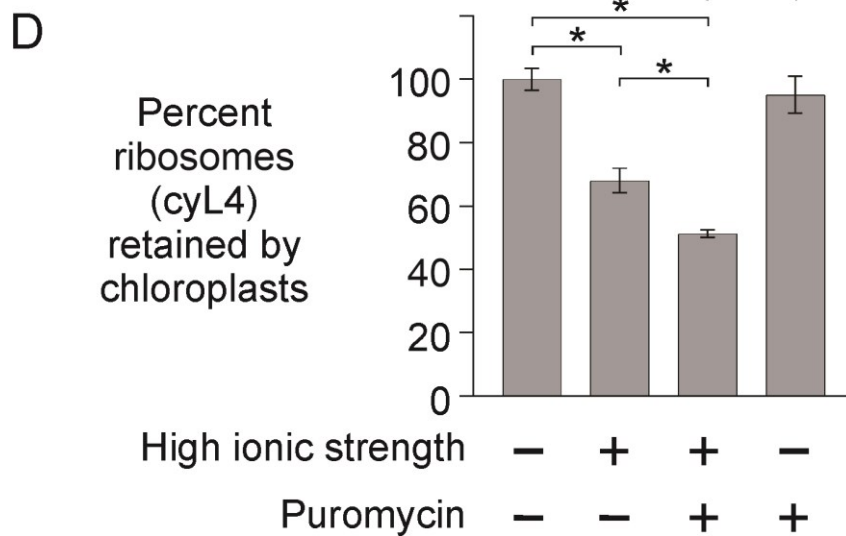
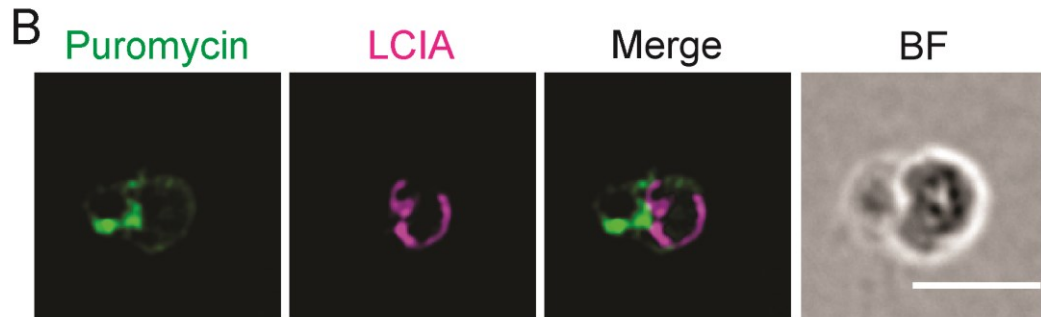
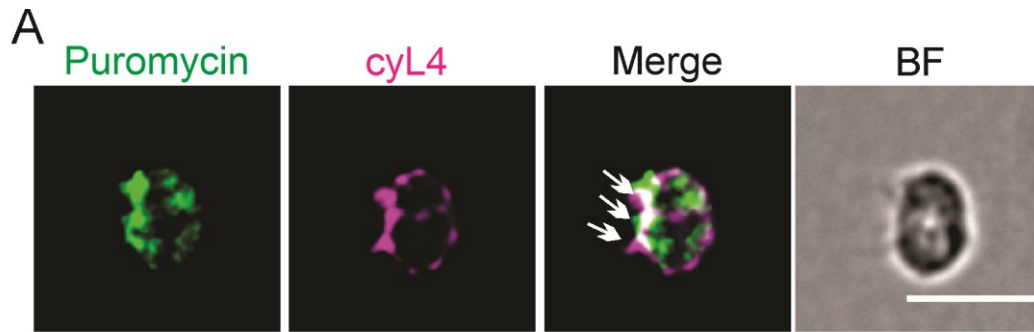


Fig. 2.3. The cyto-ribosomes on the chloroplast are translationally active and tethered by nascent polypeptides. (A and B) Results of the RiboPuromycylation method show IF signal of the puromycin-conjugated nascent polypeptides (green), as markers of translation, localized to (A) the cyto-ribosome (cyL4) IF signal (B) on the cytoplasmic side of the chloroplast envelope (LCIA) (size bar, 5.0 μm). Arrows indicate sites of colocalization of puromycin-conjugated nascent polypeptides and cyto-ribosomes. The green IF signal is specific to puromycin (Fig S2C). (C) A heat map of the average IF signal from the puromycin-conjugated nascent polypeptides from all chloroplasts in this data set ($n= 30$) shows that the individual chloroplasts are representative. (D) Bar heights indicate the average proportion of cyto-ribosomes (cyL4) retained by isolated chloroplasts following the treatments indicated. (Immunoblot results represented by this graph are presented in Fig S4.) High ionic strength was 750 mM KCl. (Error bars= 1.0 SEM, $n= 3$ biological replicates from independent cultures).

2.3.4 mRNAs encoding chloroplast proteins localize at the cyto-ribosomes on the chloroplast envelope

The results above support localized translation by chloroplast-bound cyto-ribosomes for protein import specifically into the T-zone within the chloroplast (Figure 1A). This predicts that the cyto-ribosome-bound domain of the chloroplast envelope is associated with mRNAs encoding chloroplast proteins, but not mRNAs encoding non-chloroplast proteins. We used FISH to test this prediction (Tsanov et al., 2016). The imported chloroplast proteins include subunits of the light-harvesting complexes (LHCs), which each have three hydrophobic transmembrane domains and are embedded in the membranes of photosynthetic thylakoid vesicles where they associate with PSI and PSII (Dall'Osto et al., 2015; Nelson & Ben-Shem, 2004). LHC subunits are candidates to be synthesized by chloroplast-bound cyto-ribosomes and undergo cotranslational import because most hydrophobic integral membrane proteins undergo cotranslational import, membrane insertion or both (Ott & Herrmann, 2010; Williams et al., 2014) and such hydrophobic proteins have propensity to aggregate in the cytoplasm which would hamper their import and could cause toxicity (Claros et al., 1995). Therefore, we asked whether chloroplasts retain mRNAs encoding LHCPs (Stauber et al., 2003, p.). Our FISH probe sequences are complementary to the mRNAs of *LHCBM2* (Cre12.g548400) and *LHCBM7* (Cre12.g548950), close paralogues in a large gene family encoding LHCPs (Table S1). The mRNAs detected by these probes are referred to collectively as “*LHCBM*” here. In cells, the *LHCBM* FISH signal was detected from the cytosol, where it was enriched near the chloroplast, as we reported previously (Figure 4E and Supplemental Figure 1B) (Uniacke & Zerges, 2009b). Chloroplasts retained 96% of average cellular signal, and individual chloroplasts showed localized signal closely adjacent to, but not overlapping, the chloroplast-localized cyL4 IF signal (Figure 2.4A and B). Consistency of this localization pattern across all chloroplasts imaged was seen in a display of the average *LHCBM* mRNA FISH signal

distribution (Figure 2.4E). While the cyto-ribosome-bound domain extends along the envelope between opposing lobes, the strongest average *LHCBM* mRNA FISH signal was localized at the center of this domain (contrast *cyL4* in Figure 2.1D versus *LHCBM* and *RBCS* in Figure 2.4E, illustrated in Figure 2.1A). These results reveal a physical association of *LHCBM* mRNAs with the cyto-ribosome-bound domain of the chloroplast envelope. We also used FISH to image the distributions of the cytoplasmic mRNAs encoding the small subunit of Rubisco, a chloroplast-localized Calvin-Benson cycle enzyme. The Rubisco small subunit is encoded by two highly similar paralogous nuclear genes, *RBCS1* and *RBCS2* (Cre02.g120100 and Cre02.g120150, respectively). We refer to their mRNAs collectively as “*RBCS*” because our FISH probes hybridize to both (Table S2.1). In cells, localization of the *RBCS* mRNAs in the cytosol was not evident in most images, as was reported previously (Supplemental Figure 2.1C) (Uniacke & Zerges, 2009). However, in a display of the average *RBCS* FISH signal from all cells imaged, localization was detected in the approximate location of the cyto-ribosome-bound domain of the chloroplast envelope (Figure 2.4E). Association of *RBCS* mRNAs with the chloroplast was revealed by our findings that free chloroplasts retained 80% of average cellular *RBCS* FISH signal and that individual chloroplasts showed localized signal adjacent to the *cyL4* IF signal primarily at the center of the cyto-ribosome-bound envelope domain, similar to the localization of the *LHCBM* mRNA FISH signal (Figure 2.4A and C). Display of the average *RBCS* FISH signal confirmed this localization and revealed that a greater proportion of the *RBCS* mRNA FISH signal was distributed around the entire basal (posterior) region of the chloroplast, compared to the highly localized *LHCBM* FISH signal (Figure 2.4E). These results support the translation of cytoplasmic mRNAs encoding chloroplast proteins by the cyto-ribosomes on the central region of the chloroplast envelope domain.

As a control for specificity of chloroplast localization by mRNAs encoding chloroplast proteins, we similarly analysed the FISH signal from the mRNA of *TUB2*, which encodes β 2-tubulin (Cre12.g549550) (Silflow & Rosenbaum, 1981). In cells, strong *TUB2* mRNA FISH signal was detected throughout the cytosol, as reported previously (Supplemental Figure 1D, Figure 4E) (Colon-Ramos et al., 2003). Chloroplasts retained only 2% of the cellular *TUB2* mRNA FISH signal (Figure 2.4A) and the residual *TUB2* FISH signal from chloroplasts was neither enriched at the cyto-ribosome-bound envelope domain nor did it overlap with the *cyL4* signal (Figure 2.4D and E). Moreover, *TUB2* mRNA FISH signal from chloroplasts was probably non-specific as it was in a pattern resembling that of the signal from a control FISH probe with a sequence which is not in the genome (Supplemental Figure 2.2D). Therefore, the *TUB2* mRNA pool is not translated by chloroplast-bound cyto-ribosomes. Together, these results support specificity of chloroplast-localized translation of mRNAs encoding chloroplast-localized proteins.

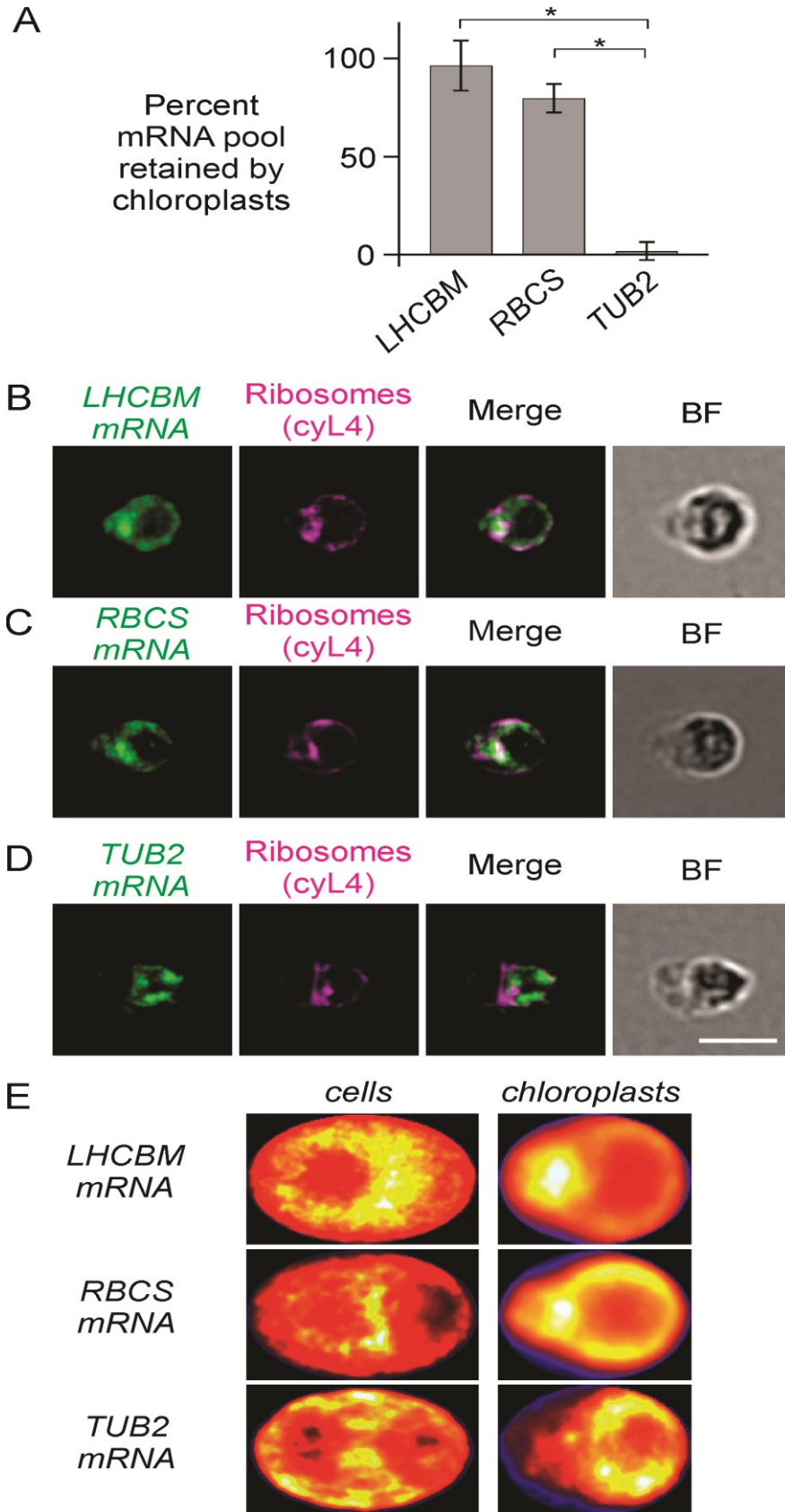


Fig. 2.4. FISH results reveal that mRNAs encoding specifically chloroplast-localized proteins are bound to isolated chloroplasts. (A) Bar heights represent percentages of the average FISH signal intensity from whole cells that were retained by chloroplasts for the mRNAs indicated. (Error bars= 1.0 SEM). (B-D) Chloroplasts IF-stained for cyto-ribosomes (cyL4) and FISH-probed for the mRNAs encoding chloroplast-localized proteins of (B) the *LHCBM* mRNAs or (C) the *RBCS* mRNAs. (D) Chloroplast FISH-probed for the *TUB2* mRNA as a control mRNA encoding a non-chloroplast protein. Size bar, 5.0 μm . (E) Heat maps show the distributions of the average FISH signals in maximal intensity projections of image stacks from all cells or chloroplasts in each data set ($n \geq 30$ cells or chloroplasts per data set).

2.3.5 Biochemical evidence of the import envelope domain

We used subcellular fractionation to obtain biochemical evidence of a domain of the chloroplast envelope that compartmentalizes translation by cytoplasmic ribosomes for chloroplast biogenesis. We predicted that such a membrane would be associated with 80S ribosomes and protein import translocons of the inner and outer chloroplast envelope, the TIC and TOC complexes, respectively. Enzymes in chlorophyll biosynthesis were also expected because newly synthesized chlorophyll and chlorophyll-binding apoprotein bind immediately and chlorophyll synthesis occurs in the T-zone of *Chlamydomonas* and at the envelope of plant chloroplasts (Czarnecki & Grimm, 2012; Joyard et al., 2009).

Previously, a membrane fraction was purified from the chloroplast of *Chlamydomonas* with features of a platform for translation of mRNAs encoded by the chloroplast genome (Zerges et al., 2002; Zerges & Rochaix, 1998). This membrane was called “low density membrane” (LDM) because it has a lower buoyant density than thylakoid membranes. LDM was shown to be similar to the inner membrane of the chloroplast envelope in pigment and membrane lipid compositions and to be associated with light-activated RNA-binding proteins (Zerges & Rochaix, 1998). To determine whether the LDM could be the microdomain of the chloroplast envelope that compartmentalizes translation by cytoplasmic ribosomes, we isolated it and characterized its profile using immunoblot analysis.

LDM was prepared from isolated chloroplasts collected as a yellow-green band from sucrose density gradients (Fig 2.5 A, fraction F2) and compared to purified thylakoid membranes from another culture, by immunoblot analyses (Fig 2.5 B, fraction F7). Fraction F2 was found to be enriched in cyL4, suggesting the presence of cyto-ribosome large subunits. It also had marker proteins for the import apparatus, TOC 159G, TIC 110, TOC 75. F2 also had the chloroplast

translation factor RBP40 and the chlorophyll marker POR. This membrane is not a thylakoid membrane because it did not have detectable levels of two abundant thylakoid membrane proteins PsaA and PsbA (Fig 2.5 C). The protein composition of F2 differed substantially from that of thylakoid membranes based on SDS-PAGE and silver staining (Fig 2.5 D). This suggests that LDM could be derived from the envelope domain that compartmentalizes translation by cytoplasmic ribosomes for chloroplast biogenesis and translation by the bacterial-type ribosomes of the chloroplast in the T-zone. Additional work is required to explore this possibility.

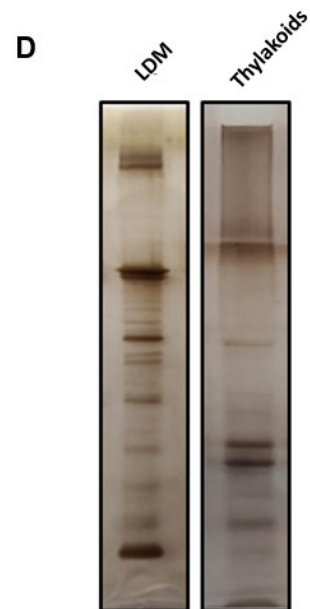
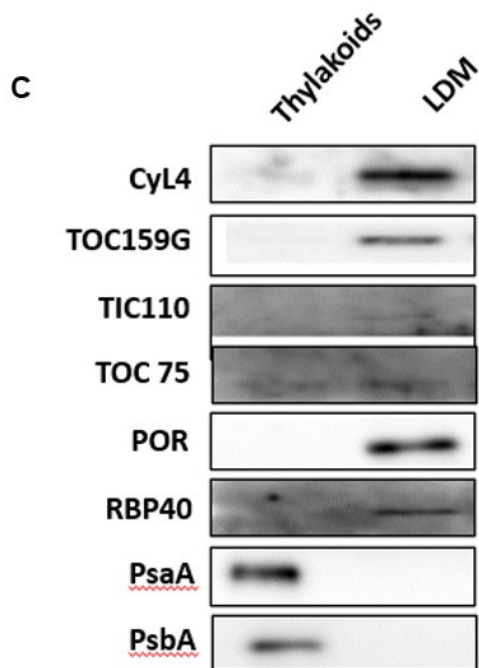
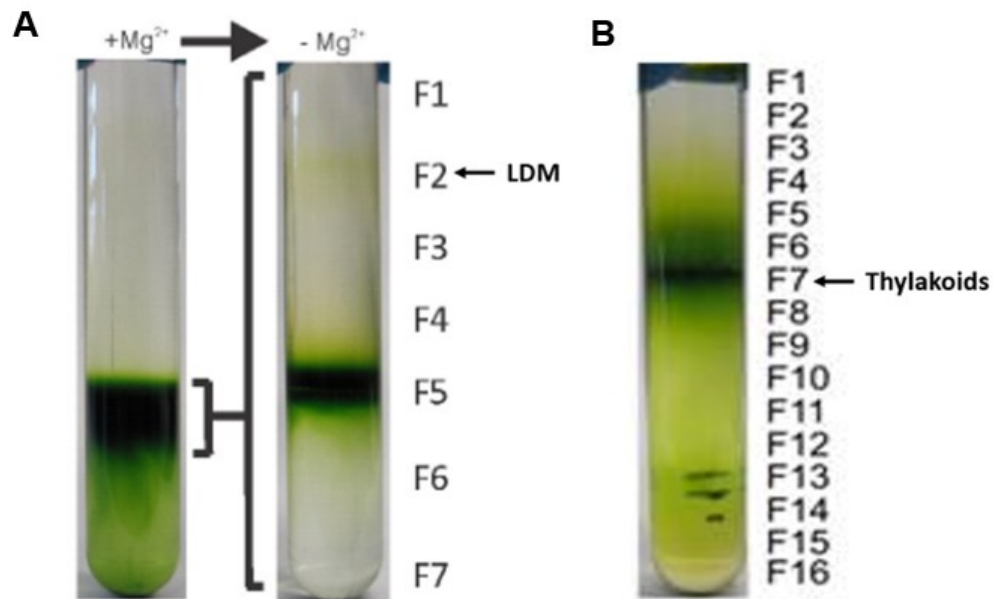


Fig 2.5. Isolation and analyses of low-density membrane.

A) Membranes from purified and fragmented chloroplasts were fractionated according to buoyant density by isopycnic sucrose gradient ultracentrifugation. The first gradient (left) fractionated membranes in the presence of Mg^{2+} ions. The dark green band was collected and fractionated on a second gradient lacking Mg^{2+} . Fraction F2 was collected as low-density membrane. B) Membranes from fragmented cells were fractionated according to their buoyant density. The dark green band in fraction F7 was collected as purified thylakoid membranes. C) Immunoblot analysis comparing fraction F2 (LDM) from the gradient on the right in panel A and fraction F7 (thylakoids) from the gradient in panel B. Marker proteins include cytoplasmic ribosome (cyL4), subunits of the chloroplast outer and inner translocon (TOC 159G, TOC 75 and TIC 110), an enzyme in the chlorophyll branch of the tetrapyrrole biosynthesis pathway, protochlorophyllide oxidoreductase (POR), a translation factor in the chloroplast (RBP40), and subunits of PSI and PSII (PsaA and PsbA, respectively). Lanes were loaded according to equal protein of each fraction to reveal the distributions of each protein across the gradient. D) Silver staining of F2 and F7 fractions described above differed substantially in terms of protein composition.

2.4 DISCUSSION

Our results reveal that the translation of mRNAs encoding chloroplast proteins is localized to the chloroplast envelope in *Chlamydomonas*. This discovery revises the long-standing model that all chloroplast proteins are synthesized throughout the cytoplasm (Weis et al., 2013). In addition, the dependency of cyto-ribosome-chloroplast associations on ribosome-nascent polypeptide connectivity supports co-translational import of chloroplast proteins (Fig. 2.3D). In this mechanism, the emerging nascent polypeptide is engaged by the TOC/TIC protein translocons in the chloroplast envelope during its co-translational import, thereby tethering the cyto-ribosome to the chloroplast. Translation localization at the ER and mitochondria also involves cyto-ribosome receptors on the organellar surfaces. These receptors were revealed by requirements for high ionic strength for ribosome dissociation from these organelles *in vitro* (Bykov et al., 2020; Chua et al., 1973; Kiebler et al., 1990; Lesnik et al., 2015). The possibility that cyto-ribosomes bind to receptors on the chloroplast surface is indicated by our finding that high ionic strength is required to dissociate approximately 50% of them (Fig. 2.3D).

Results reported here and previously reveal that chloroplast protein synthesis and targeting is spatially organized in a fashion analogous to the organization of the cytoplasmic and organellar translation systems for mitochondrial protein synthesis in *Saccharomyces cerevisiae* and humans (Gehrke et al., 2015; Matsumoto et al., 2012; Stoldt et al., 2018; Vogel, Bornhovd, et al., 2006; Zorkau et al., 2021). Mito-ribosomes synthesize subunits of the complexes of the respiratory electron transport system and ATP synthase directly into the inner membrane that form the invaginations called cristae (Vogel, Bornhovd, et al., 2006; Watson, 1972; Zorkau et al., 2021). The sites where the inner membrane invaginates to form cristae, cristae junctions, are preferential sites of the early steps of complex assembly and translation of these subunits (Vogel, Bornhovd, et al.,

2006; Watson, 1972; Zorkau et al., 2021). Hence, cristae junctions are analogous to the T-zone of the chloroplast (Sun et al., 2019). Similarly, the chloroplast envelope domain bound by translating cyto-ribosomes is analogous to clusters of cyto-ribosomes that translate on the mitochondrial outer membrane at cristae junctions (Garcia et al., 2007; Gold et al., 2017; Stoldt et al., 2018). The protein import translocons in the mitochondrial membranes are also localized at cristae junctions, analogous to the import envelope domains in the chloroplast envelope at the cyto-ribosome-bound envelope domain (Gold et al., 2017; Schottkowski et al., 2012; Vogel, Bornhovd, et al., 2006). Therefore, spatial coordination of translation on and within each of the semiautonomous organelles might be a fundamental aspect of the biogenesis of their electron transport complexes. Co-translational import of mitochondrial proteins to cristae junctions is hypothesized to facilitate their integration into the inner membrane and assembly with the locally synthesized protein products of mito-ribosomes (Formosa & Ryan, 2018; Fox, 2012; Grevel et al., 2020; Lesnik et al., 2015). Similarly, we hypothesize that LHCPs, and likely other chloroplast proteins, are synthesized at the cyto-ribosome-bound domain of the chloroplast envelope and undergo co-translational import into the T-zone to facilitate their insertion into developing thylakoid membranes and assembly with subunits synthesized by chloro-ribosomes. In this scenario, the homologues of the chloroplast SRP system, cpSRP43 and cpSRP54, engage the nascent polypeptide as it emerges from the TIC translocon and direct it to the translocon for co-translational insertion into developing thylakoid membranes in the T-zone, thereby obviating the widely accepted and exceptional post-translational roles of the chloroplast SRP system.

CHAPTER 3: SPATIAL ORGANIZATION OF THE CALVIN BENSON CYCLE IN *CHLAMYDOMONAS REINHARDTII*

ABSTRACT

Compartmentalization is an important aspect of cellular processes because it can enhance their efficiency and prevent deleterious side reactions. For example, organelles compartmentalize many metabolic pathways (Kerfeld et al., 2018). Within organelles there is a more fine-scale localization to regions called microcompartments or zones (Shimizu, 2019). This chapter describes novel findings regarding the compartmentalization of the Calvin-Benson cycle, the metabolic pathway that is responsible for CO₂ assimilation and primary carbohydrate production in photosynthesis. This pathway occurs within chloroplasts in plants and algae. Within the chloroplast of the unicellular alga *Chlamydomonas*, a microcompartment in the chloroplast, called the pyrenoid is widely accepted as the primary location of CO₂ fixation. This is because the pyrenoid contains most of the Rubisco in the cell, an enzyme that is responsible for the carbon assimilation step in the Calvin Benson Cycle. Here, we used fluorescence microscopy to reveal the spatiotemporal organization of the enzymes and related proteins in this pathway. Our results reveal a compartment in a specific part of the chloroplast, which is distinct from the pyrenoid. This compartment may have a role in the Calvin Benson Cycle, especially during the early-mid light phase of the diel cycle.

3.1 INTRODUCTION

A key challenge faced by all organisms, is the organization of the many reactions of cellular metabolism. If carried out in a single environment, many of these reactions would result in inefficient pathways or unwanted by-products (Goodman et al., 2018). In eukaryotic cells, the cytoplasmic space is compartmentalized by organelles. Organelles are further partitioned into microcompartments that separate metabolic pools and enzymes (Kerfeld et al., 2018; Shimizu, 2019). This creates elevated concentration of substrates and enzymes in one region with set thermodynamic parameters that favor the forward reactions (Flechsler et al., 2021; Zecchin et al., 2015). It can also allow for intermediates to be channeled between enzymes in a pathway while preventing the enzymes from working on inappropriate substrates (Flechsler et al., 2021; Goodman et al., 2018).

Chloroplasts are organelles found in plants and green alga. They are the developmental fate of the plastids in green tissues of the leaves and stems (Cooper, 2000; Sakamoto et al., 2008). Chloroplasts have many essential functions; in addition to their well-known role in photosynthesis, they synthesize lipids and amino acids for the cell (Barajas-López et al., 2013). Chloroplasts photosynthesize carbohydrates by using the CO₂ in the atmosphere, the electrons generated from the oxidation of water and the energy from light (Armbruster & Strand, 2020). Photosynthesis involves two major pathways, which occur in specific intra-chloroplast compartments. Light-dependent photosynthetic electron transport generates NADPH and an electrochemical proton gradient with three complexes embedded in the membranes of flattened vesicles called thylakoids within chloroplasts (Alberts et al., 2002; Wollman et al., 1999). These reactions use electrons from the oxidation of water and generate O₂ as a byproduct. They also transduce light energy to generate reducing equivalents in the form of NADPH and an electrochemical proton gradient across

thylakoid membranes, which is used to synthesize ATP by the ATP synthase (Alberts et al., 2002; Edwards et al., 2001).

The second phase of photosynthesis, the Calvin Benson Cycle, uses the NADPH generated by the light-dependent photosynthetic electron transport system and the ATP synthesized by ATP synthase to fix carbon dioxide and convert it to carbohydrates (Gurrieri et al., 2021). This cycle involves thirteen reactions that are catalyzed by eleven different enzymes. A key enzyme in this pathway is Rubisco (Cummins, 2021; Goudet et al., 2020). It adds carbon dioxide (CO_2) to a 5-carbon CO_2 acceptor molecule called ribulose-1,5-bisphosphate (RuBP). This results in the production of two 3-carbon molecules called 3-phosphoglycerate (3PGA) (Heldt & Piechulla, 2011; Raines, 2003). 3PGA is metabolized in the Calvin Benson Cycle to either regenerate RuBP or it is exported as triose phosphate which is used for the biosynthesis of sugars (glucose, fructose, sucrose) and most other organic compounds that make up a plant (Heldt & Piechulla, 2011; Raines, 2003).

Rubisco can catalyze the addition of both CO_2 and O_2 to ribulose-1,5-bisphosphate. The latter is called oxygenation (Busch, 2020; Heldt & Piechulla, 2011; Keller, 2010). A low CO_2 : high O_2 ratio inhibits the carboxylase activity of Rubisco and catalyzes its oxygenation reaction instead. This results in the production of a 2-carbon molecule called 2-phosphoglycolate (2-PG) which is a potent inhibitor of several enzymes and is metabolized through photorespiration (Busch, 2020; Eisenhut et al., 2019). Photorespiration is considered a wasteful process because it works in the opposite direction of photosynthesis; competing for ATP and NADPH and results in a loss of carbon that could otherwise be used for sugar production (Eisenhut et al., 2019; Keller, 2010).

To enhance the carboxylation activity of Rubisco, many photosynthetic organisms have developed a carbon concentrating mechanism to increase the concentration of CO_2 in the vicinity

of Rubisco (Cummins, 2021; Goudet et al., 2020). For example, C4 plants such as corn, maize and sugarcane, partition the initial CO₂ fixation step and the Calvin Benson Cycle between different cell types (mesophyll and bundle sheath cells) (Edwards et al., 2001). Crassulacean Acid Metabolism plants such as cactus and orchids, separate these steps temporally, between night and day (Bräutigam et al., 2017; Keeley & Rundel, 2003).

In *Chlamydomonas*, Rubisco inefficiency is compounded by several additional factors. Living in aquatic ecosystems, these organisms often have limiting CO₂, because the diffusion rate of CO₂ is 10,000 times slower in water than in air (Goudet et al., 2020; Hagemann et al., 2016). Also, most CO₂ in water, which is near pH 7, is converted to HCO₃⁻, which cannot cross membranes and enter cells or organelles by simple diffusion (Fei et al., 2021; Goudet et al., 2020; Yamano et al., 2015). To overcome these factors, *Chlamydomonas* has developed a biophysical carbon concentrating mechanism. This involves three key elements: 1) HCO₃⁻ transporters at the plasma membrane and chloroplast envelope, 2) carbonic anhydrases (CA) which convert the imported HCO₃⁻ in the cell to CO₂ and 3) the pyrenoid, a microcompartment in the basal region of the chloroplast that contains most of the cellular pool of Rubisco (Giordano et al., 2005; Jungnick et al., 2014).

Considering the generation of O₂ in the chloroplast by photosystem II (Sun et al., 2019; Uniacke & Zerges, 2007), we asked what this could mean for the localization of Rubisco and other Calvin Benson Cycle enzymes in *Chlamydomonas*. In the current model, aside from Rubisco, the ten remaining enzymes in this pathway are assumed to be in other parts of the chloroplast, and not the pyrenoid (Zhan et al., 2018). However, their precise location is less known. Using Venus-fusion constructs, a recent publication aimed to localize some of these proteins (Küken et al., 2018). However, although fluorescent protein tagging is a good method for analyzing dynamic

behaviours, it may not be ideal for determining intraorganellar location in chloroplasts. It is known that a protein tag might alter the structure of the target protein, and cause loss or alteration of its function (Toya et al., 2010). Also, the overexpression of the tagged protein may affect its localization (Iwai et al., 2016; Toya et al., 2010). However, the key disadvantage of using fluorescent protein tags for localization studies in the chloroplast, is the chlorophyll, the green pigment that is found in plants and green algae. Chlorophyll itself has autofluorescence and this may mask subtle localization patterns (Iwai et al., 2016). For this reason, immunofluorescence microscopy, which uses fluorescently labeled antibodies might be a better choice for localizing proteins in this organelle. Although this technique has its own downfalls such as the possibility of cross reactivity, this can be overcome by using proper controls such as deletion mutants to check for specificity. The upside however is that immunofluorescence microscopy is easier to carry out and often provides better spatial resolution (Toya et al., 2010; Vitha & Osteryoung, 2011). Furthermore, it is difficult to control the conditions of Live cell imaging of tagged proteins. For example, any localization pattern that requires specific conditions (CO_2 concentration, light), may not be maintained, while this can be easily achieved with immunolocalization techniques.

Here, we used immunofluorescence microscopy to localize enzymes and related proteins involved in the Calvin Benson Cycle. We did this under two conditions; atmospheric CO_2 concentration versus high CO_2 , where the CCM is active or inactive, respectively. We additionally explored the spatial-temporal distribution of these components using homogenous cell populations from cultures synchronized to the diel cycle (12hr:12hr light-dark cycle). This allowed us to look at specific stages of the light phase and focus on the time points when photosynthesis is maximal, unlike studies that focus only on the dark to light transition (Mitchell et al., 2014; Strenkert et al., 2019). Our results reveal a compartment in a specific part of the chloroplast, that

is distinct from the pyrenoid. This compartment may have a role in the Calvin Benson Cycle, especially during the early-mid light phase of the diel cycle.

3.2 MATERIALS AND METHODS

3.2.1 Culture conditions

Cultures of *Chlamydomonas* wild-type strain cc-125 were grown in high-salt minimal (HSM) medium and either aerated with air (for ambient CO₂ conditions), or with air enriched to 0.5 to 1% CO₂ (for high CO₂ conditions) at a flow rate of 300 to 400 ml.min⁻¹. Cultures were illuminated from the four sides and bottom by five banks of red and blue LEDs at 250 to 280 μE m⁻² s⁻¹ at 23 °C in the day and 27 °C at night. Cultures were entrained under alternating cycles of 12 h of light:12 h of dark for 2 to 3 consecutive days until they reached a density of 1×10⁶ to 2×10⁶ cells/ml. For the subsequent days, cultures were diluted into fresh HSM medium between ZT1 and ZT3 (1 and 3 hours into the light phase), thereby reducing the cell density to 1×10⁵ to 2×10⁵ cells.ml⁻¹ each day to allow for better cell synchronization. This daily dilution was carried out for at least three days. Cultures were not diluted on the day of the experiment when samples were collected at different experimental time points for either immunoblot analysis or for immunofluorescence microscopy. ZT0 (transition from dark to light) and ZT12 (transition from light to dark) cells were collected ~3 min before the respective transition.

3.2.2 Immunofluorescence staining

Immunofluorescence staining was performed as described previously in Chapter 2 (Uniacke, Colón-Ramos, et al., 2011; Uniacke & Zerges, 2007a). The primary antibodies and the dilutions used were as follows: α PRK, α FBP, α PGK, α RPE, α RPI, α SBP and α TKI (all at 1:2000) from Stéphane D Lemaire, French National Centre for Scientific Research, α RbcL (1:500) and α LCIA (1:700). Fluorescent secondary antibody used was AlexaFluor568 and AlexaFluor488 conjugated to goat anti-rabbit IgG (Thermo Fisher Scientific).

3.2.3 Probe design and preparation

Complementary 31 nt probes were designed for the *psbA* mRNA using Benchling (benchling.com). All probe sequences are provided in Table 3.1 (supplementary data). The following sequence was added to the 5' end of each 31 nt probe: CCTCCTAAGTTTCGAGCTGGACTCAGTG. This is the reverse complement of the X FLAP sequence used in Tsanov et al. (Tsanov et al., 2016a). Oligos were ordered from Integrated DNA Technologies (IDT), in lyophilized format, using 25 nmol synthesis scale, standard desalting. Each probe was resuspended in the appropriate volume of TE buffer to give a final concentration of 100 μ M. A standard volume of each probe was combined to generate an equimolar probe mix, at 20 μ M (mixed probe concentration). The X FLAP sequence itself CACTGAGTCCAGCTCGAACTTAGGAGG was dual 5' and 3' end labelled with Cy3. The equimolar probe mix was annealed to the fluorophore-labelled FLAP sequence in a heat block according to Tsanov et al. Annealed probes were stored at -20 °C.

3.2.4 FISH

Slides were first boiled in 1.0 N HCL for 15 min to reduce autofluorescence and left overnight to air-dry. A 10 μ l drop of 0.1% Poly-L-lysine (Sigma) was dispensed at one end of the slide and smeared across using another slide. The Poly-L-lysine coated slides were kept in a slide rack covered with aluminum foil and left to dry for three to seven days. On the day of the experiment, approximately 1×10^6 cells were aliquoted onto the center of the Poly-L-lysine coated microscope slide. Cells were allowed to adhere to the slide for c.a. 5 min. Cell fixation was performed using 4% paraformaldehyde (w/v) freshly diluted in 1X PBS (phosphate buffered saline) for 10 minutes. The slides were incubated twice, 10 minutes each, in methanol at -20°C . The next steps were performed on an orbital shaker at low speed. The slides were washed twice, 10 minutes each in PBS-Mg at room temperature. Permeabilization was done by incubating the slides in freshly prepared 2.0% (v/v) Triton X-100 in 1X PBS for 10 minutes. This was followed by two 10 minutes washes in 1X PBS-Mg at room temperature and a 20-minute wash in 15% formamide freshly prepared in 1X SSC (3 M NaCl and 300 mM Sodium Citrate adjusted to pH 7.0 with HCl). The hybridization mix was made according to Tsanov et al. except for the BSA concentration which was 4.5 mg/ml in the hybridization mix. A 50 μ l aliquot of the hybridization mix was placed on a cover slip. Each slide was gently blotted with a kimwipe and placed cell side down onto the hybridization solution on the coverslip. The slides were incubated overnight at 37°C in a slide hybridization oven. A piece of moist paper towel was included to maintain humidity. Post hybridization buffer containing $1\times$ SSC, 15% formamide was made fresh the next day. Slides were incubated in post hybridization buffer twice for 30 minutes each at 37°C . The slides were then washed twice, 10 minutes each, with $1\times$ PBS-Mg at room temperature. Slides were blotted dry with a KimWipe. 15 μ l of Anti-fade was added to the cell side of each slide. A coverslip was

placed on top of the Anti-fade reagent and sealed with nail polish. All solutions were made with diethyl pyrocarbonate (DEPC)-treated water.

3.2.5 Microscopy

Microscopy was carried out with a Leica DMI6000B inverted epifluorescence microscope with a 63x Plan Apo objective (NA 1.4) and further magnified by a 1.6x tube lens. Images were acquired on a Hamamatsu Orca R2 C10600-10B camera controlled by Volocity software (Improvision). Filters: Texas Red (562/40nm excitation: 624/40nm emission) for AlexaFluor568 and GFP (472/30nm excitation: 520/35nm emission) for AlexaFluor488. Acquired images were taken using Z plane stacks with a spacing of 0.2 μm per section; exposure settings, gain, and excitation intensity were kept constant where comparisons between intensities was required. For deconvolution, Z-stacks were taken by series capture at a thickness of 0.2 μm per section and were deconvoluted with AutoQuant X3 (Media Cybernetics Inc).

3.2.6 Image analysis of distributions of average fluorescence signals *in situ*

To display average signal distributions across all cell images, an automated Fiji macro called “Cell Harvester” developed by Dr. Christopher Law (Concordia Centre for Microscopy and Cell imaging) was used. All images from a data set were deconvolved and compiled into maximum z projections. The first part of the protocol uses the macro to identify the cells, based on a typical ellipse shape, and outlines each cell. The user should ensure that all incorrectly identified objects are removed at this point, any non-identified cells are manually added. The outlined cells within an acquisition are then cropped to individual files and oriented along their long axis, anterior

(lobes) on the left and the basal region (pyrenoid) on the right. Each cell image is subsequently saved in an output folder. All cropped and orientated cells within each output folder in the data set were compiled into a single folder. This library was inputted into the second part of the macro which compiled all given cells into an ‘average representative cell’, while ensuring that all cells contributed equally to the average. X and Y values were assigned to make sure all cells in the data set are set to the same scale. The output file was displayed as a heatmap in Fiji.

3.2.7 Immunoblot analysis

For the immunoblots of total protein, cells were collected at various ZT time points in the diel cycle. For each time point, an equal volume and number of cells were pelleted at 3000 xg for 5 min, at 4°C. Cell pellets were resuspended in SDS-PAGE loading buffer with 2-Mercaptoethanol (BME) and denatured at 65 °C for 45-min. Proteins were resolved on a 12% SDS-PAGE gel (Sambrook & Russell, 2006), transferred to PVDF membranes (Bio-Rad) overnight and reacted with primary and secondary antibodies diluted in 5% (w/v) dried skim milk. The primary antibody used in this study was α PRK 1:5,000 (from Dr. Stéphane Lemaire). The secondary antibody was horseradish peroxidase-conjugated goat anti-rabbit IgG antibody (KPL). Signals were detected using an ECL substrate (Thermo Fisher Scientific) with an Amersham Imager 600 (GE) according to the manufacturer’s protocol.

3.2.8 Subcellular fractionation

Membrane fractionation was performed as described previously (Schottkowski et al., 2012), with minor modifications. At each time point, 1.3×10^9 cells were harvested by centrifugation at 1,600 x g for 10 min at 4 °C. The resulting pellet was resuspended in MKT-buffer [25 mM MgCl₂, 20

mM KCl, 10 mM Tricine-KOH pH 7.5, protease inhibitor cocktail for plants (BioShop)]. Cells were broken by four passes through an ice-chilled French Pressure Cell at 1,000 psi. Efficient cell breakage was confirmed by light microscopy. The lysate was subjected to ultracentrifugation at 100,000 x g for 1 h at 4°C. The pellet was resuspended in 2 ml of 2.4 M sucrose. Upon resuspension, a 0.5 ml of 2.2 M sucrose cushion was added. A linear sucrose gradient (1.1-2 M) was then layered on top. All sucrose solutions were prepared in MKT-buffer. The gradient was subjected to ultracentrifugation at 100,000 x g (in a Beckman SW41Ti rotor) for 16 h at 4 °C. Fractions were collected from the top with a 1.0 ml micropipette with the disposable tip cut to make a bore size of 3 mm.

3.2.9 Transmission electron microscopy

Samples were collected from cultures entrained to the diel cycle and fixed in 2.5% (v/v) glutaraldehyde in 0.1M sodium cacodylate buffer containing 4% (w/v) sucrose, 0.1% (wt/v) CaCl₂ pH 7.4 and kept at 4 °C. Samples were processed as described previously (Elimam et al., 2016) by the McGill Faculty for Electron Microscopy Research (FEMR) staff in the following manner: Cells were washed three times with 0.1M sodium cacodylate for 1h, and incubated with 1% (v/v) aqueous osmium tetroxide + 1.5% (w/v) aqueous potassium ferrocyanide for 2h at 4 °C. The osmium tetroxide mixture was discarded, and samples were subjected to three washes with distilled water, each for 5 minutes. Samples were then dehydrated for 8-to-15 minutes using increasing concentrations of acetone (30%, 50%, 70%, 80%, 90% and 100%). The dehydrated samples were infiltrated with an Epon:Acetone mixture. This was done using three successive ratios as follows: an overnight treatment with a ratio of 1:1, a 24 hrs treatment with a ratio of 2:1 and an overnight treatment with a 3:1 ratio. Next, samples were incubated in 100% Epon for 4hr with no agitation, 2hr on a rotator and 2hr under a vacuum. Samples were then embedded in the

appropriate molds for 1hr under the fume hood. Samples were next embedded with Epon and polymerized in a 68 °C oven for 48 hrs. The final grids contained slices of cells that were on average 90-100 nm thin and stained with uranyl acetate and Reynold's lead.

Imaging was performed using an FEI Tecnai12, 120kv transmission electron microscope with Tecnai User Interface software and an AMTv601 CCD camera. Settings used were an aperture of 3, a spot size of 2, and variable magnifications ranging from 2900× to 68,000×.

3.3 RESULTS

3.3.1 Localization of Calvin-Benson Cycle enzymes in the chloroplast

To characterize the distributions of the Calvin Benson Cycle enzymes in the chloroplast, we used immunofluorescence microscopy. We first visualized the fluorescence signals from wild-type (cc-125) cells cultured under photoautotrophic conditions. These conditions were used in a previous study that looked at the localization of these enzymes using proteins tagged with the yellow fluorescence protein Venus (Küken et al., 2018). As expected, the Rubisco large subunit (RBCL) showed localization to the pyrenoid (Fig 3.1). However, and as was reported previously, the remaining Calvin Benson Cycle enzymes fructose-1,6-bisphosphate aldolase, phosphoglycerokinase, phosphoribulokinase, ribulose-phosphate epimerase, ribose-phosphate isomerase, sedoheptulose-1,7-bisphosphate aldolase and transketolase were not in the pyrenoid and showed a pattern consistent with the stroma. The stroma is the aqueous compartment of the chloroplast, located between the envelope and thylakoid membranes, and is analogous to the cytoplasm of a cell.

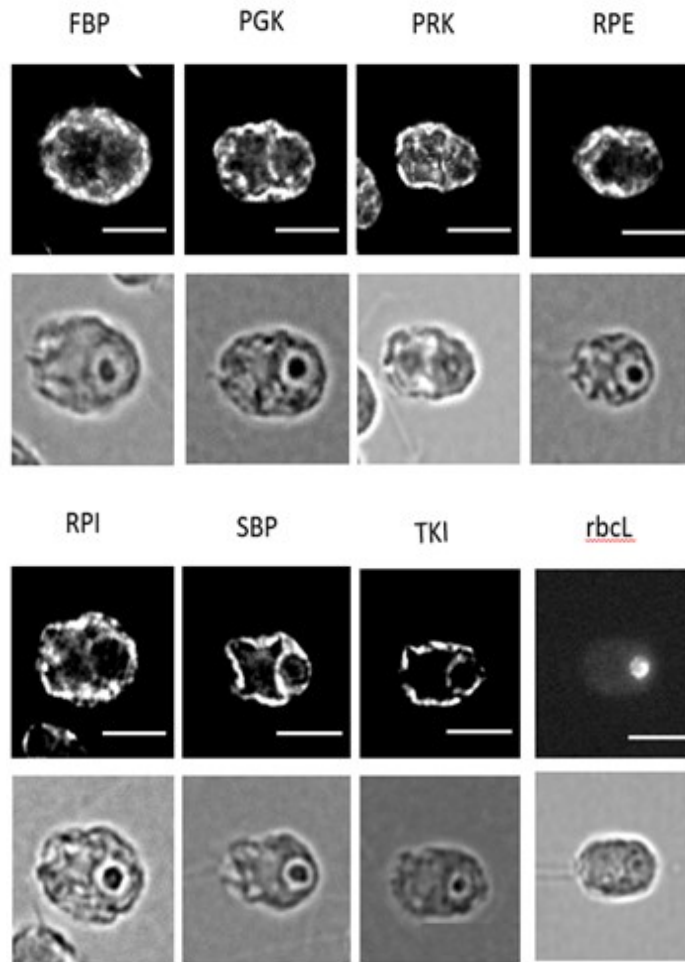


Fig 3.1. Distribution of Calvin Benson Cycle enzymes in the chloroplasts

Epifluorescence microscopy images reveal the distribution of various Calvin Benson Cycle enzymes. RBCL is enriched in the pyrenoid while the other enzymes are throughout the chloroplast except within the pyrenoid. Top rows show fluorescent channel and bottom row indicate the bright field. The white bar represents 5.0 μm . Protein names are as follows; (fructose-1,6-bisphosphate aldolase (FBP), phosphoglycerokinase (PGK), phosphoribulokinase (PRK), ribulose-phosphate epimerase (RPE), ribose-phosphate isomerase (RPI), sedoheptulose-1,7-bisphosphate aldolase (SBP) and transketolase (TKL)).

3.3.2 Re-localization of phosphoribulokinase during the light phase of the diel cycle

To examine the localization pattern in a homogenous population of cells for their stage in the diel cycle, we used cultures that were synchronized to a 12h:12h light-dark cycle (please refer to appendix 1 for evidence of culture synchrony under these conditions). Our lab and others have shown that there are stage-specific patterns of gene expression, metabolism and localization of chloroplast proteins and mRNAs (Mitchell et al., 2014; Strenkert et al., 2019; Sun et al., 2019a; Zones et al., 2015). Cells in the middle of the light phase are undergoing high rates of photosynthesis, which are not as prominent in asynchronous cultures, where many cells are undergoing mitosis (Zones et al., 2015). Therefore, if there is a predominant localization pattern at a particular diel cycle stage, we would be able to see it more clearly in synchronized cells.

To explore this, PRK was selected as the marker. Like Rubisco, this is only other enzyme known to function solely in the Calvin Benson Cycle (Kono et al., 2017; Rumpho et al., 2009). All other enzymes in this pathway, also carry out steps in other pathways and compartments which could contribute to their intracellular distributions (Rumpho et al., 2009).

Results from immunofluorescence microscopy revealed no evident localization of PRK in cells at the very beginning of the light phase (ZT0) (Fig 3.2 A). Between ZT2 and ZT4, most cells showed PRK signal localized to the chloroplast lobes. Most cells also displayed this signal in only one of the two chloroplast lobes. Later in the light phase, at ZT6, ZT8 and ZT10 time points, the PRK signal became more evenly distributed throughout the chloroplast. However, zero signal was detected from the pyrenoid (Fig 3.2 A). Therefore, comparison of results across all time points reveals that the level of PRK was increasing in the lobes.

To maintain objectivity, we quantified the average distributions of the PRK signal in the cells of each data set (i.e, cells from the same experimental culture) using a Fiji macro (Sun et al., 2019). The distribution of the average signal across all cells is displayed by a heatmap (Fig 3.2 B). The results reveal that there is some stage specificity for the localization of PRK to the chloroplast lobes. This pattern is more distinct at ZT4 when photosynthesis rates are high (Strenkert et al., 2019; Sun et al., 2019a). Upon further observation, it also became evident that the localization pattern is initially seen in one chloroplast lobe. To verify this with our Fiji macro, we manually orientated the cells so that the lobe with the stronger signal was facing the same direction (in this case, the upper lobe), and indeed the results generated by the macro confirmed this observation (Fig 3.2 B, ZT2 and ZT4 cells)

Additionally, immunoblot analysis was used to reveal temporal changes in the levels of PRK during the diel cycle. Samples were collected every hour, beginning at ZT22 (2 hours before the light phase) until ZT12 (end of the light phase). The results show an increase in the levels of PRK as the cells progress into the diel cycle, corroborating with our microscopy results Fig 3.2 C).

To check for specificity of the fluorescence signal of PRK, we did immunofluorescence staining on cells of a PRK deletion mutant. Results showed that our antibody staining was indeed specific as there was zero signal seen in cells from the mutant strain (Fig 3.2 D).

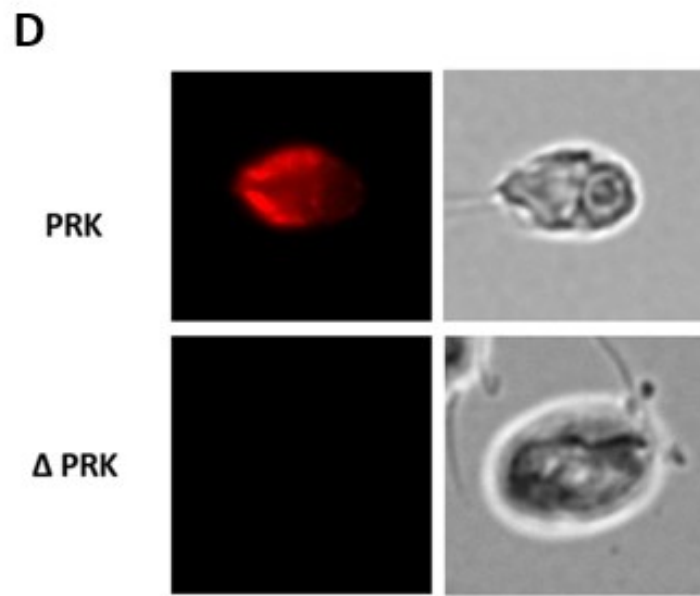
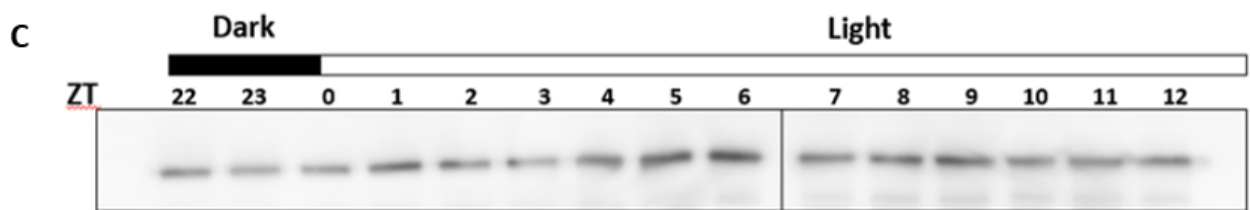
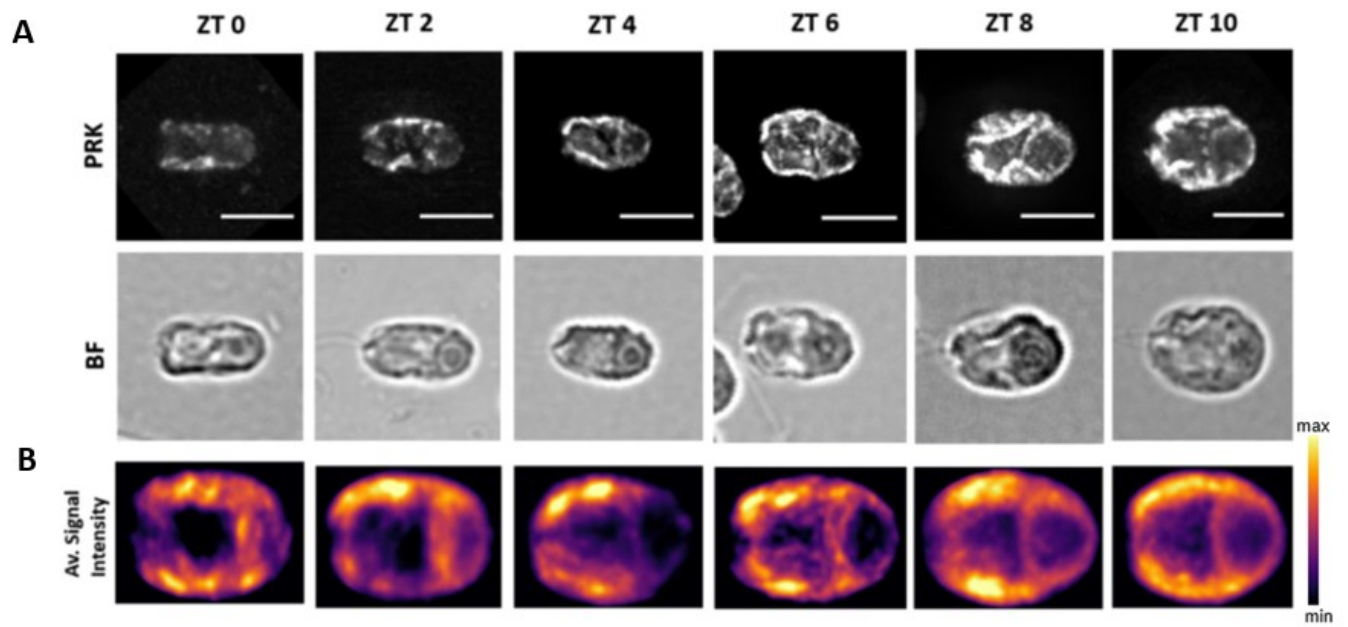


Fig 3.2. Growing chloroplasts during the light phase of the diel cycle show spatiotemporal patterning of PRK

A) Epifluorescence microscopy images reveal the distribution of PRK through the light phase of the diel cycle. PRK is enriched in the chloroplast lobes of ZT2 and ZT4 cells. B) Heatmaps show average signal intensities in a maximal intensity projection (MIP) of all cells in the data set for each time point ZT0, n=30; ZT2, n=42; ZT4, n=40; ZT6, n = 30; ZT8, n = 26; ZT10, n=20. Time course experiment was performed on cells from a single uniform culture. Scale bars indicate 5 μm . C) Results of immunoblot analyses of total protein samples from the ZT2- ZT12 time points of the diel cycle reveal the relative levels of PRK. D) Experimental control. Cells that were IF-stained for PRK (phosphoribulokinase) do not show a signal in the deletion mutant for the gene encoding it.

3.3.3 Localization of PRK across the diel cycle under 0.5% CO₂

To examine the effect of CO₂ on the distribution of PRK, wild-type cells were entrained to a 12hr:12hr light-dark cycle. These cultures were continuously aerated with 0.5% CO₂ during entrainment. Samples were taken and cells fixed for immunofluorescence staining at 2-hour intervals, from ZT0 to ZT12. Higher CO₂ levels are predicted to suppress the carbon concentrating mechanism which could in turn, affect the distribution of various enzymes in the Calvin Benson Cycle.

Immunofluorescence microscopy results showed that 0.5% CO₂ had a slight effect on the localization pattern. (Fig 3.3 A). Similar to the cultures that were grown under ambient CO₂, there was no evident localization at ZT0. However, a localized signal was visible in the chloroplast lobes at ZT2 and at ZT4. Later in the light phase, beginning at ZT6, the PRK signal increased throughout the chloroplast and became more evenly distributed. Once again, there was no staining in the pyrenoid. Because the 0.5% CO₂ treatment did not have much of an effect on the immunofluorescence pattern, it seems the critical factor determining localization is the phase of the diel cycle or some process occurring at that stage, for example high rates of photosynthesis.

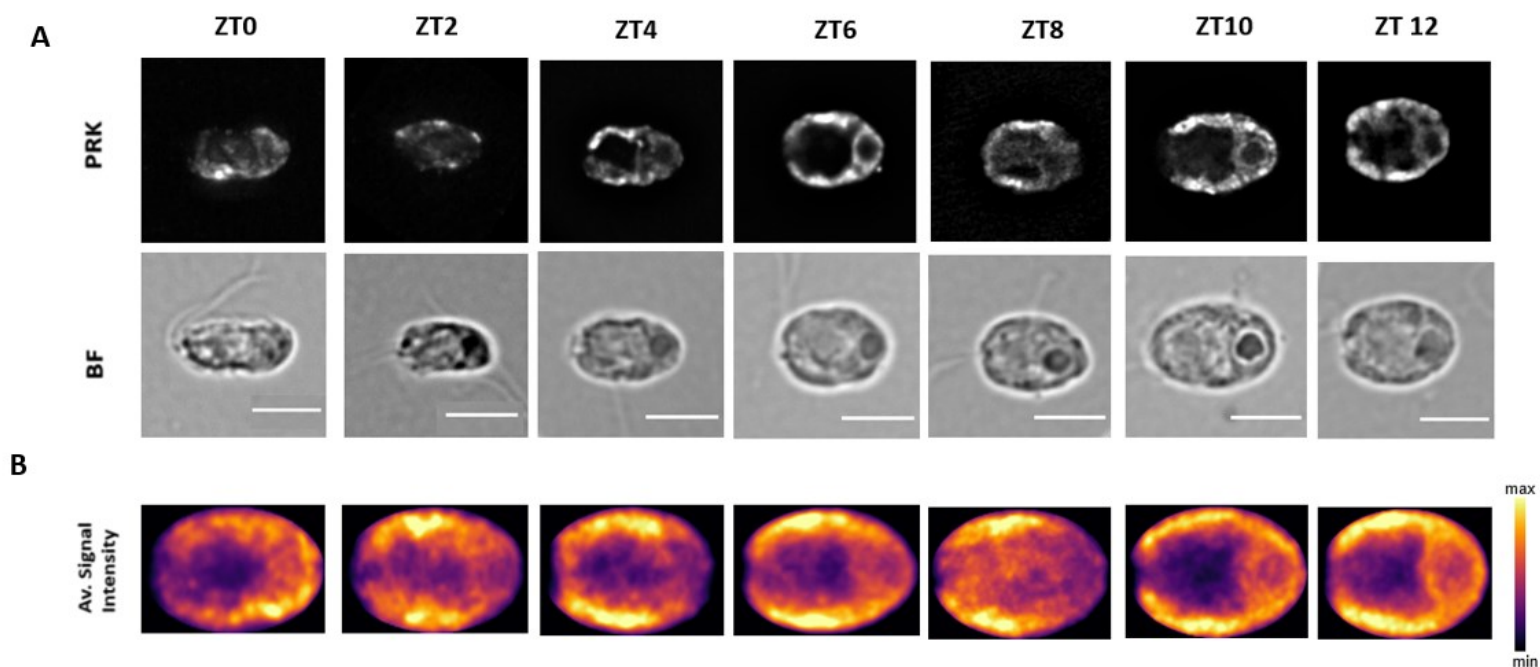


Fig 3.3. Spatiotemporal patterning of PRK in the light phase under 0.5% CO₂

A) Epifluorescence microscopy images reveal the distribution of PRK through the light phase of the diel cycle when cells are treated with 0.5% CO₂. The PRK signal is localized to the chloroplast lobes at ZT4 and later becomes evenly distributed throughout the chloroplast. B) Heatmaps show average signal intensities in a maximal intensity projection (MIP) of all cells in the data set for each time point ZT0, n = 20; ZT2, n = 26; ZT4, n = 35; ZT6, n = 30; ZT8, n = 26; ZT10, n=23. All cells are from a single uniform culture. Scale bars indicate 5.0 μm.

3.3.4 RBCL localizes to chloroplast lobes in early to mid-light phase

PRK and Rubisco are sequential enzymes in the Calvin Benson cycle. Studies have shown that Rubisco is localized primarily to the pyrenoid matrix (Küken et al., 2018; Zhan et al., 2018). However, we asked if there is any occurrence of this enzyme in the chloroplast lobes at the same time points when we see PRK localizing there. To examine this, we again synchronized wild-type cells to a 12hr:12hr light-dark cycle. The cultures were aerated with air (ambient CO₂) during their entrainment. Samples were taken at ZT4 and ZT6, representing early to mid-light phase where we had previously seen a lobe localization for PRK. Cells were immune-stained for the large subunit of Rubisco (RBCL).

Microscopy results revealed that there was very little RBCL signal in the pyrenoid at ZT4 and ZT6 time points (Fig 3.4 A-B). Instead, there was an enrichment in the chloroplast lobes. This corroborated with the pattern we had seen for PRK and suggests that under these conditions, the lobes may be a compartment for the Calvin-Benson Cycle perhaps to facilitate the channeling of substrates and metabolites between these two sequential enzymes while ensuring the efficiency of the process.

Our lab had previously revealed a T-zone in the basal region of the *Chlamydomonas* chloroplast that is the preferential site for the synthesis and assembly of photosystem subunits, as well as their chlorophyll (Sun et al., 2019a; Uniacke & Zerges, 2007a). We had also demonstrated a temporal regulation of the spatial T-zone, with ZT0-ZT4 being identified as the time points when photosystem II biogenesis is high. To show the distribution of RBCL in relation to a photosystem II marker (the *psbA* mRNA) at these time points, we carried out FISH on the same cells that were described above. As expected, the *psbA* mRNA localized to the T-zone, while RBCL was enriched in the lobes. This suggests that when photosynthesis rates are high in the basal region of the chloroplast, RBCL is sequestered to the chloroplast lobes. We previously showed that photosystem II is enriched in the basal region at these time points (Sun et al., 2019). These results raise the intriguing possibility of a spatial partitioning of O₂ production by photosystem II and CO₂ fixation by Rubisco in the basal region and lobes, respectively.

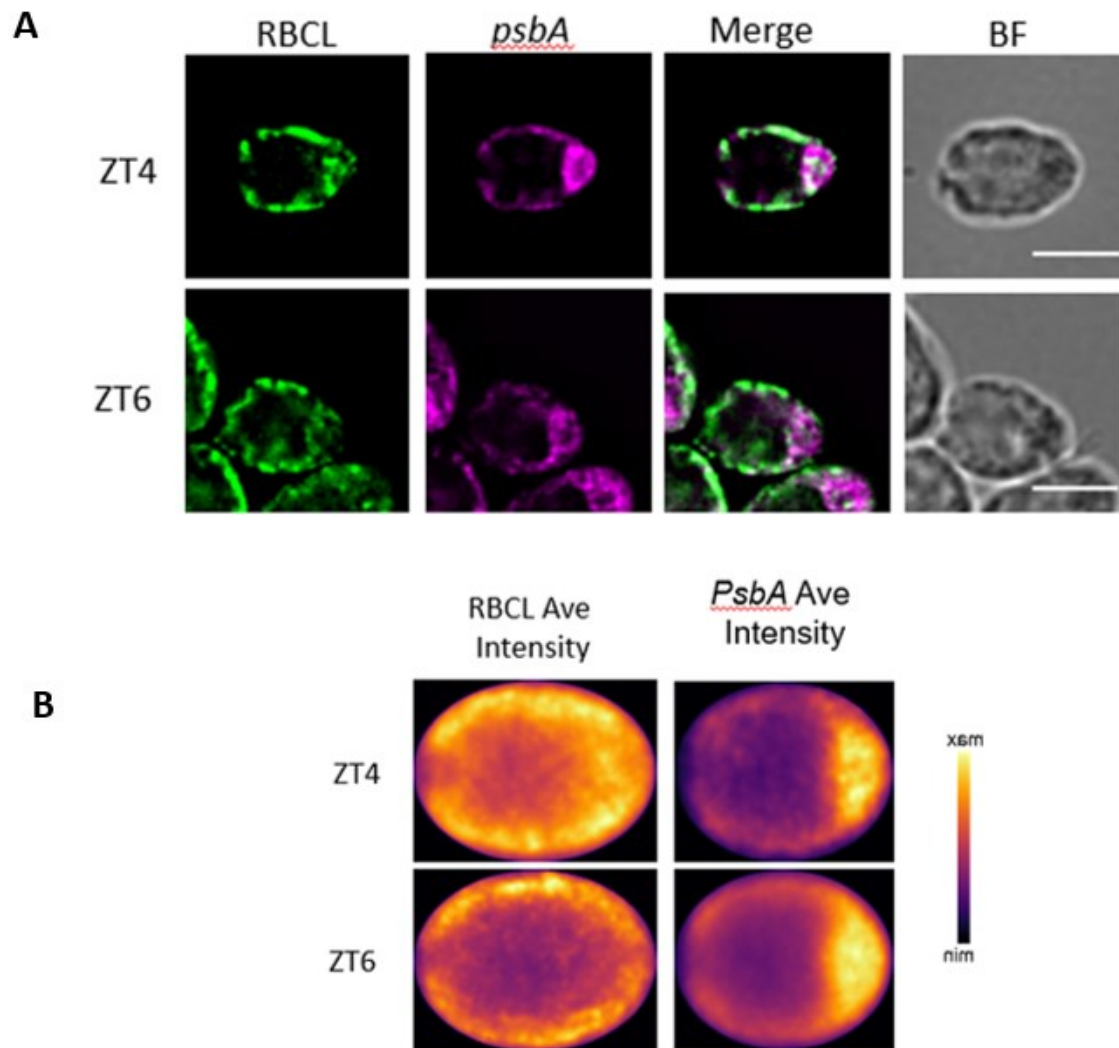


Fig 3.4. Localization of RBCL in early-mid light phase of diel cycle

A) Epifluorescence microscopy images reveal the distributions of RBCL in the chloroplast lobes and the *psbA* mRNA enriched in the T-zone of ZT4 and ZT6 cells. B) Heatmaps show the average signal intensities in a maximal intensity projection (MIP) of all cells in each data set in ZT4 cells (n = 31) and ZT6 cells (n = 34). Scale bars indicate 5.0 μm .

3.3.5 Localization of a bicarbonate transporter in *Chlamydomonas*

LCIA (Low CO₂ Inducible A) is a component of the *Chlamydomonas* carbon concentrating mechanism that facilitates the uptake and transport of HCO₃⁻ across both the plasma membrane and the chloroplast envelope to reach Rubisco (Atkinson et al., 2016; Wang et al., 2015; Yamano et al., 2015b). Previous localization studies had shown LCIA outlining the chloroplast envelope (Atkinson et al., 2016; Yamano et al., 2015b). However, those studies either used fluorescently tagged proteins or initially cultured the cells in TAP (Tris Acetate Phosphate) media which has an added carbon source.

To investigate the location of this marker using our conditions, we cultured cells photoautotrophically before staining them with an antibody against LCIA. The results showed a strong signal in the chloroplast lobes while the basal region was nearly devoid of any signal (Fig 3.5). This pattern was seen in c.a. 90% of the cells imaged and confirmed the heatmap representing the average signal distribution in the data set. The results further support the possibility of the chloroplast lobes being a compartment for the Calvin Benson Cycle as well as the CCM.

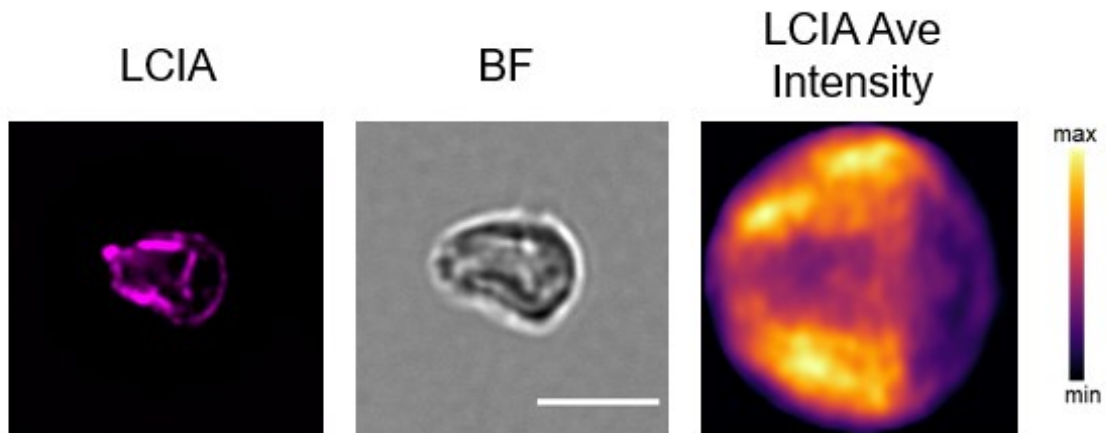


Fig 3.5. LCIA localizes to chloroplast lobes in photo-autotrophically grown cells

Epifluorescence microscopy images reveal the distributions of LCIA in the chloroplast lobes of *Chlamydomonas reinhardtii* cells grown asynchronously in ambient CO₂. The heatmap shows the average signal intensity in a maximal intensity projection (MIP) of all cells in the data set (n = 60). Scale bars indicate 5.0 μm.

3.3.6 Transmission electron microscopy images reveal constrictions at the base of chloroplast lobes

To determine if the lobes are a separate compartment and to validate our immunofluorescence results, we used electron microscopy. Cells were collected and imaged from synchronized cultures at different time points throughout the light phase. The obtained images reveal a constriction in the junction between each lobe and the basal region of the chloroplast. This was especially prominent in the early light phase (ZT2-ZT4) (Fig 3.6 A). To correlate these constrictions with the localization pattern seen in our immunofluorescence images, we scored the percentage of cells that showed this feature at each time point (Fig 3.6 B). Close to 50% of the cells at ZT2 and 70% of the cells at ZT4 had this feature. Many cells displayed this in one lobe only which also corroborated with our immunofluorescence microscopy results. Later in the light phase at ZT10, only 10% of the scored cells showed this pattern. However, it should be noted that the continuity of stroma could be detected in some optical sections of the cells, suggesting that this structural feature is perhaps a severe curvature rather than a constriction. Additional work is required to determine whether this feature contributes the localization patterns seen in our immunofluorescence images.

A

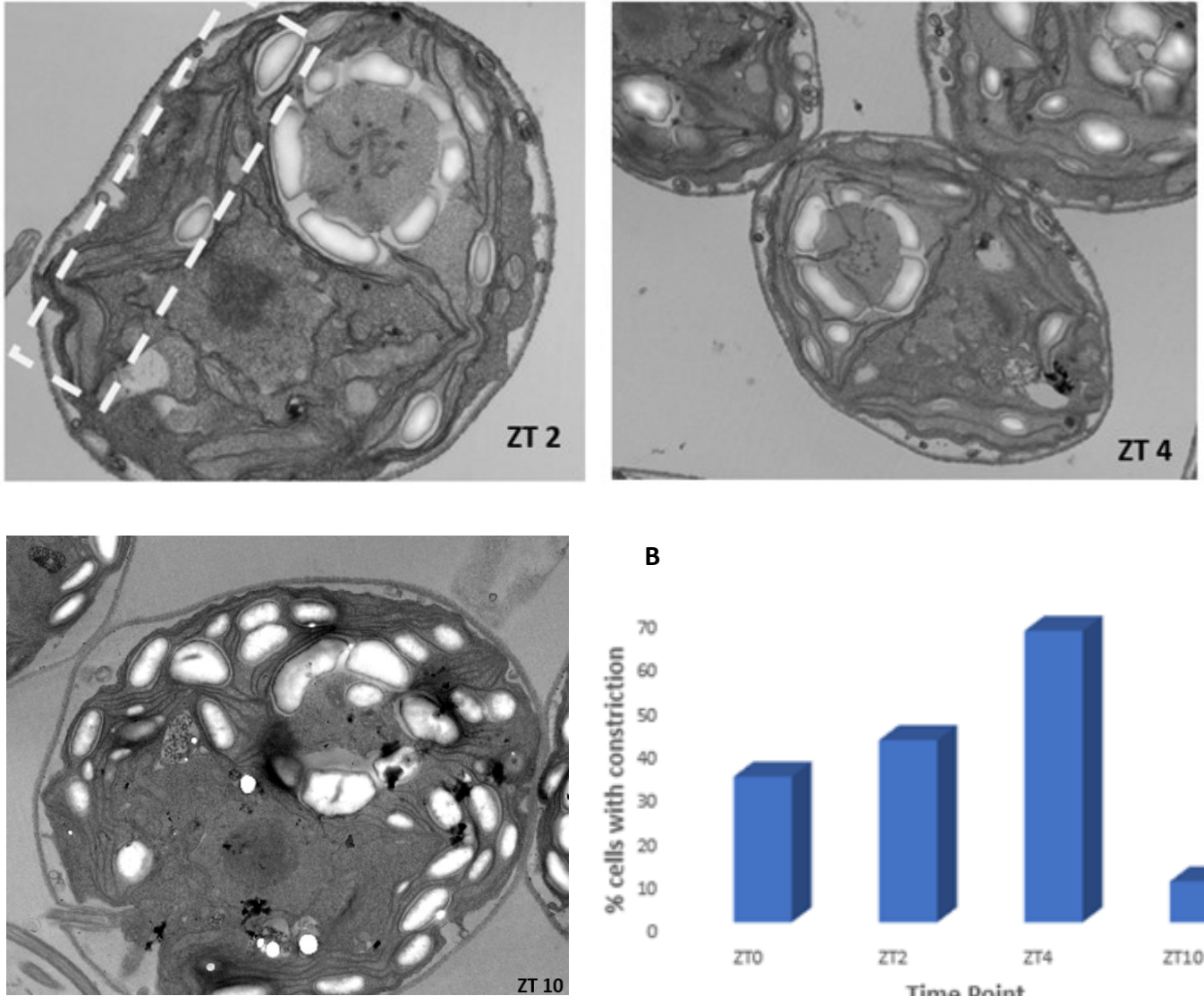


Fig 3.6. TEM ultrastructure of diurnally entrained cells

A) Image of ZT2, ZT4 and ZT10 cell. The white dashed line is outlining a lobe with a constriction.

This feature is less prominent in ZT10 cells. B) Percentage of cells showing constriction pattern

in each dataset (ZT2, n=12, ZT4, n=55, ZT10, n=32)

3.3.7 PRK is associated with thylakoid membranes

The enzymes in the Calvin Benson Cycle are often considered to be randomly distributed in the chloroplast stroma or the cytoplasm of photosynthetic bacteria. Membrane association of these enzymes has not been studied as extensively, although some of the Rubisco pool is known to be associated with thylakoid membranes (Agarwal et al., 2009; Suss et al., 1995). Here we used subcellular fractionation to determine if PRK is bound to any chloroplast membrane. PRK catalyzes the ATP-dependent reaction that generates the substrate ribulose-1,5-bisphosphate (RuBP) (Rumpho et al., 2009; Suss et al., 1995), therefore we expect that it would be positioned close to the thylakoids where the photosynthetic electron transport chain is located.

To address this, we collected cells at two different time points in the diel cycle. This included ZT4, the time point when we had seen a localization for PRK in the chloroplast lobes and ZT11, when this enzyme is evenly distributed throughout the chloroplast (Fig 3.2 A). Lysates were generated using a French Pressure Cell. The lysates were subjected to ultracentrifugation to separate soluble from insoluble material. The membranes in the pellets were separated by isopycnic density ultracentrifugation, in which membranes float to and equilibrate at their native buoyant density in the sucrose density gradient (Quail, 1979). Fractions from these gradients were then collected for western blot analysis.

PRK was found to be enriched in the dark green fractions of each gradient (Fig 3.7 A-B). These fractions were previously identified as thylakoid membranes, based on their green color caused by the pigment chlorophyll of the photosystems in thylakoid membrane. Our lab had also previously found these green fractions to be enriched in photosystem marker proteins, which are located on the thylakoid membranes (Schottkowski et al., 2012a). This suggests that the thylakoid membranes may be involved in the organization of Calvin Benson Cycle enzymes.

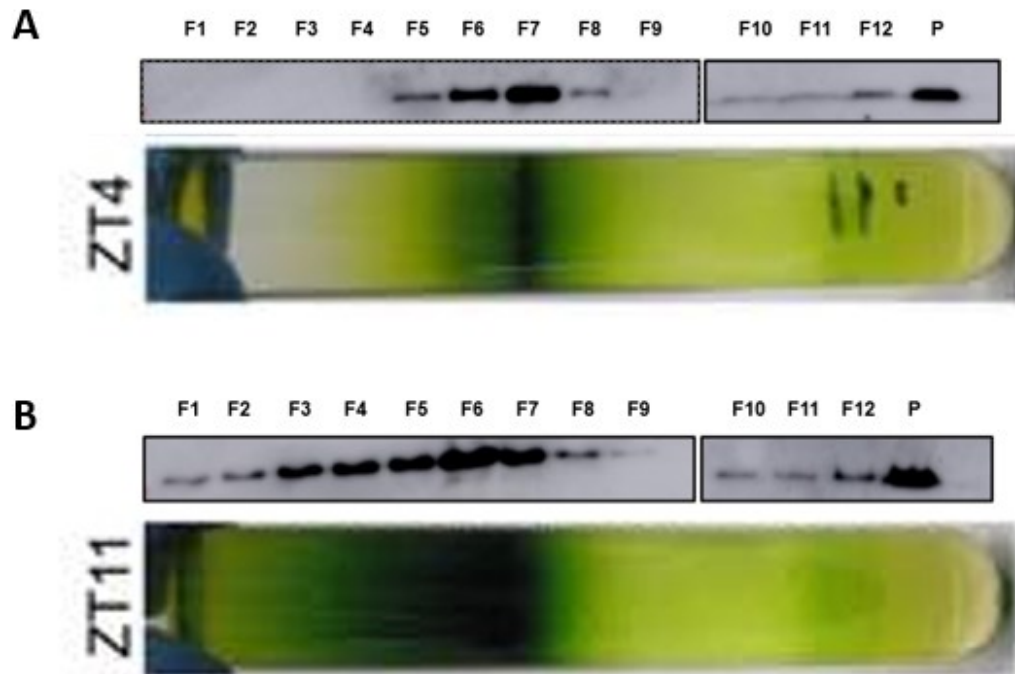


Fig 3.7. PRK is associated with thylakoid membranes

Gradient fractions were examined from CC-125 cells entrained to a 12-hr:12-hr light-dark cycle. Samples were taken for subcellular fractionation at (A) 4 hours into the light phase (B) 11 hours into the light phase. Each fraction was assayed by immunoblot analysis. PRK was enriched in the fractions corresponding to thylakoid membranes.

3.4 DISCUSSION

In this study we looked at the distribution of the Calvin Benson Cycle enzymes and related proteins in the chloroplast of *Chlamydomonas* in the light phase of the diel cycle. We confirmed that, in cells grown in photoautotrophic conditions, RBCL is largely located in the pyrenoid, although there were traces of this enzyme seen outside the pyrenoid. Meanwhile, all other enzymes in this pathway were absent from this microcompartment and distributed in other locations of the chloroplast, as had been reported previously (Küken et al., 2018; Zhan et al., 2018). To analyze spatial and temporal distribution patterns, we took advantage of diurnal synchronization in *Chlamydomonas*. Cultures were grown under 12hr:12hr light-dark cycles to obtain homogenous populations of cells. The combination of culture synchrony and frequent time-point sampling allowed us to discern phase differences in localization pattern more accurately.

PRK showed a distinct spatial and temporal patterning throughout the diel cycle. At ZT0, which represents the transition from dark to light phase, there was no definite localization of this enzyme. However, a clear localization to the chloroplast lobes was visible at ZT2-ZT4. This localized signal became evenly distributed throughout the chloroplast during the later time points (ZT6 and after). Cultures grown under high (0.5%-1%) CO₂ conditions, where the carbon concentrating mechanism is suppressed, revealed only a slight change in the distribution pattern. Therefore, it appears the stage of the diel cycle is the critical factor which determines localization.

Interestingly, RBCL showed a similar distribution to the chloroplast lobes at ZT4, with little signal seen in the pyrenoid. Together, these results support the possibility of the chloroplast lobes being a compartment for the Calvin Benson Cycle during early to mid-light phase (Fig 3.8).

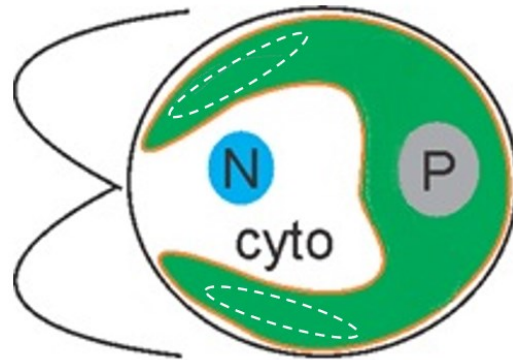


Fig 3.8. Proposed model for Calvin Benson Cycle. Dashed white line indicates compartment in the chloroplast lobes believed to be involved in Calvin Benson Cycle during early to mid-light phase.

Interestingly, previous work by our lab demonstrated that the mid-light phase (ZT0-ZT4) correlates with high rates of photosynthesis and photosystem biogenesis in the T-zone in the basal region of the chloroplast (Sun et al., 2019a; Uniacke & Zerges, 2007a). Photosystem II is a complex in the photosynthetic electron transport chain and acts as the first light-transducing complex in the redox pathway of oxygenic photosynthesis (Brudvig, 2008). It absorbs light energy through chlorophyll and other pigment molecules and oxidizes water, producing O_2 and protons (Barber, 2008; Brudvig, 2008). Considering Rubisco can react with both O_2 and CO_2 , we hypothesize that when photosynthesis rates are high, this enzyme is partitioned away to a compartment in the chloroplast lobes and away from the T-zone where photosystem biogenesis is taking place.

Additionally, the possibility of the chloroplast lobes being a separate compartment is suggested by TEM images, which reveal a constriction or severe curvature at the junctions between the lobes and the basal region of the chloroplast. However, more work is needed to validate this finding.

Finally, the localization of the bicarbonate transporter LCIA to the chloroplast lobes suggests that there could be a CCM-related function to this localization pattern. Also, studies have shown that the mid-light phase correlates with enhanced transcripts encoding the CAHs (Rai et al., 2021; Strenkert et al., 2019; Zones et al., 2015). CAHs catalyze the interconversion of CO₂ into HCO₃⁻ (Moroney et al., 2011). *CAH 1*, *CAH2*, *CAH3*, *CAH4* and *CAH5* transcripts have been shown to reach their peak during the day and are induced by low CO₂ which is the same condition as was used in our experiments (Lopez et al., 2015; Rai et al., 2021; Strenkert et al., 2019; Zones et al., 2015). Therefore, it would be interesting to look at the localization pattern of these markers and see if there is a correlation with our results.

CHAPTER 4: CONCLUSION

4.1 Overview

The results presented in this thesis reveal that chloroplasts have complex compartmentalization that is dependent on conditions. This was illustrated using the chloroplast of the unicellular alga *Chlamydomonas reinhardtii*. The stereotypic anatomy of the chloroplast in this alga (Chapter 1) makes it easy to identify spatial and temporal patterns. Using this feature to our advantage, we have revealed two novel compartments in this organelle that are engaged in different processes. These findings, with our previous discovery of a third chloroplast compartment, highlight the highly organized nature of this organelle. We also show that the presence of these compartments is dependent on conditions, particularly the stage in the diel cycle (Fig 4.1).

The first novel compartment introduced here is a region of localized translation on the chloroplast surface (Fig 4.1 magenta). This domain is located in the basal region of the chloroplast and is enriched in cytoplasmic ribosomes and two mRNAs that encode chloroplast-localized proteins (Colon-Ramos et al., 2003; Uniacke & Zerges, 2009). Our evidence suggests that this localized translation is for co-translational import, something which has never been shown before for chloroplasts.

Also in the basal region, and immediately adjacent to this domain, we had previously identified another compartment of localized translation within the chloroplast. This domain was designated as the T-zone. The T-zone is where localized chloroplast ribosomes are translating subunits of photosystem I and photosystem II (Schottkowski et al., 2012; Sun et al., 2019; Uniacke

& Zerges, 2007, 2009b) (Fig 4.1 dashed white line). Further detail on the T-zone model can be found in Appendix I.

The juxtaposition of these two domains of localized translation on and within the chloroplast reveals a complex spatial organization of the two genetic systems that organize the expression, targeting and assembly of proteins in this semi-autonomous organelle. This resembles the spatial coordination of the nuclear and mitochondrial translation systems for the synthesis of inner membrane proteins of the respiratory electron transport system and ATP synthase in *Saccharomyces cerevisiae* and humans (Gehrke et al., 2015; Matsumoto et al., 2012; Stoldt et al., 2018; Vogel, Bornhovd, et al., 2006; Zorkau et al., 2021).

In the chloroplast lobes, we reveal another compartment that is involved in the Calvin Benson Cycle (Fig 4.1 dashed yellow line). This domain is enriched in enzymes of this pathway such as PRK and RBCL as well as other enzymes and related proteins. The presence of this compartment is highly dependent on conditions, i.e., during the early to mid-light phase in the diel cycle (ZT2-ZT4). Interestingly, this is also the same period when we see the T-zone being formed. For example, all translation markers used to identify the T-zone, are enriched in the basal region of the chloroplast near the lobe junctions during the ZT0-ZT4 interval (Sun et al., 2019).

As to whether the compartment of localized translation on the cytoplasmic side of the chloroplast is also condition dependent, we are not certain. This compartment was identified using isolated chloroplasts which require the use of a cell-wall deficient strain that is not amenable to complete synchronization. Nonetheless, the cultures used for these experiments were entrained to a 12hr:12 hr light-dark regime for several consecutive days and samples were harvested approximately 4 hrs into the light phase. This resembles the ZT4 time point in synchronized cells.

Therefore, there is a possibility that the stage in the diel cycle may also play a role in the formation of this compartment of localized translation.

Finally, the results presented in this thesis, address the long-standing question of whether protein translocation into chloroplasts can operate via a co-translational translocation pathway, as established in the endoplasmic reticulum. As stated previously, the field has largely favored a post-translational protein translocation mechanism for chloroplast-localized proteins encoded by nuclear genomes. However, here, we have revealed the first evidence of localized translation for co-translational import on the chloroplast surface, which is landmark in cell biology.

Together, these findings illustrate a higher level of complexity and organization in the chloroplast of *Chlamydomonas* than has been appreciated. Moreover, they raise the possibility that similar organization can occur in higher plants and provide a new conceptual framework for research into chloroplast biogenesis.

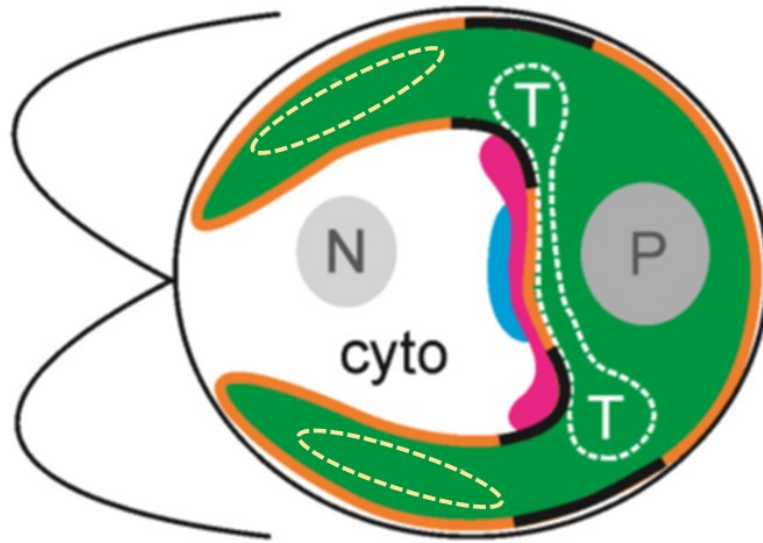


Fig 4.1. Our Model. *Chlamydomonas* is used as a model organism for analyses of the cytological organization of chloroplastic processes because it has a single chloroplast with a stereotypic morphology and prominent cytological landmarks. An illustration shows the cilia pair at the anterior cell pole, the nucleus (N), cytosol (cyto), and the chloroplast (green). The chloroplast (green) has lobes which enclose the nuclear-cytosolic region (cyto), the pyrenoid (P), the translation zone (T) and is surrounded by a dual membrane envelope (orange). The cyto-ribosome-bound domain of the envelope (magenta) includes the mRNA enriched region (cyan) and overlaps envelope domains enriched in the TOC/TIC protein import translocons (black)(Uniacke & Zerges, 2009b). Within the lobes is a compartment involved in the Calvin Benson Cycle (dashed yellow line).

4.2 Future directions

4.2.1 Translation profiling of ribosome-associated nascent polypeptide chains

The results of this thesis have opened the avenue to answer several other questions that can be addressed with future experiments. The first step would be to acquire a profile of mRNAs that are translated by cytoplasmic ribosomes on the chloroplast envelope. This can be done through two approaches. First by performing RNAseq on isolated chloroplasts, to confirm and investigate what class of mRNAs are enriched there. Second, by profiling the nascent polypeptides with proteomics. The basis of this second approach will be to label the nascent chains with biotinylated puromycin followed by their affinity purification using streptavidin beads. This will reveal if there is a subset of proteins that are translated on the chloroplast surface. For example, for the mitochondria, proximity-specific ribosome profiling has shown that most inner membrane proteins are synthesized on the mitochondria of yeast (Williams et al., 2014a). It could also provide further evidence that the localized translation on the outer chloroplast surface is for co-translational import, should the obtained translome be enriched in nuclear encoded chloroplast proteins. The presence of non-chloroplast proteins in the translome would suggest that this organelle is serving as a platform for localizing and regulating translation of proteins for a neighboring compartment, such as the mitochondria or ER. Such a result would need to be validated by FISH to control for mRNAs bound to non-chloroplast contaminants. Any bias in the chloroplast proteins encoded by the mRNAs that are translated on the chloroplast surface would suggest functions of the co-translational import.

4.2.2 Characterization of the membranes associated with chloroplast-bound ribosomes

A second intriguing avenue to explore would be to identify membranes that are derived from the biogenic envelope domain (Figure 4.1 magenta), it would be possible to use isopycnic ultracentrifugation to fractionate membranes from cells and label the membranes with ribosomes that were translating *in vivo* with biotinylated puromycin. The puromycin-conjugated truncated proteins will then be affinity purified from their corresponding fraction and all associated proteins will be identified by MS and proteomics. If successful, such results will reveal which membranes serve as a platform for translation on the chloroplast surface, such as the biogenic envelope. The proteome of such membranes could reveal proteins that are candidate factors in protein import and thylakoid biogenesis and reveal additional functions of the biogenic envelope domain.

4.2.3 Identification of partner proteins associated with the chloroplast-bound ribosomes

Chloroplast-bound ribosomes are likely interacting with other proteins. These proteins could function in the process of co-translational import, for example, docking proteins. Other partner proteins might be involved in unknown functions of co-translational protein import. Therefore, it would be interesting to epitope-tag cytoplasmic ribosomal proteins for their affinity purification from cells or chloroplast lysates. MS analyses of such fractions could reveal candidates for co-translational import.

4.2.4 Localization of chloroplast translation markers

My efforts to optimize and adapt a new FISH protocol to *Chlamydomonas* cells and chloroplasts has paved the way to study the localization of other mRNAs in this organism. This is a relatively cost-effective method that has shown to be promising in our hands and can be used to expand the T-zone model. This can be done for example by localizing other PET chain complexes such as Cytb₆f as well as ATP synthase and related components. This will shed further light into the spatial and temporal organization involved in the biogenesis of chloroplasts.

REFERENCES

- Adelman, M. R., Sabatini, D. D., & Blobel, G. (1973). RIBOSOME-MEMBRANE INTERACTION: Nondestructive Disassembly of Rat Liver Rough Microsomes into Ribosomal and Membranous Components. *Journal of Cell Biology*, 56(1), 206–229. <https://doi.org/10.1083/jcb.56.1.206>
- Agarwal, R., Ortleb, S., Sainis, J. K., & Melzer, M. (2009). Immunoelectron Microscopy for Locating Calvin Cycle Enzymes in the Thylakoids of *Synechocystis* 6803. *Molecular Plant*, 2(1), 32–42. <https://doi.org/10.1093/mp/ssn075>
- Alberts, B., Johnson, A., Lewis, J., Raff, M., Roberts, K., & Walter, P. (2002a). Chloroplasts and Photosynthesis. *Molecular Biology of the Cell. 4th Edition*. <https://www.ncbi.nlm.nih.gov/books/NBK26819/>
- Alberts, B., Johnson, A., Lewis, J., Raff, M., Roberts, K., & Walter, P. (2002b). The Compartmentalization of Cells. *Molecular Biology of the Cell. 4th Edition*. <https://www.ncbi.nlm.nih.gov/books/NBK26907/>
- Andrès, C., Agne, B., & Kessler, F. (2010). The TOC complex: Preprotein gateway to the chloroplast. *Biochimica et Biophysica Acta (BBA) - Molecular Cell Research*, 1803(6), 715–723. <https://doi.org/10.1016/j.bbamcr.2010.03.004>
- Armbruster, U., & Strand, D. D. (2020). Regulation of chloroplast primary metabolism. *Photosynthesis Research*, 145(1), 1–3. <https://doi.org/10.1007/s11120-020-00765-4>
- Atkinson, N., Feike, D., Mackinder, L. C. M., Meyer, M. T., Griffiths, H., Jonikas, M. C., Smith, A. M., & McCormick, A. J. (2016). Introducing an algal carbon-concentrating mechanism into higher plants: Location and incorporation of key components. *Plant Biotechnology Journal*, 14(5), 1302–1315. <https://doi.org/10.1111/pbi.12497>
- Atteia, A., Adrait, A., Brugière, S., Tardif, M., van Lis, R., Deusch, O., Dagan, T., Kuhn, L., Gontero, B., Martin, W., Garin, J., Joyard, J., & Rolland, N. (2009). A Proteomic Survey of *Chlamydomonas reinhardtii* Mitochondria Sheds New Light on the Metabolic Plasticity of the Organelle and on the Nature of the α -Proteobacterial Mitochondrial Ancestor. *Molecular Biology and Evolution*, 26(7), 1533–1548. <https://doi.org/10.1093/molbev/msp068>
- Avendaño-Monsalve, M. C., Ponce-Rojas, J. C., & Funes, S. (2020). From cytosol to mitochondria: The beginning of a protein journey. *Biol. Chem*, 401((6–7)), 645–661. <https://doi.org/10.1515/hsz-2020-0110>
- Aviram, N., & Schuldiner, M. (2017). Targeting and translocation of proteins to the endoplasmic reticulum at a glance. *Journal of Cell Science*, 130(24), 4079–4085. <https://doi.org/10.1242/jcs.204396>
- Badger, M. R., & Price, G. D. (1994). The Role of Carbonic Anhydrase in Photosynthesis. *Annual Review of Plant Physiology and Plant Molecular Biology*, 45(1), 369–392. <https://doi.org/10.1146/annurev.pp.45.060194.002101>
- Barajas-López, J. de D., Blanco, N. E., & Strand, Å. (2013). Plastid-to-nucleus communication, signals controlling the running of the plant cell. *Biochimica et Biophysica Acta (BBA) - Molecular Cell Research*, 1833(2), 425–437. <https://doi.org/10.1016/j.bbamcr.2012.06.020>

- Barber, J. (2008). Photosynthetic generation of oxygen. *Philosophical Transactions of the Royal Society B: Biological Sciences*, 363(1504), 2665–2674. <https://doi.org/10.1098/rstb.2008.0047>
- Béthune, J., Jansen, R.-P., Feldbrügge, M., & Zarnack, K. (2019). Membrane-Associated RNA-Binding Proteins Orchestrate Organelle-Coupled Translation. *Trends in Cell Biology*, 29(2), 178–188. <https://doi.org/10.1016/j.tcb.2018.10.005>
- Biel, K., & Fomina, I. (2015). Benson-Bassham-Calvin cycle contribution to the organic life on our planet. *Photosynthetica*. <https://doi.org/10.1007/s11099-015-0112-7>
- Bowsher, C. G., & Tobin, A. K. (2001). Compartmentation of metabolism within mitochondria and plastids. *Journal of Experimental Botany*, 52(356), 513–527. <https://doi.org/10.1093/jexbot/52.356.513>
- Bräutigam, A., Schlüter, U., Eisenhut, M., & Gowik, U. (2017). On the Evolutionary Origin of CAM Photosynthesis[OPEN]. *Plant Physiology*, 174(2), 473–477. <https://doi.org/10.1104/pp.17.00195>
- Brudvig, G. W. (2008). Water oxidation chemistry of photosystem II. *Philosophical Transactions of the Royal Society B: Biological Sciences*, 363(1494), 1211–1219. <https://doi.org/10.1098/rstb.2007.2217>
- Busch, F. A. (2020). Photorespiration in the context of Rubisco biochemistry, CO₂ diffusion and metabolism. *The Plant Journal*, 101(4), 919–939. <https://doi.org/10.1111/tpj.14674>
- Busch, F. A., Sage, T. L., Cousins, A. B., & Sage, R. F. (2013). C₃ plants enhance rates of photosynthesis by reassimilating photorespired and respired CO₂. *Plant, Cell & Environment*, 36(1), 200–212. <https://doi.org/10.1111/j.1365-3040.2012.02567.x>
- Bykov, Y. S., Rapaport, D., Herrmann, J. M., & Schuldiner, M. (2020). Cytosolic Events in the Biogenesis of Mitochondrial Proteins. *Trends in Biochemical Sciences*, 45(8), 650–667. <https://doi.org/10.1016/j.tibs.2020.04.001>
- Campbell, P. N. (1989). The targeting of proteins in eukaryotic cells. *Biochemical Education*, 17(3), 114–121. [https://doi.org/10.1016/0307-4412\(89\)90088-5](https://doi.org/10.1016/0307-4412(89)90088-5)
- Carde, J. P., Joyard, J., & Douce, R. (1982). Electron Microscopic Studies of Envelope Membranes from Spinach Plastids. *Biology of the Cell*, 44, 315–324.
- Chepko, G., Weistrop, J. S., & Margulies, M. M. (1979). The absence of cytoplasm ribosomes on the envelopes of chloroplasts and mitochondria in plants: Implications for the mechanism of transport of proteins into these organelles. *Protoplasma*, 100(3), 385–392. <https://doi.org/10.1007/BF01279324>
- Chua, N. H., Blobel, G., Siekevitz, P., & Palade, G. E. (1973). Attachment of chloroplast polysomes to thylakoid membranes in *Chlamydomonas reinhardtii*. *Proc Natl Acad Sci U S A*, 70(5), 1554–1558.
- Chua, N. H., & Gillham, N. W. (1977). The sites of synthesis of the principal thylakoid membrane polypeptides in *Chlamydomonas reinhardtii*. *Journal of Cell Biology*, 74(2), 441–452. <https://doi.org/10.1083/jcb.74.2.441>
- Chua, N. H., & Schmidt, G. W. (1979). Transport of proteins into mitochondria and chloroplasts. *J Cell Biol*, 81(3), 461–483.

Claros, M. G., Perea, J., Shu, Y., Samatey, F. A., Popot, J. L., & Jacq, C. (1995). Limitations to in vivo import of hydrophobic proteins into yeast mitochondria. The case of a cytoplasmically synthesized apocytochrome b. *Eur J Biochem*, 228(3), 762-71.

Colon-Ramos, D. A., Salisbury, J. L., Sanders, M. A., Shenoy, S. M., Singer, R. H., & Garcia-Blanco, M. A. (2003). Asymmetric distribution of nuclear pore complexes and the cytoplasmic localization of beta2-tubulin mRNA in *Chlamydomonas reinhardtii*. *Dev Cell*, 4(6), 941–952.

Cooper, G. M. (2000). Chloroplasts and Other Plastids. *The Cell: A Molecular Approach. 2nd Edition*. <https://www.ncbi.nlm.nih.gov/books/NBK9905/>

Cummins, P. L. (2021). The Coevolution of RuBisCO, Photorespiration, and Carbon Concentrating Mechanisms in Higher Plants. *Frontiers in Plant Science*, 12, 1753. <https://doi.org/10.3389/fpls.2021.662425>

Czarnecki, O., & Grimm, B. (2012). Post-translational control of tetrapyrrole biosynthesis in plants, algae, and cyanobacteria. *Journal of Experimental Botany*, 63(4), 1675–1687. <https://doi.org/10.1093/jxb/err437>

Dall'Osto, L., Bressan, M., & Bassi, R. (2015). Biogenesis of light harvesting proteins. *Biochim Biophys Acta*. <https://doi.org/10.1016/j.bbabi.2015.02.009>

Das, S., Vera, M., Gandin, V., Singer, R. H., & Tutucci, E. (2021). Intracellular mRNA transport and localized translation. *Nature Reviews Molecular Cell Biology*, 1–22. <https://doi.org/10.1038/s41580-021-00356-8>

Edwards, G. E., Franceschi, V. R., Ku, M. S. B., Voznesenskaya, E. V., Pyankov, V. I., & Andreo, C. S. (2001). Compartmentation of photosynthesis in cells and tissues of C4 plants. *Journal of Experimental Botany*, 52(356), 577–590. <https://doi.org/10.1093/jexbot/52.356.577>

Eisenhut, M., Roell, M.-S., & Weber, A. P. M. (2019). Mechanistic understanding of photorespiration paves the way to a new green revolution. *New Phytologist*, 223(4), 1762–1769. <https://doi.org/10.1111/nph.15872>

Elimam, H., Papillon, J., Kaufman, D. R., Guillemette, J., Aoudjit, L., Gross, R. W., Takano, T., & Cybulsky, A. V. (2016). Genetic Ablation of Calcium-independent Phospholipase A2 γ Induces Glomerular Injury in Mice. *The Journal of Biological Chemistry*, 291(28), 14468–14482. <https://doi.org/10.1074/jbc.M115.696781>

Engel, B. D., Schaffer, M., Kuhn Cuellar, L., Villa, E., Pnitzko, J. M., & Baumeister, W. (2015). Native architecture of the *Chlamydomonas* chloroplast revealed by in situ cryo-electron tomography. *ELife*, 4, e04889. <https://doi.org/10.7554/eLife.04889>

English, A. R., & Voeltz, G. K. (2013). Endoplasmic Reticulum Structure and Interconnections with Other Organelles. *Cold Spring Harbor Perspectives in Biology*, 5(4), a013227. <https://doi.org/10.1101/cshperspect.a013227>

Erb, T. J., & Zarzycki, J. (2018). A short history of RubisCO: The rise and fall (?) of Nature's predominant CO₂ fixing enzyme. *Current Opinion in Biotechnology*, 49, 100–107. <https://doi.org/10.1016/j.copbio.2017.07.017>

- Fei, C., Wilson, A. T., Mangan, N. M., Wingreen, N. S., & Jonikas, M. C. (2021). *Diffusion barriers and adaptive carbon uptake strategies enhance the modeled performance of the algal CO₂-concentrating mechanism* (p. 2021.03.04.433933). <https://doi.org/10.1101/2021.03.04.433933>
- Ferenczi, A., Pyott, D. E., Xipnitou, A., & Molnar, A. (2017). Efficient targeted DNA editing and replacement in *Chlamydomonas reinhardtii* using Cpf1 ribonucleoproteins and single-stranded DNA. *Proceedings of the National Academy of Sciences of the United States of America*, *114*(51), 13567–13572. <https://doi.org/10.1073/pnas.1710597114>
- Fingerhut, J. M., & Yamashita, Y. M. (2020). mRNA localization mediates maturation of cytoplasmic cilia in *Drosophila* spermatogenesis. *Journal of Cell Biology*, *219*(9). <https://doi.org/10.1083/jcb.202003084>
- Flechsler, J., Heimerl, T., Huber, H., Rachel, R., & Berg, I. A. (2021). Functional compartmentalization and metabolic separation in a prokaryotic cell. *Proceedings of the National Academy of Sciences*, *118*(25). <https://doi.org/10.1073/pnas.2022114118>
- Formosa, L. E., & Ryan, M. T. (2018). Mitochondrial OXPHOS complex assembly lines. *Nature Cell Biology*, *20*(5), 511–513. <https://doi.org/10.1038/s41556-018-0098-z>
- Fox, T. D. (2012). Mitochondrial Protein Synthesis, Import, and Assembly. *Genetics*, *192*(4), 1203–1234. <https://doi.org/10.1534/genetics.112.141267>
- Freeman Rosenzweig, E. S., Xu, B., Kuhn Cuellar, L., Martinez-Sanchez, A., Schaffer, M., Strauss, M., Cartwright, H. N., Ronceray, P., Pnitzko, J. M., Förster, F., Wingreen, N. S., Engel, B. D., Mackinder, L. C. M., & Jonikas, M. C. (2017). The Eukaryotic CO₂-Concentrating Organelle Is Liquid-like and Exhibits Dynamic Reorganization. *Cell*, *171*(1), 148-162.e19. <https://doi.org/10.1016/j.cell.2017.08.008>
- Gabaldón, T., & Pittis, A. A. (2015). Origin and evolution of metabolic sub-cellular compartmentalization in eukaryotes. *Biochimie*, *119*, 262–268. <https://doi.org/10.1016/j.biochi.2015.03.021>
- Garcia, M., Darzacq, X., Delaveau, T., Jourden, L., Singer, R. H., & Jacq, C. (2007a). Mitochondria-associated Yeast mRNAs and the Biogenesis of Molecular Complexes. *Molecular Biology of the Cell*, *18*(2), 362–368. <https://doi.org/10.1091/mbc.E06-09-0827>
- Garcia, M., Darzacq, X., Delaveau, T., Jourden, L., Singer, R. H., & Jacq, C. (2007b). Mitochondria-associated Yeast mRNAs and the Biogenesis of Molecular Complexes. *Molecular Biology of the Cell*, *18*(2), 362–368. <https://doi.org/10.1091/mbc.e06-09-0827>
- Gehrke, S., Wu, Z., Klinkenberg, M., Sun, Y., Auburger, G., Guo, S., & Lu, B. (2015). PINK1 and Parkin Control Localized Translation of Respiratory Chain Component mRNAs on Mitochondria Outer Membrane. *Cell Metabolism*, *21*(1), 95–108. <https://doi.org/10.1016/j.cmet.2014.12.007>
- Giordano, M., Beardall, J., & Raven, J. A. (2005). CO₂ CONCENTRATING MECHANISMS IN ALGAE: Mechanisms, Environmental Modulation, and Evolution. *Annual Review of Plant Biology*, *56*(1), 99–131. <https://doi.org/10.1146/annurev.arplant.56.032604.144052>
- Giordano, M., & Raven, J. A. (2014). Nitrogen and sulfur assimilation in plants and algae. *Aquatic Botany*, *118*, 45–61. <https://doi.org/10.1016/j.aquabot.2014.06.012>

- Gold, V. A., Chroscicki, P., Bragoszewski, P., & Chacinska, A. (2017a). Visualization of cytosolic ribosomes on the surface of mitochondria by electron cryo-tomography. *EMBO Rep*, *18*(10), 1786–1800. <https://doi.org/10.15252/embr.201744261>
- Gold, V. A., Chroscicki, P., Bragoszewski, P., & Chacinska, A. (2017b). Visualization of cytosolic ribosomes on the surface of mitochondria by electron cryo-tomography. *EMBO Reports*, *18*(10), 1786–1800. <https://doi.org/10.15252/embr.201744261>
- Goodenough, U., Lin, H., & Lee, J.-H. (2007). Sex determination in *Chlamydomonas*. *Seminars in Cell & Developmental Biology*, *18*(3), 350–361. <https://doi.org/10.1016/j.semcd.2007.02.006>
- Goodman, R. P., Calvo, S. E., & Mootha, V. K. (2018). Spatiotemporal compartmentalization of hepatic NADH and NADPH metabolism. *Journal of Biological Chemistry*, *293*(20), 7508–7516. <https://doi.org/10.1074/jbc.TM117.000258>
- Gorman, D. S., & Levine, R. P. (1965). Cytochrome f and plastocyanin: Their sequence in the photosynthetic electron transport chain of *Chlamydomonas reinhardi*. *Proceedings of the National Academy of Sciences*, *54*(6), 1665–1669. <https://doi.org/10.1073/pnas.54.6.1665>
- Goudet, M. M. M., Orr, D. J., Melkonian, M., Müller, K. H., Meyer, M. T., Carmo-Silva, E., & Griffiths, H. (2020). Rubisco and carbon-concentrating mechanism co-evolution across chlorophyte and streptophyte green algae. *New Phytologist*, *227*(3), 810–823. <https://doi.org/10.1111/nph.16577>
- Gould, S. B. (2018). Membranes and evolution. *Current Biology*, *28*(8), R381–R385. <https://doi.org/10.1016/j.cub.2018.01.086>
- Gowik, U., & Westhoff, P. (2011). The Path from C3 to C4 Photosynthesis. *Plant Physiology*, *155*(1), 56–63. <https://doi.org/10.1104/pp.110.165308>
- Grevel, A., Pfanner, N., & Becker, T. (2020a). Coupling of import and assembly pathways in mitochondrial protein biogenesis. *Biological Chemistry*, *401*(1), 117–129. <https://doi.org/10.1515/hsz-2019-0310>
- Grevel, A., Pfanner, N., & Becker, T. (2020b). Coupling of import and assembly pathways in mitochondrial protein biogenesis. *Biological Chemistry*, *401*(1), 117–129. <https://doi.org/10.1515/hsz-2019-0310>
- Grossman, A. (2000). Acclimation of *Chlamydomonas reinhardtii* to its nutrient environment. *Protist*, *151*(3), 201–224. <https://doi.org/10.1078/1434-4610-00020>
- Gurreri, L., Fermani, S., Zaffagnini, M., Sparla, F., & Trost, P. (2021). Calvin–Benson cycle regulation is getting complex. *Trends in Plant Science*, *26*(9), 898–912. <https://doi.org/10.1016/j.tplants.2021.03.008>
- Hagemann, M., Kern, R., Maurino, V. G., Hanson, D. T., Weber, A. P. M., Sage, R. F., & Bauwe, H. (2016). Evolution of photorespiration from cyanobacteria to land plants, considering protein phylogenies and acquisition of carbon concentrating mechanisms. *Journal of Experimental Botany*, *67*(10), 2963–2976. <https://doi.org/10.1093/jxb/erw063>
- Haimovich, G., Cohen-Zontag, O., & Gerst, J. E. (2016). A role for mRNA trafficking and localized translation in peroxisome biogenesis and function? *Biochim Biophys Acta*, *1863*(5), 911–921. <https://doi.org/10.1016/j.bbamcr.2015.09.007> S0167-4889(15)00300-6 [pii]

- Harris, E. H. (1989). 7—Photosynthesis. In E. H. Harris (Ed.), *The Chlamydomonas Sourcebook* (pp. 259–297). Academic Press. <https://doi.org/10.1016/B978-0-12-326880-8.50012-2>
- Harris, E. H., Stern, D., & Witman, G. (2009). *The Chlamydomonas Sourcebook 3-Vol Set*. Elsevier Science.
- He, S., Chou, H.-T., Matthies, D., Wunder, T., Meyer, M. T., Atkinson, N., Martinez-Sanchez, A., Jeffrey, P. D., Port, S. A., Patena, W., He, G., Chen, V. K., Hughson, F. M., McCormick, A. J., Mueller-Cajar, O., Engel, B. D., Yu, Z., & Jonikas, M. C. (2020). The structural basis of Rubisco phase separation in the pyrenoid. *Nature Plants*, *6*(12), 1480–1490. <https://doi.org/10.1038/s41477-020-00811-y>
- Heldt, H.-W., & Piechulla, B. (2011). 6—The Calvin cycle catalyzes photosynthetic CO₂ assimilation. In H.-W. Heldt & B. Piechulla (Eds.), *Plant Biochemistry (Fourth Edition)* (pp. 163–191). Academic Press. <https://doi.org/10.1016/B978-0-12-384986-1.00006-5>
- Hernández, M. L., & Cejudo, F. J. (2021). Chloroplast Lipids Metabolism and Function. A Redox Perspective. *Frontiers in Plant Science*, *12*, 1636. <https://doi.org/10.3389/fpls.2021.712022>
- Hoffman, A. M., Chen, Q., Zheng, T., & Nicchitta, C. V. (2019). Heterogeneous translational landscape of the endoplasmic reticulum revealed by ribosome proximity labeling and transcriptome analysis. *Journal of Biological Chemistry*, *294*(22), 8942–8958. <https://doi.org/10.1074/jbc.RA119.007996>
- Hovland, R., Hesketh, J. E., & PRYME, I. F. (1996). The Compartmentalization of Protein Synthesis: Importance of Cytoskeleton and Role in mRNA Targeting. *Int. J. Biochem. Cell Biol*, *28*(10), 1089–1105.
- Iñiguez, C., Capó-Bauçà, S., Niinemets, Ü., Stoll, H., Aguiló-Nicolau, P., & Galmés, J. (2020). Evolutionary trends in RuBisCO kinetics and their co-evolution with CO₂ concentrating mechanisms. *The Plant Journal*, *101*(4), 897–918. <https://doi.org/10.1111/tpj.14643>
- Iwai, M., Yokono, M., Kurokawa, K., Ichihara, A., & Nakano, A. (2016). Live-cell visualization of excitation energy dynamics in chloroplast thylakoid structures. *Scientific Reports*, *6*(1), 29940. <https://doi.org/10.1038/srep29940>
- Jan, C. H., Williams, C. C., & Weissman, J. S. (2014). Principles of ER cotranslational translocation revealed by proximity-specific ribosome profiling. *Science*, *346*(6210), 1257521. <https://doi.org/10.1126/science.1257521>
- Jarvis, P., & López-Juez, E. (2013). Biogenesis and homeostasis of chloroplasts and other plastids. *Nature Reviews Molecular Cell Biology*, *14*(12), 787–802. <https://doi.org/10.1038/nrm3702>
- Jarvis, P., & Lopez-Juez, E. (2014). Biogenesis and homeostasis of chloroplasts and other plastids (vol 14, pg 787, 2013). *Nature Reviews Molecular Cell Biology*, *15*(2), 147–147. <https://doi.org/10.1038/Nrm3744>
- Jarvis, P., & Soll, J. (2002). Toc, tic, and chloroplast protein import. *Biochimica Et Biophysica Acta*, *1590*(1–3), 177–189. [https://doi.org/10.1016/s0167-4889\(02\)00176-3](https://doi.org/10.1016/s0167-4889(02)00176-3)
- Johnson, M. P. (2016). Photosynthesis. *Essays in Biochemistry*, *60*(3), 255–273. <https://doi.org/10.1042/EBC20160016>

- Joyard, J., Ferro, M., Masselon, C., Seigneurin-Berny, D., Salvi, D., Garin, J., & Rolland, N. (2009). Chloroplast proteomics and the compartmentation of plastidial isoprenoid biosynthetic pathways. *Molecular Plant*, 2(6), 1154–1180. <https://doi.org/10.1093/mp/ssp088>
- Jungnick, N., Ma, Y., Mukherjee, B., Cronan, J. C., Speed, D. J., Laborde, S. M., Longstreth, D. J., & Moroney, J. V. (2014). The carbon concentrating mechanism in *Chlamydomonas reinhardtii*: Finding the missing pieces. *Photosynthesis Research*, 121(2), 159–173. <https://doi.org/10.1007/s11120-014-0004-x>
- Keeley, J. E., & Rundel, P. W. (2003). Evolution of CAM and C4 Carbon-Concentrating Mechanisms. *International Journal of Plant Sciences*, 164(S3), S55–S77. <https://doi.org/10.1086/374192>
- Keeling, P. J. (2010). The endosymbiotic origin, diversification and fate of plastids. *Philosophical Transactions of the Royal Society B: Biological Sciences*, 365(1541), 729–748. <https://doi.org/10.1098/rstb.2009.0103>
- Kellems, R. E., Allison, V. F., & Butow, R. A. (1974). Cytoplasmic Type 80 S Ribosomes Associated with Yeast Mitochondria II. EVIDENCE FOR THE ASSOCIATION OF CYTOPLASMIC RIBOSOMES WITH THE OUTER MITOCHONDRIAL MEMBRANE IN SITU. *Journal of Biological Chemistry*, 249(10), 3297–3303.
- Keller, M. (2010). Chapter 4—Photosynthesis and Respiration. In M. Keller (Ed.), *The Science of Grapevines* (pp. 107–123). Academic Press. <https://doi.org/10.1016/B978-0-12-374881-2.00004-0>
- Kerfeld, C. A., Aussignargues, C., Zarzycki, J., Cai, F., & Sutter, M. (2018). Bacterial microcompartments. *Nature Reviews Microbiology*, 16(5), 277–290. <https://doi.org/10.1038/nrmicro.2018.10>
- Kiebler, M., Pfaller, R., Sollner, T., Griffiths, G., Horstmann, H., Pfanner, N., & Neupert, W. (1990). Identification of a mitochondrial receptor complex required for recognition and membrane insertion of precursor proteins. *Nature*, 348(6302), 610–616. <https://doi.org/10.1038/348610a0>
- Kim, D. H., & Hwang, I. (2013). Direct Targeting of Proteins from the Cytosol to Organelles: The ER versus Endosymbiotic Organelles. *Traffic*, 14(6), 613–621. <https://doi.org/10.1111/tra.12043>
- Kirchhoff, H. (2014). Dynamic Architecture of Plant Photosynthetic Membranes. In S. M. Theg & F.-A. Wollman (Eds.), *Plastid Biology* (pp. 129–154). Springer. https://doi.org/10.1007/978-1-4939-1136-3_5
- Kirchhoff, H. (2019). Chloroplast ultrastructure in plants. *New Phytologist*, 223(2), 565–574. <https://doi.org/10.1111/nph.15730>
- Kono, T., Mehrotra, S., Endo, C., Kizu, N., Matusda, M., Kimura, H., Mizohata, E., Inoue, T., Hasunuma, T., Yokota, A., Matsumura, H., & Ashida, H. (2017). A RuBisCO-mediated carbon metabolic pathway in methanogenic archaea. *Nature Communications*, 8(1), 14007. <https://doi.org/10.1038/ncomms14007>
- Kremer, J. R., Mastrorade, D. N., & McIntosh, J. R. (1996). Computer Visualization of Three-Dimensional Image Data Using IMOD. *Journal of Structural Biology*, 116(1), 71–76. <https://doi.org/10.1006/jsbi.1996.0013>
- Kühlbrandt, W. (2015). Structure and function of mitochondrial membrane protein complexes. *BMC Biology*, 13(1), 89. <https://doi.org/10.1186/s12915-015-0201-x>

- Küken, A., Sommer, F., Yaneva-Roder, L., Mackinder, L. C., Höhne, M., Geimer, S., Jonikas, M. C., Schroda, M., Stitt, M., Nikoloski, Z., & Mettler-Altmann, T. (2018). Effects of microcompartmentation on flux distribution and metabolic pools in *Chlamydomonas reinhardtii* chloroplasts. *ELife*, *7*, e37960. <https://doi.org/10.7554/eLife.37960>
- Lesnik, C., Cohen, Y., Atir-Lande, A., Schuldiner, M., & Arava, Y. (2014). OM14 is a mitochondrial receptor for cytosolic ribosomes that supports co-translational import into mitochondria. *Nature Communications*, *5*(1), 5711. <https://doi.org/10.1038/ncomms6711>
- Lesnik, C., Golani-Armon, A., & Arava, Y. (2015). Localized translation near the mitochondrial outer membrane: An update. *RNA Biology*, *12*(8), 801–809. <https://doi.org/10.1080/15476286.2015.1058686>
- Li, X., Zhang, R., Patena, W., Gang, S. S., Blum, S. R., Ivanova, N., Yue, R., Robertson, J. M., Lefebvre, P. A., Fitz-Gibbon, S. T., Grossman, A. R., & Jonikas, M. C. (2016). An Indexed, Mapped Mutant Library Enables Reverse Genetics Studies of Biological Processes in *Chlamydomonas reinhardtii*. *The Plant Cell*, *28*(2), 367–387. <https://doi.org/10.1105/tpc.15.00465>
- Lopez, D., Hamaji, T., Kropat, J., De Hoff, P., Morselli, M., Rubbi, L., Fitz-Gibbon, S., Gallaher, S. D., Merchant, S. S., Umen, J., & Pellegrini, M. (2015). Dynamic Changes in the Transcriptome and Methylome of *Chlamydomonas reinhardtii* throughout Its Life Cycle. *Plant Physiology*, *169*(4), 2730–2743. <https://doi.org/10.1104/pp.15.00861>
- Lui, J., Castelli, L. M., Pizzinga, M., Simpson, C. E., Hoyle, N. P., Bailey, K. L., Campbell, S. G., & Ashe, M. P. (2014). Granules harboring translationally active mRNAs provide a platform for P-body formation following stress. *Cell Rep*, *9*(3), 944–954. <https://doi.org/10.1016/j.celrep.2014.09.040> S2211-1247(14)00823-7 [pii]
- Mackinder, L. C. M., Meyer, M. T., Mettler-Altmann, T., Chen, V. K., Mitchell, M. C., Caspari, O., Rosenzweig, E. S. F., Pallesen, L., Reeves, G., Itakura, A., Roth, R., Sommer, F., Geimer, S., Mühlhaus, T., Schroda, M., Goodenough, U., Stitt, M., Griffiths, H., & Jonikas, M. C. (2016). A repeat protein links Rubisco to form the eukaryotic carbon-concentrating organelle. *Proceedings of the National Academy of Sciences*, *113*(21), 5958–5963. <https://doi.org/10.1073/pnas.1522866113>
- Martin, W. (2010). Evolutionary origins of metabolic compartmentalization in eukaryotes. *Philosophical Transactions of the Royal Society B: Biological Sciences*, *365*(1541), 847–855. <https://doi.org/10.1098/rstb.2009.0252>
- Mason, C. B., Bricker, T. M., & Moroney, J. V. (2006a). A rapid method for chloroplast isolation from the green alga *Chlamydomonas reinhardtii*. *Nat Protoc*, *1*(5), 2227–2230.
- Mason, C. B., Bricker, T. M., & Moroney, J. V. (2006b). A rapid method for chloroplast isolation from the green alga *Chlamydomonas reinhardtii*. *Nature Protocols*, *1*(5), 2227–2230. <https://doi.org/10.1038/nprot.2006.348>
- Matsumoto, S., Uchiumi, T., Saito, T., Yagi, M., Takazaki, S., Kanki, T., & Kang, D. (2012). Localization of mRNAs encoding human mitochondrial oxidative phosphorylation proteins. *Mitochondrion*, *12*(3), 391–398. <https://doi.org/10.1016/j.mito.2012.02.004>

- Merchant, S. S., Allen, M. D., Kropat, J., Moseley, J. L., Long, J. C., Tottey, S., & Terauchi, A. M. (2006). Between a rock and a hard place: Trace element nutrition in *Chlamydomonas*. *Biochimica et Biophysica Acta (BBA) - Molecular Cell Research*, 1763(7), 578–594. <https://doi.org/10.1016/j.bbamcr.2006.04.007>
- Merchant, S. S., Prochnik, S. E., Vallon, O., Harris, E. H., Karpowicz, S. J., Witman, G. B., Terry, A., Salamov, A., Fritz-Laylin, L. K., Maréchal-Drouard, L., Marshall, W. F., Qu, L.-H., Nelson, D. R., Sanderfoot, A. A., Spalding, M. H., Kapitonov, V. V., Ren, Q., Ferris, P., Lindquist, E., ... Grossman, A. R. (2007). The *Chlamydomonas* Genome Reveals the Evolution of Key Animal and Plant Functions. *Science*, 318(5848), 245–250. <https://doi.org/10.1126/science.1143609>
- Meyer, M. T., Itakura, A. K., Patena, W., Wang, L., He, S., Emrich-Mills, T., Lau, C. S., Yates, G., Mackinder, L. C. M., & Jonikas, M. C. (n.d.). Assembly of the algal CO₂-fixing organelle, the pyrenoid, is guided by a Rubisco-binding motif. *Science Advances*, 6(46), eabd2408. <https://doi.org/10.1126/sciadv.abd2408>
- Mitchell, M. C., Meyer, M. T., & Griffiths, H. (2014). Dynamics of Carbon-Concentrating Mechanism Induction and Protein Relocalization during the Dark-to-Light Transition in Synchronized *Chlamydomonas reinhardtii*. *Plant Physiology*, 166(2), 1073–1082. <https://doi.org/10.1104/pp.114.246918>
- Moroney, J. V., Ma, Y., Frey, W. D., Fusilier, K. A., Pham, T. T., Simms, T. A., DiMario, R. J., Yang, J., & Mukherjee, B. (2011). The carbonic anhydrase isoforms of *Chlamydomonas reinhardtii*: Intracellular location, expression, and physiological roles. *Photosynthesis Research*, 109(1), 133–149. <https://doi.org/10.1007/s11120-011-9635-3>
- Moroney, J. V., & Ynalvez, R. A. (2007). Proposed Carbon Dioxide Concentrating Mechanism in *Chlamydomonas reinhardtii*. *Eukaryotic Cell*, 6(8), 1251–1259. <https://doi.org/10.1128/EC.00064-07>
- Mullock, B. M., & Luzio, J. P. (2013). Theory of Organelle Biogenesis: A Historical Perspective. In *Madame Curie Bioscience Database [Internet]*. Landes Bioscience. <https://www.ncbi.nlm.nih.gov/books/NBK6609/>
- Mussgnug, J. H. (2015). Genetic tools and techniques for *Chlamydomonas reinhardtii*. *Applied Microbiology and Biotechnology*, 99(13), 5407–5418. <https://doi.org/10.1007/s00253-015-6698-7>
- Nakai, M. (2018). New Perspectives on Chloroplast Protein Import. *Plant and Cell Physiology*, 59(6), 1111–1119. <https://doi.org/10.1093/pcp/pcy083>
- Nelson, N., & Ben-Shem, A. (2004a). The complex architecture of oxygenic photosynthesis. *Nature Reviews. Molecular Cell Biology*, 5(12), 971–982. <https://doi.org/10.1038/nrm1525>
- Nelson, N., & Ben-Shem, A. (2004b). The complex architecture of oxygenic photosynthesis. *Nat Rev Mol Cell Biol*, 5(12), 971–982. <https://doi.org/nrm1525> [pii] 10.1038/nrm1525
- Ott, M., & Herrmann, J. M. (2010). Co-translational membrane insertion of mitochondrially encoded proteins. *Biochimica et Biophysica Acta (BBA) - Molecular Cell Research*, 1803(6), 767–775. <https://doi.org/10.1016/j.bbamcr.2009.11.010>
- Panasenko, O. O., Somasekharan, S. P., Villanyi, Z., Zagatti, M., Bezrukov, F., Rashpa, R., Cornut, J., Iqbal, J., Longis, M., Carl, S. H., Peña, C., Panse, V. G., & Collart, M. A. (2019). Co-translational assembly of

- proteasome subunits in NOT1-containing assemblyosomes. *Nature Structural & Molecular Biology*, 26(2), 110–120. <https://doi.org/10.1038/s41594-018-0179-5>
- Peeters, N., & Small, I. (2001). Dual targeting to mitochondria and chloroplasts. *Biochimica et Biophysica Acta (BBA) - Molecular Cell Research*, 1541(1), 54–63. [https://doi.org/10.1016/S0167-4889\(01\)00146-X](https://doi.org/10.1016/S0167-4889(01)00146-X)
- Pröschold, T., Harris, E. H., & Coleman, A. W. (2005). Portrait of a Species: *Chlamydomonas reinhardtii*. *Genetics*, 170(4), 1601–1610. <https://doi.org/10.1534/genetics.105.044503>
- Quail, P. (1979). *Plant cell fractionation*. https://scholar.google.com/citations?view_op=view_citation&hl=en&user=xzNOM3kAAAAJ&citation_for_view=xzNOM3kAAAAJ:BrmTIyaxIBUC
- Rabl, R., Soubannier, V., Scholz, R., Vogel, F., Mendl, N., Vasiljev-Neumeyer, A., Körner, C., Jagasia, R., Keil, T., Baumeister, W., Cyrklaff, M., Neupert, W., & Reichert, A. S. (2009). Formation of cristae and crista junctions in mitochondria depends on antagonism between Fcj1 and Su e/g. *The Journal of Cell Biology*, 185(6), 1047–1063. <https://doi.org/10.1083/jcb.200811099>
- Rai, A. K., Chen, T., & Moroney, J. V. (2021). Mitochondrial carbonic anhydrases are needed for optimal photosynthesis at low CO₂ levels in *Chlamydomonas*. *Plant Physiology*, kiab351. <https://doi.org/10.1093/plphys/kiab351>
- Raines, C. A. (2003). The Calvin cycle revisited. *Photosynthesis Research*, 75(1), 1–10. <https://doi.org/10.1023/A:1022421515027>
- Redman, C. M., & Sabatini, D. D. (1966). Vectorial discharge of peptides released by puromycin from attached ribosomes. *Proceedings of the National Academy of Sciences of the United States of America*, 56(2), 608–615.
- Rochaix, J.-D. (2001). Assembly, Function, and Dynamics of the Photosynthetic Machinery in *Chlamydomonas reinhardtii*. *Plant Physiology*, 127(4), 1394–1398. <https://doi.org/10.1104/pp.010628>
- Rose, R. J. (2019). Sustaining Life: Maintaining Chloroplasts and Mitochondria and their Genomes in Plants. *The Yale Journal of Biology and Medicine*, 92(3), 499–510.
- Rumpho, M. E., Pochareddy, S., Worful, J. M., Summer, E. J., Bhattacharya, D., Pelletreau, K. N., Tyler, M. S., Lee, J., Manhart, J. R., & Soule, K. M. (2009). Molecular Characterization of the Calvin Cycle Enzyme Phosphoribulokinase in the Stramenopile Alga *Vaucheria litorea* and the Plastid Hosting Mollusc *Elysia chlorotica*. *Molecular Plant*, 2(6), 1384–1396. <https://doi.org/10.1093/mp/ssp085>
- Sakamoto, W., Miyagishima, S., & Jarvis, P. (2008). Chloroplast Biogenesis: Control of Plastid Development, Protein Import, Division and Inheritance. *The Arabidopsis Book / American Society of Plant Biologists*, 6, e0110. <https://doi.org/10.1199/tab.0110>
- Salomé, P. A., & Merchant, S. S. (2019). A Series of Fortunate Events: Introducing *Chlamydomonas* as a Reference Organism. *The Plant Cell*, 31(8), 1682–1707. <https://doi.org/10.1105/tpc.18.00952>
- Sambrook, J., & Russell, D. (2006). SDS-Polyacrylamide Gel Electrophoresis of Proteins. *CSH Protocols*, 2006. <https://doi.org/10.1101/pdb.prot4540>

- Sasso, S., Stibor, H., Mittag, M., & Grossman, A. R. (2018). From molecular manipulation of domesticated *Chlamydomonas reinhardtii* to survival in nature. *ELife*, *7*, e39233. <https://doi.org/10.7554/eLife.39233>
- Satoh, K. (2003). The identification of the Photosystem II reaction center: A personal story. *Photosynthesis Research*, *76*(1), 233. <https://doi.org/10.1023/A:1024933610778>
- Schmidt, E. K., Clavarino, G., Ceppi, M., & Pierre, P. (2009). SUnSET, a nonradioactive method to monitor protein synthesis. *Nat Methods*, *6*(4), 275–277. <https://doi.org/10.1038/nmeth.1314> [pii]
- Schottkowski, M., Peters, M., Zhan, Y., Rifai, O., Zhang, Y., & Zerges, W. (2012a). Biogenic membranes of the chloroplast in *Chlamydomonas reinhardtii*. *Proceedings of the National Academy of Sciences of the United States of America*, *109*(47), 19286–19291. <https://doi.org/10.1073/pnas.1209860109>
- Schottkowski, M., Peters, M., Zhan, Y., Rifai, O., Zhang, Y., & Zerges, W. (2012b). Biogenic membranes of the chloroplast in *Chlamydomonas reinhardtii*. *Proc Natl Acad Sci U S A*, *109*(47), 19286–19291. <https://doi.org/10.1073/pnas.1209860109> [pii]
- Shi, L.-X., & Theg, S. M. (2013). The chloroplast protein import system: From algae to trees. *Biochimica et Biophysica Acta (BBA) - Molecular Cell Research*, *1833*(2), 314–331. <https://doi.org/10.1016/j.bbamcr.2012.10.002>
- Shimizu, S. (2019). Organelle zones in mitochondria. *The Journal of Biochemistry*, *165*(2), 101–107. <https://doi.org/10.1093/jb/mvy068>
- Shin, S.-E., Lim, J.-M., Koh, H. G., Kim, E. K., Kang, N. K., Jeon, S., Kwon, S., Shin, W.-S., Lee, B., Hwangbo, K., Kim, J., Ye, S. H., Yun, J.-Y., Seo, H., Oh, H.-M., Kim, K.-J., Kim, J.-S., Jeong, W.-J., Chang, Y. K., & Jeong, B. (2016). CRISPR/Cas9-induced knockout and knock-in mutations in *Chlamydomonas reinhardtii*. *Scientific Reports*, *6*(1), 27810. <https://doi.org/10.1038/srep27810>
- Silflow, C. D., & Rosenbaum, J. L. (1981). Multiple α - and β -tubulin genes in *chlamydomonas* and regulation of tubulin mRNA levels after deflagellation. *Cell*, *24*(1), 81–88. [https://doi.org/10.1016/0092-8674\(81\)90503-1](https://doi.org/10.1016/0092-8674(81)90503-1)
- Singh, S. K., Sundaram, S., & Kishor, K. (2014). Carbon-Concentrating Mechanism. In S. K. Singh, S. Sundaram, & K. Kishor (Eds.), *Photosynthetic Microorganisms: Mechanism For Carbon Concentration* (pp. 5–38). Springer International Publishing. https://doi.org/10.1007/978-3-319-09123-5_2
- Soll, J., & Schleiff, E. (2004). Protein import into chloroplasts. *Nature Reviews Molecular Cell Biology*, *5*(3), 198–208. <https://doi.org/10.1038/nrm1333>
- Sommer, M. S., & Schleiff, E. (2014). Protein Targeting and Transport as a Necessary Consequence of Increased Cellular Complexity. *Cold Spring Harbor Perspectives in Biology*, *6*(8), a016055. <https://doi.org/10.1101/cshperspect.a016055>
- Spalding, M. H. (2008). Microalgal carbon-dioxide-concentrating mechanisms: *Chlamydomonas* inorganic carbon transporters. *Journal of Experimental Botany*, *59*(7), 1463–1473. <https://doi.org/10.1093/jxb/erm128>

- Stauber, E. J., Fink, A., Markert, C., Kruse, O., Johanningmeier, U., & Hippler, M. (2003). Proteomics of *Chlamydomonas reinhardtii* light-harvesting proteins. *Eukaryot Cell*, 2(5), 978–994.
- Stoldt, S., Wenzel, D., Kehrein, K., Riedel, D., Ott, M., & Jakobs, S. (2018). Spatial orchestration of mitochondrial translation and OXPHOS complex assembly. *Nat Cell Biol*, 20(5), 528–534. <https://doi.org/10.1038/s41556-018-0090-7> 10.1038/s41556-018-0090-7 [pii]
- Strenkert, D., Schmollinger, S., Gallaher, S. D., Salomé, P. A., Purvine, S. O., Nicora, C. D., Mettler-Altmann, T., Soubeyrand, E., Weber, A. P. M., Lipton, M. S., Basset, G. J., & Merchant, S. S. (2019). Multi-omics resolution of molecular events during a day in the life of *Chlamydomonas*. *Proceedings of the National Academy of Sciences*, 116(6), 2374–2383. <https://doi.org/10.1073/pnas.1815238116>
- Strittmatter, P., Soll, J., & Bölter, B. (2010). The chloroplast protein import machinery: A review. *Methods in Molecular Biology (Clifton, N.J.)*, 619, 307–321. https://doi.org/10.1007/978-1-60327-412-8_18
- Sun, Y., Valente-Paterno, M., Bakhtiari, S., Law, C., Zhan, Y., & Zerges, W. (2019a). Photosystem Biogenesis Is Localized to the Translation Zone in the Chloroplast of *Chlamydomonas*. *The Plant Cell*, 31(12), 3057–3072. <https://doi.org/10.1105/tpc.19.00263>
- Sun, Y., Valente-Paterno, M. I., Bakhtiari, S., Law, C., Zhan, Y., & Zerges, W. (2019b). Photosystem Biogenesis Is Localized to the Translation Zone in the Chloroplast of *Chlamydomonas*. *Plant Cell*. <https://doi.org/10.1105/tpc.19.00263>
- Suss, K. H., Prokhorenko, I., & Adler, K. (1995). In Situ Association of Calvin Cycle Enzymes, Ribulose-1,5-Bisphosphate Carboxylase/Oxygenase Activase, Ferredoxin-NADP+ Reductase, and Nitrite Reductase with Thylakoid and Pyrenoid Membranes of *Chlamydomonas reinhardtii* Chloroplasts as Revealed by Immunoelectron Microscopy. *Plant Physiology*, 107(4), 1387–1397.
- Thomson, S. M., Pulido, P., & Jarvis, R. P. (2020). Protein import into chloroplasts and its regulation by the ubiquitin-proteasome system. *Biochemical Society Transactions*, 48(1), 71–82. <https://doi.org/10.1042/BST20190274>
- Toya, M., Iida, Y., & Sugimoto, A. (2010). Chapter 19—Imaging of Mitotic Spindle Dynamics in *Caenorhabditis elegans* Embryos. In L. Cassimeris & P. Tran (Eds.), *Methods in Cell Biology* (Vol. 97, pp. 359–372). Academic Press. [https://doi.org/10.1016/S0091-679X\(10\)97019-2](https://doi.org/10.1016/S0091-679X(10)97019-2)
- Tsanov, N., Samacoits, A., Chouaib, R., Traboulsi, A.-M., Gostan, T., Weber, C., Zimmer, C., Zibara, K., Walter, T., Peter, M., Bertrand, E., & Mueller, F. (2016a). SmiFISH and FISH-quant – a flexible single RNA detection approach with super-resolution capability. *Nucleic Acids Research*, 44(22), e165. <https://doi.org/10.1093/nar/gkw784>
- Tsanov, N., Samacoits, A., Chouaib, R., Traboulsi, A.-M., Gostan, T., Weber, C., Zimmer, C., Zibara, K., Walter, T., Peter, M., Bertrand, E., & Mueller, F. (2016b). SmiFISH and FISH-quant – a flexible single RNA detection approach with super-resolution capability. *Nucleic Acids Research*, 44(22), e165–e165. <https://doi.org/10.1093/nar/gkw784>
- Ullmann, G. M. (2001). Chapter 6—Charge Transfer Properties of Photosynthetic and Respiratory Proteins† this work was partially written at the Freie Universität Berlin, Department of Biology, Chemistry, and Pharmacy, Institute of Chemistry, Takustr. 6, 14195 Berlin (Germany) and The Scripps Research

Institute, Department of Molecular Biology, 10550 N. Torrey Pines Rd., TPC-15, La Jolla, CA 92037 USA. In H. S. Nalwa (Ed.), *Supramolecular Photosensitive and Electroactive Materials* (pp. 525–584). Academic Press. <https://doi.org/10.1016/B978-012513904-5/50008-9>

Uniacke, J., Colón-Ramos, D., & Zerges, W. (2011). FISH and immunofluorescence staining in *Chlamydomonas*. *Methods Mol Biol*, *714*, 15–29. https://doi.org/10.1007/978-1-61779-005-8_2

Uniacke, J., Colón-Ramos, D., & Zerges, W. (2011). FISH and Immunofluorescence Staining in *Chlamydomonas*. In J. E. Gerst (Ed.), *RNA Detection and Visualization: Methods and Protocols* (pp. 15–29). Humana Press. https://doi.org/10.1007/978-1-61779-005-8_2

Uniacke, J., & Zerges, W. (2007a). Photosystem II Assembly and Repair Are Differentially Localized in *Chlamydomonas*. *The Plant Cell*, *19*(11), 3640–3654. <https://doi.org/10.1105/tpc.107.054882>

Uniacke, J., & Zerges, W. (2007b). Photosystem II assembly and repair are differentially localized in *Chlamydomonas*. *Plant Cell*, *19*(11), 3640–3654. <https://doi.org/tpc.107.054882> [pii] 10.1105/tpc.107.054882

Uniacke, J., & Zerges, W. (2009a). Chloroplast protein targeting involves localized translation in *Chlamydomonas*. *Proceedings of the National Academy of Sciences*, *106*(5), 1439–1444. <https://doi.org/10.1073/pnas.0811268106>

Uniacke, J., & Zerges, W. (2009b). Chloroplast protein targeting involves localized translation in *Chlamydomonas*. *Proc Natl Acad Sci U S A*, *106*(5), 1439–1444. <https://doi.org/10.1073/pnas.0811268106> 0811268106 [pii]

Vitha, S., & Osteryoung, K. W. (2011). Immunofluorescence microscopy for localization of Arabidopsis chloroplast proteins. *Methods in Molecular Biology (Clifton, N.J.)*, *774*, 33–58. https://doi.org/10.1007/978-1-61779-234-2_3

Vogel, F., Bornhovd, C., Neupert, W., & Reichert, A. S. (2006). Dynamic subcompartmentalization of the mitochondrial inner membrane. *J Cell Biol*, *175*(2), 237–247. <https://doi.org/jcb.200605138> [pii] 10.1083/jcb.200605138

Vogel, F., Bornhövd, C., Neupert, W., & Reichert, A. S. (2006). Dynamic subcompartmentalization of the mitochondrial inner membrane. *The Journal of Cell Biology*, *175*(2), 237–247. <https://doi.org/10.1083/jcb.200605138>

Vothknecht, U. C., & Westhoff, P. (2001). Biogenesis and origin of thylakoid membranes. *Biochimica et Biophysica Acta (BBA) - Molecular Cell Research*, *1541*(1), 91–101. [https://doi.org/10.1016/S0167-4889\(01\)00153-7](https://doi.org/10.1016/S0167-4889(01)00153-7)

Wallace, D. C. (1982). Structure and evolution of organelle genomes. *Microbiological Reviews*, *46*(2), 208–240.

Wang, Y., Stessman, D. J., & Spalding, M. H. (2015). The CO₂ concentrating mechanism and photosynthetic carbon assimilation in limiting CO₂: How *Chlamydomonas* works against the gradient. *The Plant Journal*, *82*(3), 429–448. <https://doi.org/10.1111/tpj.12829>

- Watson, K. (1972). THE ORGANIZATION OF RIBOSOMAL GRANULES WITHIN MITOCHONDRIAL STRUCTURES OF AEROBIC AND ANAEROBIC CELLS OF SACCHAROMYCES CEREVISAE. *Journal of Cell Biology*, 55(3), 721–726. <https://doi.org/10.1083/jcb.55.3.721>
- Weis, B. L., Schleiff, E., & Zerges, W. (2013a). Protein targeting to subcellular organelles via mRNA localization. *Biochim Biophys Acta*, 1833(2), 260–273.
- Weis, B. L., Schleiff, E., & Zerges, W. (2013b). Protein targeting to subcellular organelles via mRNA localization. *Biochimica et Biophysica Acta (BBA) - Molecular Cell Research*, 1833(2), 260–273. <https://doi.org/10.1016/j.bbamcr.2012.04.004>
- Wellen, K. E., & Snyder, N. W. (2019). Should we consider subcellular compartmentalization of metabolites, and if so, how do we measure them? *Current Opinion in Clinical Nutrition and Metabolic Care*, 22(5), 347–354. <https://doi.org/10.1097/MCO.0000000000000580>
- Williams, C. C., Jan, C. H., & Weissman, J. S. (2014a). Targeting and plasticity of mitochondrial proteins revealed by proximity-specific ribosome profiling. *Science (New York, N.Y.)*, 346(6210), 748–751. <https://doi.org/10.1126/science.1257522>
- Williams, C. C., Jan, C. H., & Weissman, J. S. (2014b). Targeting and plasticity of mitochondrial proteins revealed by proximity-specific ribosome profiling. *Science*, 346(6210), 748–751. <https://doi.org/10.1126/science.1257522>
- Wingfield, J. L., & Lechtreck, K.-F. (2018). Chlamydomonas Basal Bodies as Flagella Organizing Centers. *Cells*, 7(7), 79. <https://doi.org/10.3390/cells7070079>
- Wollman, F.-A., Minai, L., & Nechushtai, R. (1999). The biogenesis and assembly of photosynthetic proteins in thylakoid membranes. This article is dedicated to the memory of our colleague and friend, Alma Gal. Her presence played a major role in our decision to prepare this review article. *Biochimica et Biophysica Acta (BBA) - Bioenergetics*, 1411(1), 21–85. [https://doi.org/10.1016/S0005-2728\(99\)00043-2](https://doi.org/10.1016/S0005-2728(99)00043-2)
- Yamano, T., Sato, E., Iguchi, H., Fukuda, Y., & Fukuzawa, H. (2015a). Characterization of cooperative bicarbonate uptake into chloroplast stroma in the green alga *Chlamydomonas reinhardtii*. *Proc Natl Acad Sci U S A*, 112(23), 7315–7320. <https://doi.org/10.1073/pnas.1501659112>
- Yamano, T., Sato, E., Iguchi, H., Fukuda, Y., & Fukuzawa, H. (2015b). Characterization of cooperative bicarbonate uptake into chloroplast stroma in the green alga *Chlamydomonas reinhardtii*. *Proceedings of the National Academy of Sciences*, 112(23), 7315–7320. <https://doi.org/10.1073/pnas.1501659112>
- Zecchin, A., Stapor, P. C., Goveia, J., & Carmeliet, P. (2015). Metabolic pathway compartmentalization: An underappreciated opportunity? *Current Opinion in Biotechnology*, 34, 73–81. <https://doi.org/10.1016/j.copbio.2014.11.022>
- Zerges, W. (2000). Translation in chloroplasts. *Biochimie*, 82(6–7), 583–601. [https://doi.org/10.1016/s0300-9084\(00\)00603-9](https://doi.org/10.1016/s0300-9084(00)00603-9)
- Zerges, W., & Rochaix, J. D. (1998). Low density membranes are associated with RNA-binding proteins and thylakoids in the chloroplast of *Chlamydomonas reinhardtii*. *J Cell Biol*, 140(1), 101–110.

Zerges, W., Wang, S., & Rochaix, J.-D. (2002). Light activates binding of membrane proteins to chloroplast RNAs in *Chlamydomonas reinhardtii*. *Plant Molecular Biology*, *50*(3), 573–585. <https://doi.org/10.1023/a:1020246007858>

Zhan, Y., Marchand, C. H., Maes, A., Mauries, A., Sun, Y., Dhaliwal, J. S., Uniacke, J., Arragain, S., Jiang, H., Gold, N. D., Martin, V. J. J., Lemaire, S. D., & Zerges, W. (2018). Pyrenoid functions revealed by proteomics in *Chlamydomonas reinhardtii*. *PLoS ONE*, *13*(2), e0185039. <https://doi.org/10.1371/journal.pone.0185039>

Zipor, G., Haim-Vilmovsky, L., Gelin-Licht, R., Gadir, N., Brocard, C., & Gerst, J. E. (2009). Localization of mRNAs coding for peroxisomal proteins in the yeast, *Saccharomyces cerevisiae*. *Proceedings of the National Academy of Sciences*, *106*(47), 19848–19853. <https://doi.org/10.1073/pnas.0910754106>

Zones, J. M., Blaby, I. K., Merchant, S. S., & Umen, J. G. (2015). High-Resolution Profiling of a Synchronized Diurnal Transcriptome from *Chlamydomonas reinhardtii* Reveals Continuous Cell and Metabolic Differentiation. *The Plant Cell*, *27*(10), 2743–2769. <https://doi.org/10.1105/tpc.15.00498>

Zorkau, M., Albus, C. A., Berlinguer-Palmini, R., Chrzanowska-Lightowlers, Z. M. A., & Lightowlers, R. N. (2021). High-resolution imaging reveals compartmentalization of mitochondrial protein synthesis in cultured human cells. *Proceedings of the National Academy of Sciences*, *118*(6). <https://doi.org/10.1073/pnas.2008778118>

SUPPLEMENTAL DATA

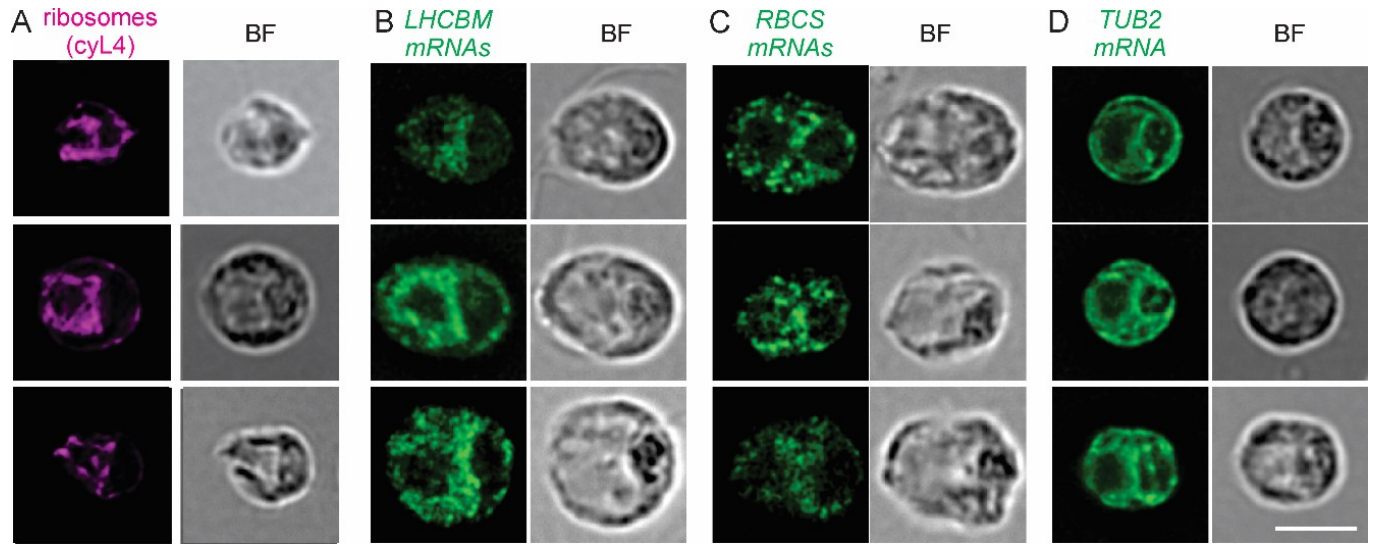


Figure S2.1. Localization patterns reported previously. Epifluorescence microscopy images of cells that were (A) IF-stained for cyL4 or (B-D) FISH-probed for (B) the LHCBM mRNAs, (C) the RBCS mRNAs or the (D) TUB2 mRNA. These cells show patterns that were reported previously (Colon-Ramos et al., 2003; Uniacke & Zerges, 2009b); cyL4, LHCBM mRNAs and RBCS mRNAs, and TUB2 mRNA. Error bar = 5.0 μ m. Create a page break and paste in the Figure above the caption.

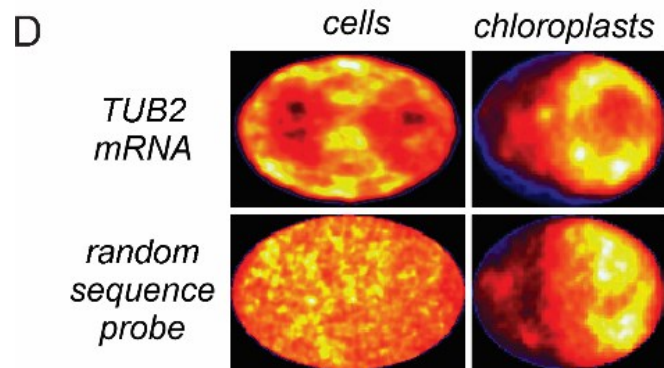
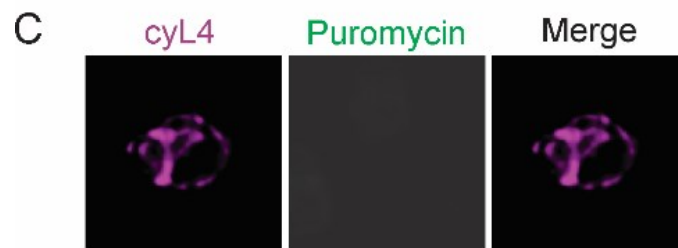
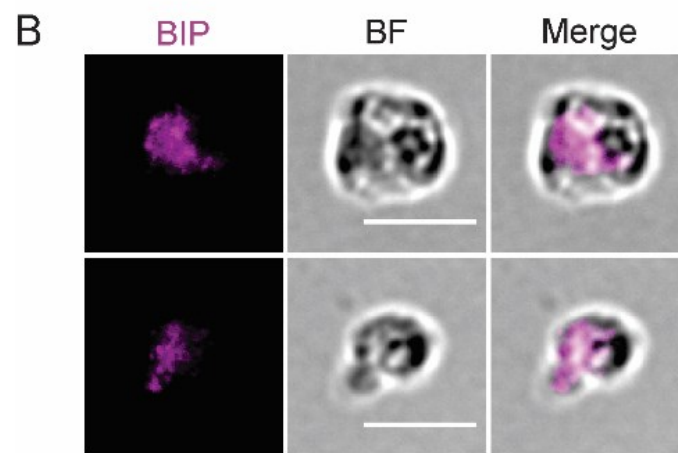
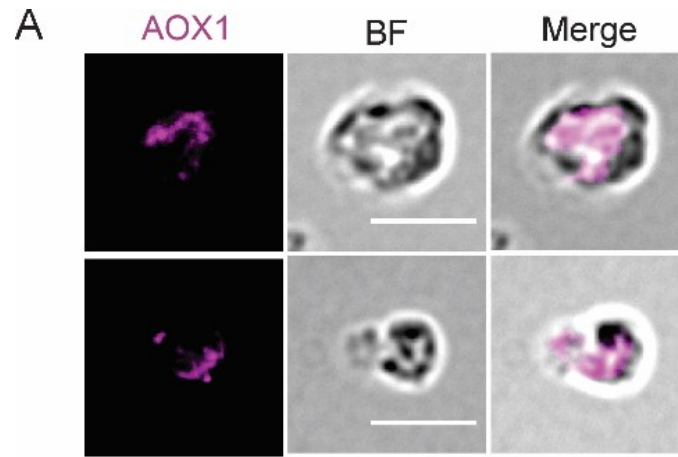


Figure S2.2. Experimental controls. Isolated chloroplasts that were IF-stained for marker proteins for (A) mitochondria (AOX1) or (B) endoplasmic reticulum (BIP) do not show the localization pattern seen for (C) the ribosome marker protein (cyL4). (C) In the RiboPuromylation method results (Figure 3), the puromycin IF signal seen at the localized IF signal from cytoplasmic ribosomes (cyL4) on isolated chloroplasts is specific; it was not detected from chloroplasts that were not treated with puromycin. (D) The average distributions of the TUB2 mRNA FISH signal from all imaged cells and chloroplasts is compared to average distributions of the background signal from a control FISH probe with a random sequence that is not in the *Chlamydomonas* genome. The distributions of the average TUB2 mRNA and control FISH signals differ in cells, supporting the former as representing this mRNA. From chloroplasts, the signals are both weak and their distributions are similar, suggesting that much or all TUB2 mRNA FISH signal from chloroplasts is background.

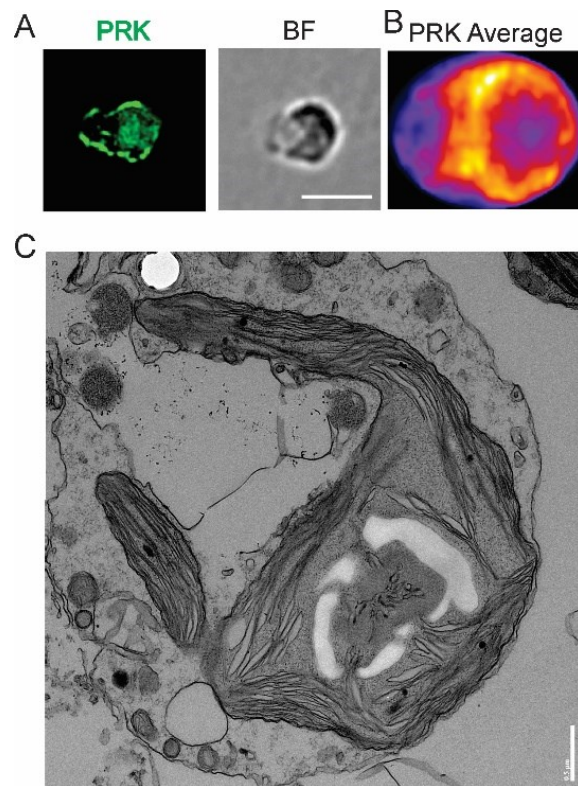


Figure S2.3. The isolated chloroplasts retain normal morphology (see Figure 1A for reference).

(A) An isolated chloroplast IF stained for phosphoribulose kinase (PRK) to reveal the entire chloroplast and its retention of normal morphology during isolation. (B) A heatmap of the average PRK signal across all chloroplasts of the data set shows entire chloroplast and contrasts the heatmaps of the IF-signals of *cyL4* (Figure 1D), puromycin (Figure 3C), and the FISH signals from the *LHCB* and *RBCS* mRNAs (Figure 4E) ($n=30$). (C) Transmission EM image of an isolated chloroplast shows that it has normal morphology. Cells were collected from cultures entrained to the diurnal cycle and processed as described previously (Sun et al., 2019b). Images were acquired on a FEI Tecnai 12 120kv Transmission electron microscope using the Tecnai User Interface software and an AMTv601 CCD Camera. Settings used were an aperture of 3, a spot size of 2, and variable magnifications ranging from 2,900X to 68,000X.

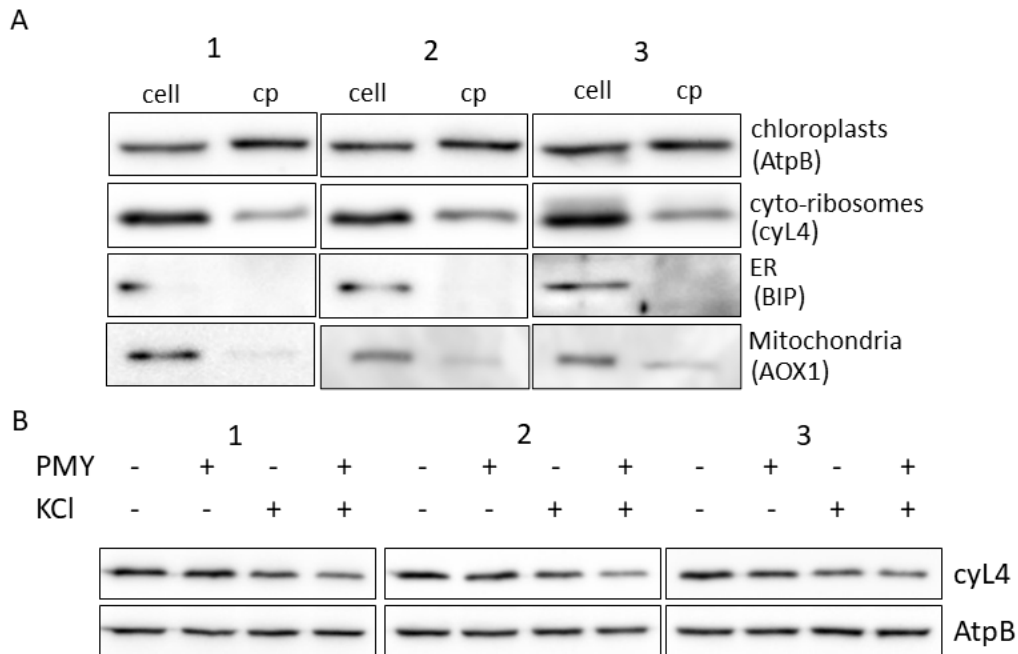


Figure S2.4. (A) These immunoblot results are represented by the bar heights in Figure 1B. Trials 1-3 are three biological replicate experiments, each performed from an independent culture. (B) These immunoblot results are represented by the bar heights in Figure 3C. Note the different order of treatments here and in the bar graph in Fig. 3D. Trials 1-3 are three biological replicate experiments, each performed from an independent culture and all conducted in parallel, including the immunoblots transfer, immune-reaction steps, and ECL imaging. KCl, incubation in 750 mM KCl; puromycin, PMY. The chloroplast protein AtpB was used as a loading control.

Movie S2.1. 3D reconstruction of ribosome-bound domain in the chloroplast

Slices from a tomographic volume and different views of the corresponding 3D reconstruction. The tomograph shows the region of the chloroplast envelope that was bound by cyto-ribosomes as seen by IF microscopy (Fig. 1C). The 3D model illustrates the cytoplasmic face of the outer chloroplast envelope (light grey) and cyto-ribosomes on the envelope (blue spheres). Corresponds to Figure 2C-E.

Movie S2.2. 3D reconstruction of lobe region in the chloroplast

Slices from a tomographic volume and different views of the corresponding 3D reconstruction showing the chloroplast lobe. The 3D model illustrates the cytoplasmic face of the outer chloroplast envelope (light grey), the stromal face of the inner membrane (dark grey) and cyto-ribosomes on the envelope (blue spheres). Corresponds to Fig. 2F-G.

Table S2.1. Sequences of FISH probes used in chapter 2

		Probe Name	Probe Sequence (5' to 3')
FLAP;		FLAP X-Cy3	Cy3/C ACT GAG TCC AGC TCG AAA CTT AGG AGG/Cy3
LHCB M	LHCBM7 Cre12.g548950 *≥95% sequence identity to the mRNA of LHCBM2 Cre12.g548400		mRNA-specific sequences of the probes are given below (5' to 3'). The complete sequence of each has a the same 3' extension with the reverse complement of FLAP X-CY3 probe; CCTCCTAAGTTTCGAGCTGGACTCAGTG
		LHCII- 1	GAGGACTTCATGATGGCGGCCATTTTGA TTG
		LHCII- 2*	AAGAAGCCGAACATGGAGAACATAGCC AGGC
		LHCII- 3	GTACATGCAGCTGCCGAGGGCCAAAAT TTA
		LHCII- 4	GCTCCTAAGCCTGTGAAAAGAGGCTCAC ACT
		LHCII- 5*	GTCGCCCTCCGAGAAGGGGCCAGGAA CTTC

		LHCII- 6*	GACAGACCGGCGGTGTCCCAGCCGTAGT CGC
		LHCII- 7	GATCAGCTCCAGCTCGCGGTAGCGCTTG AAG
		LHCII- 8*	CCTTGAACCAGACAGCCTCACCGAACGG GAT
		LHCII- 9*	AGGTAGTTCAGGCCGCCCTCAGCGAAGA TCT
		LHCII-10*	ATGATGGACTGGGCGTGGATCAGGTTCT CGT
		LHCII-11*	TCAGCCAGGCCCATCACCACAACCTGGA AGG
		LHCII-12*	ATCTCCTTCACCTTCAGCTCAGCGAAGG TGT
		LHCII-13	CGTAGCACCGCCACTTCGGTTAATCGCA CGT
		LHCII-14	CAAAACCCGAACACAAAACCTGAACCTCC GTA
		LHCII-15	GTGAACTTGGTGGCGTAGGCCGAACGCGT TCA
		LHCII-16*	TTGGCCAGGTGGTCGTCCAGGTTCTGGA TGG

		LHCII-17*	ATGCAGCCCAGAGCGCCCAGCATGGCCC AGC
		LHCII-18	ACCGGCTGCTCACGGTGGAGCGCACGGA GCT
		LHCII-19	CACCGCGCTCCTCTTCATCTCCGCTCAAT CA
		LHCII-20	GTGGCCGTCAAGCCATTTTTAGTCTTCTC AA
		LHCII-21	TGCCGTGTTACACAACAAGGGCAAATCG CAA
		LHCII-22	TAGACAGCTAGAACAAGCAGGCTGTA AAGA
		LHCII-23	TCAGCCAGGCCAGGGGGTCAAAGGCA CCAC
		LHCII-24*	CCACTCGATGGCAGCGCGGGGCACCACG CGA
RBCS	RBCS2 Cre02.g120150 * \geq 95% sequence identity to the mRNA of		

	RBCS1 ($\geq 95\%$ identity) Cre02.g120100		
		RbcS- 1	ACCCCATCAAACATCATCCTGGTTTGGC TGC
		RbcS- 2	GGCGGCCATTTTAAGATGTTGAGTGACT TCT
		RbcS- 3*	GTCCAGACCATCATCTGGTTGGCCTGAG CCG
		RbcS- 4*	GGTCCAGTAGCGGTTGTCGTAGTACAGC TGC
		RbcS- 5*	ATGATCTGCACCTGCTTCTGGTTGTCGA AGG
		RbcS- 6*	TTGGTGCAGGCGACGATCTCGCGCAGCA CCT
		RbcS- 7	ACACGTAGGCCTTGTCCGACTCAGCGAA CTC
		RbcS- 8	AATGTAGTCGACCTGGGCGGCGATCTGC TCG
		RbcS- 9*	GCCACGGCCGCGGAGACGGAGGACTTG GCAA
		RbcS-10	TTACACGGAGCGCTTGTTGGCGGGCTGC CAG

		RbcS-11*	TCGCGGCAGCCGAACATGGGCAGCTTCC ACA
		RbcS-12*	CAAGACACGCTGCCGAAGCGGATGGCC GACT
		RbcS-13*	GCCTTGACGGCGGGCTTCAGCGCGGCCA TGG
		RbcS-14	TAGGAGAAGGTCTCGAACATCTTGTGT TGA
		RbcS-15	AGCAGTATCTTCCATCCACCGCCGTTCC TCA
		RbcS-16	GCACGAAACGGGGAGCTAAGCTACCGC TTCA
		RbcS-17	TGCAAAACTCCTCCGCTTTTTACGTGTTG AA
		RbcS-18	GGGGCAAGGCTCAGATCAACGAGCGCC TCCA
TUB2	Cre12.g549550		
		Tubulin-1	CGATCACAAGCTCGAGTGGCCTGTGTAG AAG
		Tubulin-2	AAACCATGACGGCAAAAACATTATCAA GCAT
		Tubulin-3	TACGAAGAGTTCTTGTCTGCACGTTCA GCA

		Tubulin-4	GCCTCCACACCAAAGCGTCAAATGGCAA TCA
		Tubulin-5	CAGCTGCTATGGCCTATCACACAAGAGC TAA
Non-specific sequenc e		Scramble	CTGAGTTAAGGCTTTCCACGGACGAGTT AAT

Table S 3.1. Sequences of FISH probes used in Chapter 3

		Probe Name	Probe Sequence (5' to 3')
FLAP; Fluor- conjugate d oligo for labeling mRNA-		FLAP X- Cy3	Cy3/C ACT GAG TCC AGC TCG AAA CTT AGG AGG/Cy3

specific probes			
PSBA	PSBA		mRNA-specific sequences of the probes are given below (5' to 3'). The complete sequence of each has a the same 3' extension with the reverse complement of FLAP X-CY3 probe; CCTCCTAAGTTTCGAGCTGGACTCAGTG
		PsbA-2	AAGAAGACATGGGATCATGATTACACCGAAC
		PsbA-3	G TTCACGGATACCATCGATGTCTACTGGCGGA
		PsbA-4	CAGCACCTGTAATGATGTTGTTACCGTAAAGA
		PsbA-6	ATAATTCCCCTCACGACCCATGTAGCAGTAT
		PsbA-9	TGAAAGTACCAGAGATACCTAAAGGCATACCG
		PsbA-11	AATAATGAACCACCGAATACACCAGCAACACC
		PsbA-12	TCGTTAGCTGATTCGTTTTTCAGTTGTTTCACG
		PsbA-13	GACGACCAAAGTAACCATGAGCAGCTACAA TG
		PsbA-15	TGCCATAGTTGATAAACCTAAAGCAGTGAA CC
		PsbA-16	CACGACCTTGTGAGTCTACTACTGATTGGTT G

APPENDIX I: Photosystem Biogenesis Is Localized to the Translation Zone in the Chloroplast of *Chlamydomonas* (Sun et al., 2019)

Yi Sun,^{a,1} Melissa Valente-Paterno,^{a,1} Shiva Bakhtiari,^a Christopher Law,^b Yu Zhan,^a and William Zerges^{a,2}

^aDepartment of Biology and Centre for Structural and Functional Genomics, Concordia University, Montreal, Quebec H4B 1R6, Canada

^bCentre for Microscopy and Cellular Imaging, Concordia University, Montreal, Quebec H4B 1R6, Canada

ORCID IDs: 0000-0002-2366-7153 (Y.S.); 0000-0001-8470-3739 (M.V.-P.); 0000-0002-8737-3170 (S.B.); 0000-0002-6946-8029 (C.L.); 0000-0002-8965-9631 (Y.Z.); 0000-0003-4575-5100 (W.Z.).

Intracellular processes can be localized for efficiency or regulation. For example, localized mRNA translation by chloroplastic ribosomes occurs in the biogenesis of PSII, one of the two photosystems of the photosynthetic electron transport chain in the chloroplasts of plants and algae. The biogenesis of PSI and PSII requires the synthesis and assembly of their constituent polypeptide subunits, pigments, and cofactors. Although these biosynthetic pathways are well characterized, less is known about when and where they occur in developing chloroplasts. Here, we used fluorescence microscopy in the unicellular alga *Chlamydomonas reinhardtii* to reveal spatiotemporal organization in photosystem biogenesis. We focused on translation by chloroplastic ribosomes and chlorophyll biosynthesis in two developmental contexts of active photosystem biogenesis: (1) growth of the mature chloroplast and (2) greening of a nonphotosynthetic chloroplast. The results reveal that a translation zone is the primary location of the biogenesis of PSI and PSII. This discretely localized region within the chloroplast contrasts with the distributions of photosystems throughout this organelle and, therefore, is likely a hub where anabolic pathways converge for photosystem biogenesis.

INTRODUCTION

Intracellular processes can be localized for a variety of benefits (e.g., enhanced efficiency, regulation, and the prevention of deleterious side reactions). Within the cells of plants and algae, photosynthesis and other essential processes are performed in chloroplasts. These processes include photosynthetic electron transport (PET) and ATP synthesis, which occur in the membranes of vesicles called thylakoids within this organelle. The PET system includes three major complexes: PSII, the cytochrome *b₆f* complex (Cytb₆f), and PSI. The photosystems act as solar-powered molecular battery chargers by using light energy to drive electrons from low-energy to high-energy redox half-reactions, analogous to the charging of the half-cells of a battery. The high energy half-reactions are then used to drive downstream redox reactions in photosynthesis (Nelson and Ben-Shem, 2004).

The biogenesis of the photosystems requires the concerted synthesis and assembly of their component protein subunits, pigments, and cofactors. The spatial organization of these biogenic processes is complex due to the evolution of the plastids from a cyanobacterial endosymbiont (Elias and Archibald, 2009). Many subunits are encoded by the organellar genome and synthesized by bacterial-type chloroplastic ribosomes (Jarvis and López-Juez, 2013). Other subunits are synthesized in the cytoplasm and imported into the chloroplast. The PSII subunit PsbA

(also known as D1) is synthesized into thylakoid membranes exposed to the chloroplast stroma for the repair of photodamaged PSII complexes (Mattoo and Edelman, 1987; van Wijk et al., 1996; Chotewutmontri and Barkan, 2018).

In plants, subunit synthesis for de novo photosystem biogenesis occurs in association with membranes that are presumed to be stroma-exposed thylakoid membranes (Zoschke and Barkan, 2015; Legen and Schmitz-Linneweber, 2017). However, in the unicellular green alga *Chlamydomonas* (*Chlamydomonas reinhardtii*), a translation zone (T-zone) is the primary location of the synthesis of the PSII subunits that are encoded by the plastid genome (Uniacke and Zerges, 2007, 2009; Schottkowski et al., 2012). The T-zone is more discretely localized than the broad distribution of PSII in the membranes of thylakoids throughout the chloroplast. It is unknown whether the T-zone is also the location of the biogenesis of other PET complexes.

A similar narrative describes our understanding of the biosynthesis of chlorophyll, the major photopigment in PSI, PSII, and their light-harvesting complexes (LHCs). The enzymes in the chlorophyll branch of the tetrapyrrole biosynthetic pathway are well characterized and many are membrane associated (Czarnecki and Grimm, 2012). However, precisely where these enzymes act within chloroplasts is controversial (Joyard et al., 2009). In the cyanobacterium *Synechocystis* PCC 6803, chlorophyll synthase is physically associated with the machinery that drives cotranslational insertion of nascent photosystem polypeptides into the thylakoid membrane (Chidgey et al., 2014). At least one enzyme in the chlorophyll biosynthetic pathway is associated with polysomes in the chloroplasts of barley (*Hordeum vulgare*; Kannangara et al., 1997). It remains to be determined whether chlorophyll biosynthesis and photosystem biogenesis are colocalized in chloroplasts.

¹ These authors contributed equally to this work.

² Address correspondence to william.zerges@concordia.ca.

The author responsible for distribution of materials integral to the findings presented in this article in accordance with the policy described in the Instructions for Authors (www.plantcell.org) is William Zerges (william.zerges@concordia.ca).

www.plantcell.org/cgi/doi/10.1105/tpc.19.00263

IN A NUTSHELL

Background: Cells localize intracellular processes to subcellular organelles in order to enhance their efficiency. For example, in plant and algal cells, chloroplasts carry out photosynthesis. Within chloroplasts, photosystems I and II carry out the initial steps in photosynthesis by harvesting light energy and converting it to chemical energy. These photosystems are composed of protein subunits, chlorophyll, and cofactors. Many photosystem subunits are encoded by the genome of the chloroplast and synthesized by ribosomes within this bacterial-like evolutionary descendent of an ancient cyanobacterium. The *de novo* generation of the photosystems is widely believed to occur throughout the chloroplast. The precise location(s) of chlorophyll synthesis in chloroplasts is controversial. Previous work in our laboratory revealed localized synthesis of photosystem II subunits in a discrete "translation zone" in the chloroplast of the unicellular green alga *Chlamydomonas reinhardtii*. However, it is unknown whether the translation zone organizes the synthesis and assembly of photosystem I subunits or chlorophyll biosynthesis.

Question: We asked whether the translation zone organizes the generation of both photosystems in two distinct developmental contexts; growth for subsequent chloroplast division or differentiation from a non-photosynthetic progenitor organelle.

Findings: Our results demonstrate that the translation zone is where the protein subunits and chlorophyll are synthesized and assembled to generate both photosystems I and II in chloroplasts undergoing chloroplast growth or chloroplast differentiation. In addition, to increase the objectivity of our fluorescence microscopy image analyses, we developed a protocol and program that displays the average intracellular distributions of specific proteins and mRNAs from all cells in each experiment in a single image or graph.

Next steps: Future research will characterize the ultrastructure of the translation zone, the intra-chloroplast dynamics involved in photosystem biogenesis therein, biochemical components and mechanisms involved in the localization of ribosomes and mRNAs to the translation zone, and a potential spatiotemporal coordination of translation in the chloroplast and cytoplasm for photosystem biogenesis.

Chloroplast biogenesis occurs in different developmental contexts. It is required for the growth of mature chloroplasts prior to their division by binary fission, for example, in expanding green tissues of leaves and stems (Sun and Zerges, 2015). Another mode of biogenesis occurs as proplastids differentiate to chloroplasts in young green tissues (Solymosi and Schoefs, 2010). Finally, cells of etiolated angiosperm seedlings contain etioplasts that, upon illumination, differentiate to chloroplasts in a process called greening (Hooper, 2007).

The proper timing of protein synthesis is important in many cell biological processes. For example, chloroplast development in both maize (*Zea mays*) and *Chlamydomonas* involves complex dynamics of the expression of the chloroplast genome and nuclear genes encoding trans-acting factors that regulate posttranscriptional steps of chloroplast gene expression (Ildoie et al., 2014; Zones et al., 2015; Chotewutmontri and Barkan, 2016; Strenkert et al., 2019). Leaf development in maize involves complex patterned changes in the translation of chloroplast mRNAs (Chotewutmontri and Barkan, 2016). It is currently of interest to determine how the levels of the photosynthesis complexes and chloroplastic ribosomes change with respect to these dynamics in the transcriptome and translome.

Chlamydomonas is an amenable model organism for studying chloroplast biogenesis. Spatial patterns are readily identifiable due to the stereotypic anatomy of the chloroplast and its several prominent cytological markers (Uniacke et al., 2011). Moreover, liquid cultures yield ample quantities of cells in defined stages of chloroplast biogenesis. For example, the growth of a photosynthetic chloroplast can be studied in wild-type cultures entrained to a 12/12-h light-dark (diel) cycle (Sun and Zerges, 2015; Zones et al., 2015). Under these conditions, cells synchronously grow in size in the light phase and undergo mitosis in the dark phase (Supplemental Figure 1). Alternatively, the greening process can be modeled with the

yellow-in-the-dark-1 (*y1*) mutant (Ohad et al., 1967a, 1967b; Malnoë et al., 1988). *y1* lacks the light-independent protochlorophyllide oxidoreductase (POR), an enzyme in the chlorophyll biosynthetic pathway (Cahoon and Timko, 2000). *y1* cells cultured in the dark cannot synthesize chlorophyll and, therefore, lack PSI and PSII. Illumination restores chlorophyll synthesis by activating a light-dependent POR, thereby initiating the biogenesis of PSI and PSII in a process that resembles greening in angiosperms.

Here, we characterized the spatiotemporal organization of photosystem biogenesis in two developmental contexts that are associated with chloroplast biogenesis: (1) rapid chloroplast growth in the light phase of the diel cycle and (2) rapid photosystem biogenesis in greening *y1* cells. We used indirect immunofluorescence (IF) staining and fluorescence in situ hybridization (FISH) to reveal distributions of endogenous proteins and mRNAs, respectively. To increase the objectivity of our fluorescence microscopy image analyses, we developed a macro and protocol to determine average intrachloroplastic distributions of IF and FISH signals in complete data sets. Therefore, our conclusions are based on both qualitative visual analyses and quantitative analyses by this macro. In addition, we performed live-cell imaging of chlorophyll fluorescence as a marker for the location of its biosynthesis. The results extend the role of the T-zone to the biogenesis of PSI and the biosynthesis of chlorophyll.

RESULTS

Photosynthesis Complexes and Chloroplastic Ribosomes Accumulate during Chloroplast Growth in the Light Phase of the Diel Cycle

In order to characterize spatiotemporal patterns of PET complex biogenesis in growing chloroplasts, we sought culture conditions

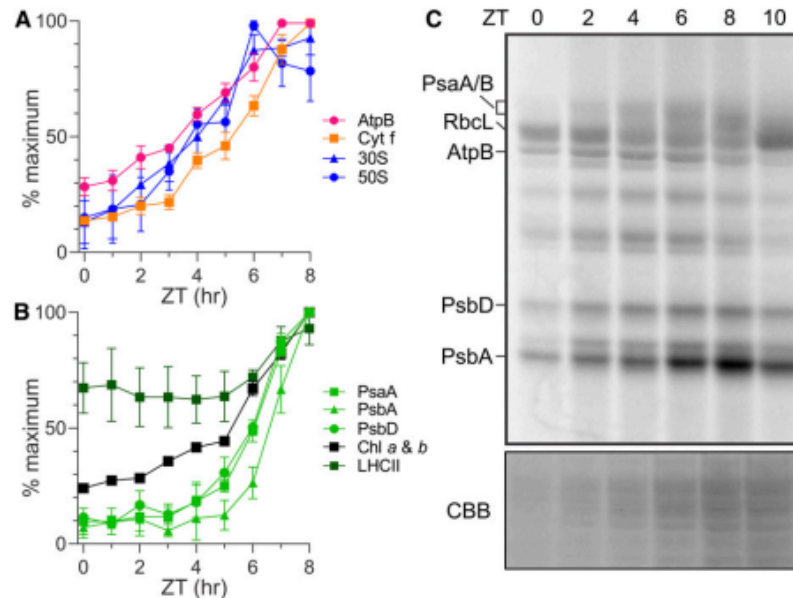


Figure 1. Temporal Changes of Protein Synthesis and Accumulation in the Growing Chloroplast during the Light Phase of the Diel Cycle.

(A) and (B) Results of immunoblot analyses of total protein samples from ZT time points in the ZT0-ZT8 interval of the light phase reveal the relative levels of marker proteins (parentheses) of the following complexes: ATP synthase (AtpB), *Cytb₆f* (Cytf), and the 30S and 50S subunits of the chloroplast ribosome (S-21 and L7/L12, respectively; **(A)**) and PSI (PsaA), PSII (PsbA and PsbD), the LHCII proteins, and chlorophyll **(B)**. Results are from three biological replicates using independent cultures. Error bars indicate 1 s.e. Identical protein samples were used for all analyses in each panel. Immunoblots from one replicate are shown in Supplemental Figure 2A. Supplemental Figures 2B and 2C show the same plots as in **(A)** and **(B)**, respectively, but with all three data points for each ZT time point.

(C) Protein synthesis rates in the chloroplast are revealed by 10-min *in vivo* pulse ³⁵S labeling of PsaA/B, AtpB, PsbD, and PsbA. Also indicated is the ³⁵S-labeled large subunit of Rubisco (RbcL). Preferentially elevated rates of PsbA synthesis for the PSII damage-repair cycle were detected in the ZT6-ZT8 interval. The doublet bands of PsbD represent phosphorylated and nonphosphorylated forms (Herrin et al., 1992). Cycloheximide inhibited cytoplasmic ribosomes to reveal products of chloroplast ribosomes. A portion of the gel with proteins was stained with Coomassie Brilliant Blue (CBB).

under which *Chlamydomonas* (1) undergoes high rates of chloroplast biogenesis for cellular growth, (2) yields samples at defined stages of cellular growth, and (3) is not undergoing mitosis, which likely affects biogenesis. Therefore, we entrained cultures of a wild-type strain to the diel cycle with a 12/12-h light/dark regime (Supplemental Figure 1). Time in the 24-h diel cycle is measured in Zeitgeber time (ZT) hours. The time points ZT0 and ZT12 are the transitions from dark to light and light to dark, respectively. To reveal temporal changes in the steady state levels of the PET complexes and the chloroplast ATP synthase during the light phase, we monitored changes in the levels of representative subunit proteins with immunoblot analysis (Figures 1A and 1B; Supplemental Figures 2A–2C). In the PET system, each subunit represents the level of its complex because unassembled subunits are rapidly degraded (de Vitry et al., 1989). We also monitored the levels of marker proteins of the 30S and 50S subunits of the chloroplast ribosome, S-21 and L7/L12, respectively, and LHCII (Randolph-Anderson et al., 1989).

As cells grew in size during the light phase, the levels of the photosynthesis complexes and ribosomal subunits increased (Figures 1A and 1B; Supplemental Figures 2A–2C). The levels of

the chloroplast ATP synthase and the 30S and 50S subunits of the chloroplast ribosome increased in the ZT0-ZT6 interval (Figure 1A). The synthesis of AtpB (also known as CF1-β), a subunit of the F1 particle of ATP synthase, increased in the ZT0-ZT2 interval, based on results of a radioisotope pulse-labeling assay (Figure 1C; Supplemental Figure 2D). *Cytb₆f* level increased slowly in the ZT0-ZT3 interval and more rapidly thereafter (Figure 1A). (Our pulse-labeling experiments did not detect the synthesis of ribosomal proteins or *Cytb₆f* subunits.) Finally, the levels of PSI and PSII increased in the ZT5-ZT8 interval, although the synthesis of PSI and PSII subunits increased earlier (i.e., at the beginning of the light phase; Figures 1B and 1C; Supplemental Figures 2A, 2C, and 2D). LHCII and chlorophyll also increased in the ZT5-ZT8 interval, but to lesser degrees than did PSI and PSII, consistent with the large proportion of total chlorophyll that is in this complex (Figure 1B; Supplemental Figures 2A and 2C; Minagawa and Takahashi, 2004). These temporal patterns of accumulation are consistent with the programmed differentiation in chloroplast development revealed by previous results of transcriptome and ribosome profiling (Idoine et al., 2014; Zones et al., 2015; Chotewutmontri and Barkan, 2016).

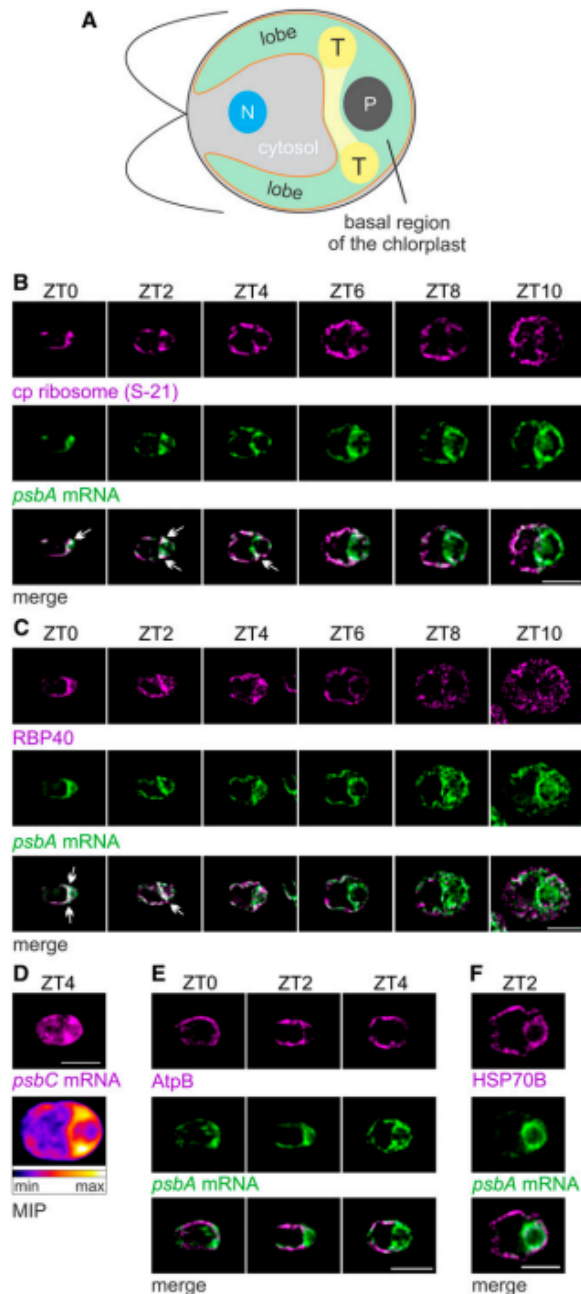


Figure 2. Growing Chloroplasts during the Light Phase of the Diel Cycle Show Spatiotemporal Patterning of Markers of PSII Biogenesis.

(A) An illustration of a *Chlamydomonas* cell shows the chloroplast (green) with its T-zone (T, yellow), basal region, lobes, envelope (orange) and pyrenoid (P). Also shown are the cytosol and the nucleus (N).

(B) Epifluorescence microscopy images reveal the distributions of chloroplastic ribosomal protein S-21 and the *psbA* mRNA enriched in the

Finally, the synthesis of the PSII subunit PsbA preferentially increased in the ZT6–ZT8 interval in the light phase of the diel cycle, relative to that of PsbD (also known as D2; Figure 1C; Supplemental Figure 2D). This preferentially elevated PsbA synthesis is well known to replace PsbA subunits damaged by aberrant photochemical reactions (Theis and Schroda, 2016).

PSII Translation Markers Localize to the T-Zone Early in the Light Phase of the Diel Cycle

Chlamydomonas shows temporally complex patterns of gene expression for chloroplast biogenesis in the light phase of the diel cycle (Zones et al., 2015; Strenkert et al., 2019). Therefore, we asked whether PSII subunit synthesis is also spatially organized and, if so, how the localization patterns relate to the kinetics of PSII subunit synthesis and accumulation. From cultures entrained to the diel cycle, cells were sampled at 2-h intervals between ZT0 and ZT10 and then analyzed for their intrachloroplastic distributions of three translation markers: (1) the *psbA* mRNA, (2) the chloroplastic ribosomal protein S-21, and (3) RBP40 (also known as RB38), a translation factor required for early steps in the translation of PsbD (Barnes et al., 2004; Schwarz et al., 2007). PsbA and PsbD are encoded by the chloroplastic genome and translated by 70S chloroplastic ribosomes (Erickson et al., 1984; Rochaix et al., 1984). An illustration of a *Chlamydomonas* cell shows the relevant compartments (Figure 2A). These analyses revealed in most cells from the ZT0–ZT4 interval that the *psbA* mRNA and S-21 were enriched in patches in the basal region of the chloroplast near lobe junctions (Figure 2B). Many cells also showed a band of these colocalized signals extending between opposing lobe junctions. We designated this region as the T-zone in the growing chloroplast. This T-zone is located slightly anterior to the location of the T-zone in cells of

T-zone of ZT0 cells ($n = 27$), ZT2 cells ($n = 28$), in approximately half of the ZT4 cells ($n = 45$), but not in most ZT6 cells ($n = 78$), ZT8 cells ($n = 44$), or ZT10 cells ($n = 41$). Arrows indicate the strongest overlaps. Each signal was manually adjusted to similar brightness across all images in each panel to allow comparisons of in situ distributions.

(C) RBP40 and the *psbA* mRNA localized to the T-zone in approximately half of the ZT0 cells ($n = 123$), in most ZT2 cells ($n = 136$) and ZT4 cells ($n = 129$), but not in most ZT6 cells ($n = 117$), ZT8 cells ($n = 101$), or ZT10 cells ($n = 113$).

(D) The *psbC* mRNA was enriched in the T-zone of ZT4 cells (top image). The heat map shows average signal intensities in a maximal intensity projection (MIP) of all cells in this data set ($n = 56$).

(E) The thylakoid membrane complex ATP synthase (AtpB) was not localized to the T-zone in most ZT0 cells ($n = 18$), ZT2 cells ($n = 64$), and ZT4 cells ($n = 83$).

(F) A protein of the chloroplast stroma (HSP70B) was not localized to the T-zone (marked by the *psbA* mRNA) in ZT2 cells ($n = 79$).

Bright-field images of all cells shown here are presented in Supplemental Figure 3 to show their proper anterior-posterior orientations (from left to right). Bars = 5.0 μm .

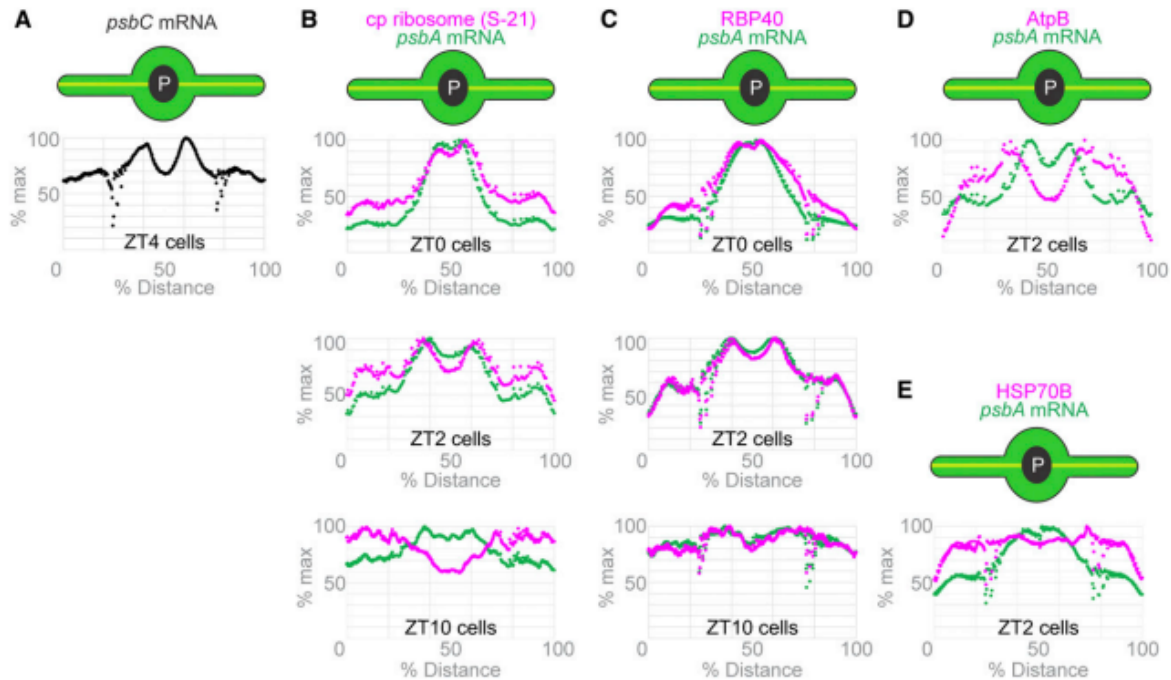


Figure 3. Plots of Average Fluorescence Signal Intensity along the Chloroplast Axis from All Cells of Each Data Set Support T-Zone Localization of the Translation Markers Early in the Light Phase of the Diel Cycle.

Chloroplasts are illustrated as their axis (yellow line) is presented on the horizontal axis of each graph. Our macro determines the average signal intensity along this axis.

(A) The average signal intensity of the *psbC* mRNA FISH signal in ZT4 cells (Figure 2D; $n = 56$) is plotted versus position on the chloroplast axis.

(B) to (E) The average signal intensities of the *psbA* mRNA FISH signal (green) and the IF signals of the S-21 chloroplastic ribosomal protein (ZT0, $n = 27$; ZT2, $n = 28$; and ZT10, $n = 41$; **[B]**), RBP40 (ZT0, $n = 111$; ZT2, $n = 118$, and ZT10, $n = 123$; **[C]**), the AtpB subunit of ATP synthase ($n = 65$; **[D]**), and the stromal marker HSP70B ($n = 93$; **[E]**) are plotted along the chloroplast axis (as percentage of the total length).

asynchronous cultures under other conditions (Uniacke and Zerges, 2007). Later in the light phase, beginning at ZT6, the S-21 IF signal increased in the lobes such that it became distributed throughout the chloroplast (except in the pyrenoid). The *psbA* mRNA remained enriched in the T-zone throughout the light phase. The strongest RBP40 IF signal was from the T-zone in the ZT0-ZT4 interval and dispersed later in the ZT6-ZT10 interval (Figure 2C). Thus, the three translation markers were enriched specifically in this T-zone in the ZT0-ZT4 interval, when we also observed the major increases in PSII subunit synthesis (Figure 1C; Supplemental Figure 2D). T-zone localization of translation marker signals was not evident while the rates of PsbD synthesis declined in the ZT8-ZT10 interval. The increased level of S-21 in the lobes of the chloroplast in the ZT6-ZT8 interval may reflect PsbA synthesis for PSII repair because these events coincided and the latter is known to occur on thylakoid membranes throughout the chloroplast (Figures 1C and 2B; Mattoo and Edelman, 1987; van Wijk et al., 1996).

As the *psbA* mRNA is translated for both the biogenesis and repair of PSII, it does not serve as a definitive marker for the

location of PSII biogenesis. Therefore, we asked whether the *psbC* mRNA, which encodes a PSII subunit that does not undergo a damage and repair cycle (CP43), also localizes to the T-zone in ZT4 cells (Chotewutmontri and Barkan, 2018). These ZT4 cells showed the highest *psbC* mRNA FISH signal in the T-zone, hence providing further support of the T-zone as the primary location of PSII biogenesis in the growing chloroplast (Figure 2D).

The localization of the translation markers to the T-zone does not reflect a feature of chloroplast anatomy, for example, densely populated thylakoid lamella or pockets of stroma in the T-zone, because it was not seen for AtpB, a subunit of the ATP synthase in thylakoid membranes, or a marker protein for the chloroplast stroma, HSP70B (Figures 2E and 2F). Moreover, our thin (0.2 μm) optical sections minimize contributions of local differences in chloroplast volume to signal intensities. In addition, transmission electron microscopy (TEM) images revealed that cells early in the light phase (ZT0 to ZT3) had the expected chloroplast ultrastructure and morphology, including thylakoid lamellae and stroma throughout the chloroplast (Supplemental Figure 4). Therefore, the enrichment of the translation markers in the T-zone

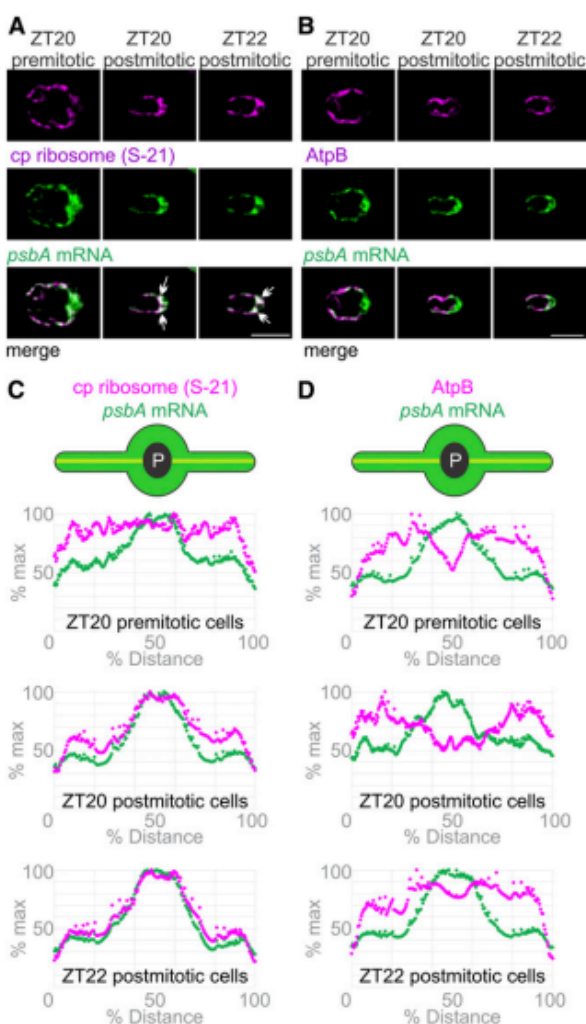


Figure 4. The Chloroplast Ribosome Marker Protein and the *psbA* mRNA Localize to the T-Zone after Cell Division in the Dark Phase of the Diel Cycle.

(A) Epifluorescence microscopy images revealed in the premitotic cells at ZT20 ($n = 15$) that the *psbA* mRNA (green) was higher in the basal region than the lobes while the chloroplast ribosomal protein S-21 (magenta) was distributed throughout the chloroplast. In most postmitotic ZT20 cells ($n = 103$) and postmitotic ZT22 cells ($n = 72$), the strongest signals from the *psbA* mRNA and the chloroplast ribosomal protein S-21 colocalized to the T-zone (arrows). Bar = 5.0 μm .

(B) The AtpB subunit of the chloroplast ATP synthase (magenta) was not localized with the *psbA* mRNA in premitotic ZT20 cells ($n = 9$), in postmitotic ZT20 cells ($n = 39$), or in ZT22 cells ($n = 103$). Bar = 5.0 μm .

(C) and **(D)** The patterns in **(A)** and **(B)** were confirmed by plots of the average signal intensities versus the chloroplast axis. Cell numbers were, for the *psbA* mRNA and S-21, ZT20 premitotic ($n = 15$), ZT20 postmitotic ($n = 54$), and ZT22 ($n = 72$); **(C)**, and for the *psbA* mRNA and AtpB, ZT20 premitotic ($n = 9$), ZT20 postmitotic ($n = 54$), and ZT22 ($n = 112$); **(D)**.

likely reflects their localization and not some anatomical feature of the chloroplast unrelated to biogenesis.

Average Signal Distributions Confirm Localization of Translation Markers to the T-Zone

The precision of visual analyses for localization patterns at suborganellar levels in fluorescence microscopy images can be affected by the researcher's unconscious bias and limited ability to simultaneously compare many images. To increase the objectivity of our analyses and discern localization patterns in *Chlamydomonas*, we developed a method to analyze fluorescence microscopy images by averaging signal intensity over many cells (Supplemental File). This macro takes a maximum intensity projection for each cell, collects the projections from all cells in a data set, and then rescales each cell such that its long and short axes are equal in length to those of the largest cell in the data set. It then superimposes the projections to generate an image of the average signal intensities (Figure 2D; Supplemental File). This analysis can further convert the average FISH signal intensity from the *psbC* mRNA in Figure 2D to the plot in Figure 3A of the percentages of the maximum value versus position on the chloroplast axis. The chloroplast axis was designated as a line from the tip of one lobe across the pyrenoid to the tip of the opposing lobe (see illustrations in Figure 3). The resulting plot shows two peaks of maximal average intensity where the axis traverses the T-zone on either side of the pyrenoid (seen as a dip of low average intensity).

To better show the relationship between two signals, we determined the average signal intensity of each in the chloroplast lobes, the T-zone, and the pyrenoid (Supplemental File) and then plotted the percentages of their maximum values versus position on the chloroplast axis (Figure 3). Results of these analyses revealed that the signals of the three translation markers displayed maxima overlapping in the T-zones of cells from ZT0 and ZT2 (Figures 3B and 3C). At ZT0, a single peak of overlapping translation marker signals was seen where the axis crosses the T-zone. The nonstaining pyrenoid is small then (i.e., in the hours following mitosis) and, thus, it makes only a slight dip at the apex of this peak (compare Supplemental Figures 4B and 4C; Freeman Rosenzweig et al., 2017). At ZT2, the larger pyrenoid is now at the center of the chloroplast axis and separates two peaks of overlapping translation marker signals where the axis crosses the T-zone in opposing lobe junctions. By ZT10, the maxima had diminished for the *psbA* mRNA and were no longer seen for S-21 and RBP40, as the latter signals increased in the lobes (Figures 3B and 3C). The average signals of the control markers for thylakoid membranes and stroma, AtpB and HSP70B, respectively, did not show maxima in the T-zone (marked by the *psbA* mRNA maxima) at any of the time points examined (Figures 3D and 3E). These results confirm the results of visual analyses in the previous subsection and, thereby, provide further support of the T-zone being the primary location of PSII subunit synthesis early in the light phase.

The lobes of the chloroplast in some cells showed a gap in all fluorescent signals, which was located immediately

anterior to the junction with the basal region (Figure 2B, ZT2 and ZT4 cells; Figures 3A, 3C, and 3E). Each of these gaps is caused by a constriction of the entire lobe, as can be seen in the TEM image in Supplemental Figure 4B. These constrictions appear on both lobes in some cells for unknown reasons. Additional work is required to understand their structure and functions.

Localization of the *psbA* mRNA and Chloroplastic Ribosome to the T-Zone Is Established following Mitosis

T-zone localization of the translation markers was established sometime during the dark phase; it was absent at ZT10 and present at ZT0 (Figures 2B, 2C, 3B, and 3C). To determine when this localization is established, cells at the end of the dark phase (ZT20 and ZT22) were analyzed for their in situ distributions of the *psbA* mRNA and the chloroplastic ribosomal protein S-21. At ZT20, we observed large and small cells. The large cells were premitotic while the small cells were postmitotic; they were similar in size to the daughter cells that predominated at ZT22 and constituted all cells at ZT0 (Supplemental Figure 1A). Premitotic ZT20 cells did not show T-zone localization of the *psbA* mRNA or S-21 (Figures 4A and 4C). The former was enriched in the basal region but not localized specifically in the T-zone, while the latter was dispersed throughout the chloroplast, except in the pyrenoid. Postmitotic ZT20 and ZT22 cells, however, showed T-zone localization of the *psbA* mRNA and S-21 (Figures 4A and 4C). This localization pattern was not seen for AtpB, revealing that it does not reflect the distribution of thylakoid membranes, the accepted location of *psbA* translation (Zoschke and Bock, 2018; Figures 4B and 4D). Therefore, localization of the *psbA* mRNA and the chloroplastic ribosome to the T-zone is established soon after mitosis and maintained throughout the remainder of the dark phase and during the initial 4 h of the light phase (Figures 2B and 2C). Previous reports describe increases in the synthesis rates of chloroplast genome-encoded subunits of PSI and PSII in the dark phase, when we observed the establishment of this localization pattern (~ZT22; Howell et al., 1977; Lee and Herrin, 2002). Our pulse-labeling assay was not sufficiently sensitive to monitor these rates of synthesis in the dark phase. Thus, the chloroplast translation machinery and mRNAs localize to the T-zone when photosystem subunit synthesis is activated near the end of the dark phase.

Chlorophyll Biosynthesis Is Localized to the T-Zone

Newly synthesized chlorophyll is incorporated into PSI and PSII within seconds in *Chlamydomonas* (White and Hooper, 1994). This suggests that chlorophyll biosynthesis is colocalized with the synthesis of chlorophyll binding proteins, as has been shown in cyanobacteria (Chidgey et al., 2014). In addition, the oxidative cyclase CRD1, an enzyme in the chlorophyll biosynthesis pathway, is localized to the pyrenoid perimeter (i.e., in the T-zone; Allen et al., 2008). Therefore, we asked whether chlorophyll biosynthesis is localized to the T-zone by IF staining cells in the light phase of the diel cycle for the light-dependent POR.

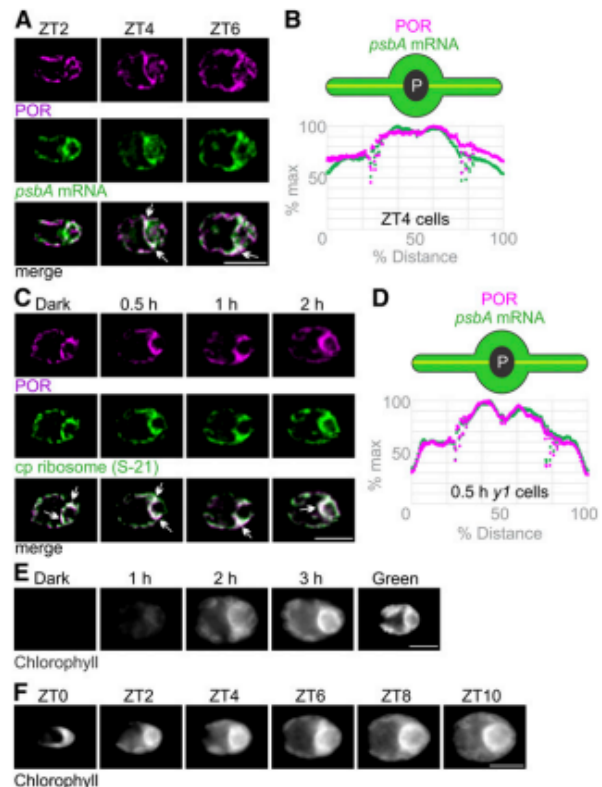


Figure 5. The T-Zone Is the Primary Location of Chlorophyll Biosynthesis.

(A) Epifluorescence microscopy images show that the fluorescent signals of POR (magenta) and the *psbA* mRNA (green) were throughout the chloroplast in most ZT2 cells ($n = 95$) and colocalized in the T-zone (arrows) in most ZT4 cells ($n = 73$) and ZT6 cells ($n = 47$). Bar = 5.0 μm .

(B) For ZT4 cells, this pattern was confirmed by plots of average signal intensities versus position on the chloroplast axis ($n = 112$).

(C) Images show the IF signals of POR (magenta) and S-21 (green) colocalized in the T-zones of most dark- $y1$ cells ($n = 111$), 0.5 h- $y1$ cells ($n = 62$), 1 h- $y1$ cells ($n = 71$), and 2 h- $y1$ cells ($n = 56$). Bar = 5.0 μm .

(D) This pattern was confirmed for 0.5 h- $y1$ cells by plots of average signal intensities versus position on the chloroplast axis ($n = 33$).

(E) In live-imaged dark- $y1$ cells ($n = 62$), no autofluorescence was seen because they lack chlorophyll. The strongest chlorophyll fluorescence was seen in the T-zones of most live 1 h- $y1$ cells ($n = 52$), 2 h- $y1$ cells ($n = 40$), and 3 h- $y1$ cells ($n = 40$) and throughout the chloroplast of all green- $y1$ cells ($n = 55$). Bar = 5.0 μm .

(F) At ZT0 ($n = 14$), chlorophyll fluorescence was higher in the basal region than in the lobes, but not particularly localized to the T-zone. The strongest chlorophyll autofluorescence was seen in the T-zones of most cells at ZT2 ($n = 16$), ZT4 ($n = 15$), ZT6 ($n = 19$), ZT8 ($n = 17$), and ZT10 ($n = 13$). Bar = 5.0 μm .

Epifluorescence microscopy images show the POR IF signal throughout the chloroplast in ZT2 cells. However, ZT4 and ZT6 cells showed strong POR IF signal in the T-zone (marked by the FISH signal of the *psbA* mRNA; Figures 5A and 5B). Therefore, the localization of POR to the T-zone coincided with the accelerated increase in chlorophyll level at ZT5 and with the increases

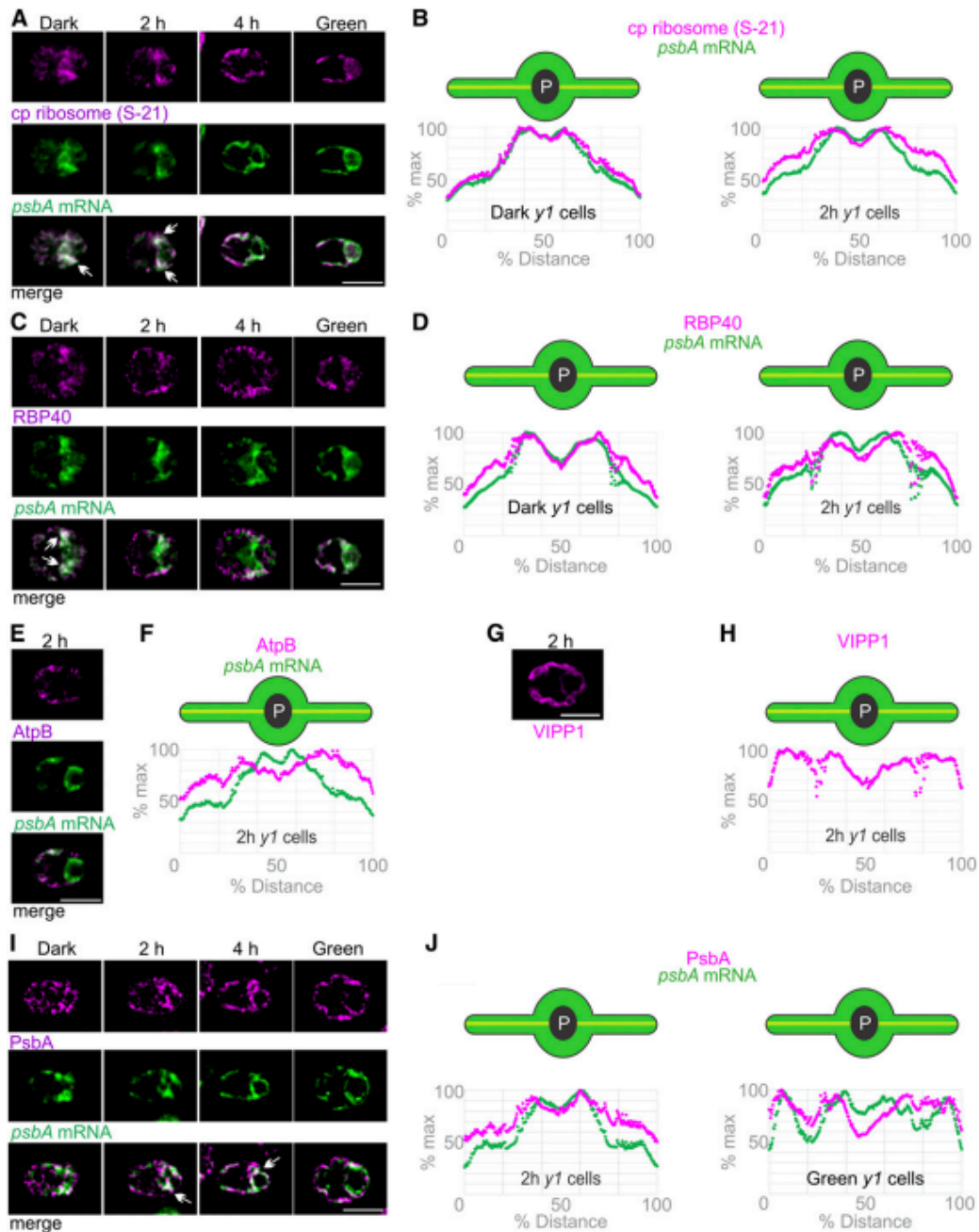


Figure 6. The T-Zone in Greening *y1* Cells Revealed by the in Situ Localization of Translation Markers.

(A) Images show the strongest signals from chloroplastic ribosomal protein S-21 (magenta) and the *psbA* mRNA (green) colocalized in the T-zone in most dark-*y1* cells ($n = 91$) and 2 h-*y1* cells ($n = 145$) and approximately half of 4 h-*y1* cells ($n = 138$) but not in most green-*y1* cells ($n = 89$). Arrows indicate where the strongest signals from both channels overlap in the T-zone. Bar = 5.0 μm .

(B) Plots of the average signal intensities versus position on the chloroplast axis confirm these patterns in dark-*y1* cells ($n = 52$) and 2 h-*y1* cells ($n = 95$). **(C)** Cell images show RBP40 (magenta) and the *psbA* mRNA (green) colocalized in the T-zone in approximately half of dark-*y1* cells ($n = 41$) and in minorities of 2 h-*y1* cells ($n = 75$) and 4 h-*y1* cells ($n = 103$) but not in green-*y1* cells ($n = 82$). Bar = 5.0 μm .

(D) Plots of average intensities of these signals showed peaks in the T-zone of dark-*y1* cells ($n = 65$) and 2 h-*y1* cells ($n = 109$).

(E) In 2 h-*y1* cells, AtpB (magenta) was maximal in the lobes and not localized to the T-zone with the *psbA* mRNA (green) in most 2 h-*y1* cells ($n = 76$). Bar = 5.0 μm .

in the levels of PSI and PSII (Figure 1B; Supplemental Figures 2A and 2C).

We asked whether chlorophyll biosynthesis is localized to the T-zone in greening *y1* cells. We confirmed that *y1* cells cultured in the dark (dark-*y1* cells) have low levels of PSI and PSII, low synthesis rates of PSI and PSII subunits (PsaA, PsbA, and PsbD), and that these levels and rates increase during greening due to the activation by light of chlorophyll biosynthesis and, consequently, photosystem biogenesis (Supplemental Figure 5; Ohad et al., 1967a; Malnoë et al., 1988). When we analyzed the in situ distribution of the POR, we found that it colocalized with S-21 in the T-zone in dark-*y1* cells and in *y1* cells after 0.5, 1, and 2 h of greening (hereafter 0.5 h-*y1* cells, 1 h-*y1* cells, and 2 h-*y1* cells, respectively; Figures 5C and 5D). This result suggests that the T-zone is a primary location of chlorophyll biosynthesis in greening *y1* cells.

To test this possibility further, we exploited the fact that dark-*y1* cells begin greening without chlorophyll and then accumulate it during greening (Ohad et al., 1967a). Chlorophyll fluorescence should first appear in the T-zone if it is a principal location of chlorophyll biosynthesis. In live-imaged dark-*y1* cells, only weak autofluorescence was seen because they lack chlorophyll. As was expected, green-*y1* cells (*y1* cells cultured in constant light) exhibited chlorophyll fluorescence throughout their chloroplast (i.e., in the known distribution of thylakoids; Figure 5E). By contrast, in *y1* cells after 1, 2, or 3 h of greening, the strongest chlorophyll fluorescence was seen along the anterior perimeter of the pyrenoid (i.e., the T-zone). Similarly, in individual greening *y1* cells followed in time-lapse movies of maximum intensity projections, chlorophyll fluorescence was seen first in the T-zone (Supplemental Video). Later, the strongest chlorophyll fluorescence expanded anteriorly and was seen throughout the chloroplast by the end of greening. These results provide further support that the T-zone is the primary location of chlorophyll biosynthesis in the greening chloroplast.

Similarly, we visualized chlorophyll fluorescence in live cells from ZT0 to ZT10 in the diel cycle (Figure 5F). At ZT0, chlorophyll fluorescence was higher in the basal region than in the lobes, but it was not particularly localized to the T-zone. Later, and throughout the light phase, the strongest chlorophyll fluorescence was seen along the anterior perimeter of the pyrenoid (i.e., the T-zone), as was observed in greening *y1* cells (Figures 5E and 5F). This strong chlorophyll fluorescence appeared before the accelerated increase in chlorophyll level at ZT5 (Figure 1B), suggesting that it is from newly synthesized chlorophyll whose excitation is not yet quenched by processes in the photosystems and their LHCs

(Müller et al., 2001). These results support the T-zone as being the primary location of chlorophyll biosynthesis in the growing chloroplast.

PSII Translation Markers Localize to the T-Zone of Greening *y1* Cells

We then analyzed the in situ distributions of the PSII translation markers in the chloroplast of greening *y1* cells (Figure 6). In dark-*y1* cells and 2 h-*y1* cells, the strongest signals from the *psbA* mRNA and S-21 overlapped in the T-zone (Figures 6A and 6B). In 4 h-*y1* cells or green-*y1* cells, the *psbA* mRNA FISH signal was still enriched in the T-zone while S-21 was more broadly distributed throughout the chloroplast, except in the pyrenoid. Similarly, RBP40 and the *psbA* mRNA localized to the T-zone in dark-*y1* cells and 2 h-*y1* cells (Figures 6C and 6D). This pattern was less evident in 4 h-*y1* cells and not evident in green-*y1* cells. These results provide evidence that the T-zone is the primary location of PSII subunit synthesis early in *y1* greening.

The localization of these translation markers to the T-zone does not reflect local enrichments of thylakoids and stroma in *y1* cells because neither AtpB nor a marker for stoma and thylakoids, VIPP1 (Liu et al., 2005), was localized in this pattern in 2 h-*y1* cells (Figures 6E–6H). As was mentioned above, the thin (0.2 μm) optical sections minimize the effects on signal intensity of any differences in volume between the T-zone and other parts of the chloroplast. Therefore, the enrichment of the PSII translation markers in the T-zone in dark-*y1* and 2 h-*y1* cells reflects their localization and not a local enrichment of thylakoids or stroma compared with elsewhere in the chloroplast.

Since the translation markers localized to the T-zone in dark-*y1* cells (i.e., before PSII subunit synthesis was induced by illumination; Figures 6A–6D; Supplemental Figures 5C and 6D), we sought a direct marker for PSII subunit synthesis to determine whether the T-zone is a primary location of active translation. We were able to use the PsbA protein because dark-*y1* cells have only trace amounts such that most of the PsbA pool early in greening is newly synthesized (Supplemental Figures 5A and 5B). Therefore, the first PsbA to appear in greening should mark its location of synthesis. Consistent with this rationale, the PsbA IF signal in dark-*y1* cells was very weak and not in any particular localization pattern (Figure 6I). (The brightness of the PsbA IF signal in the dark-*y1* cell image was enhanced to show its distribution.) In 2 h-*y1* cells and 4 h-*y1* cells, the PsbA IF signal initially increased in the T-zone, where it colocalized with the

Figure 6. (continued).

(F) This was confirmed by a plot of the AtpB IF signal intensity versus position on the chloroplast axis ($n = 54$).

(G) VIPP1, a marker for thylakoids and stroma, also was not localized to the T-zone in most 2 h-*y1* cells ($n = 51$). Bar = 5.0 μm .

(H) This was confirmed by a plot of the VIPP1 IF signal intensity versus position on the chloroplast axis ($n = 44$).

(I) PsbA is a marker for newly synthesized PSII proteins early in *y1* greening (see text); it was T-zone localized (arrows) in most 2 h-*y1* cells ($n = 95$) and 4 h-*y1* cells ($n = 40$) but not in most dark-*y1* cells ($n = 79$) or any green-*y1* cells ($n = 36$). The PsbA signal was manually enhanced in the dark-*y1* cell to allow comparisons of its in situ distributions but not relative levels across the conditions. Bar = 5.0 μm .

(J) The average intensity of the PsbA IF signals was maximal in the T-zone in 2 h-*y1* cells ($n = 89$) but not in green-*y1* cells ($n = 34$).

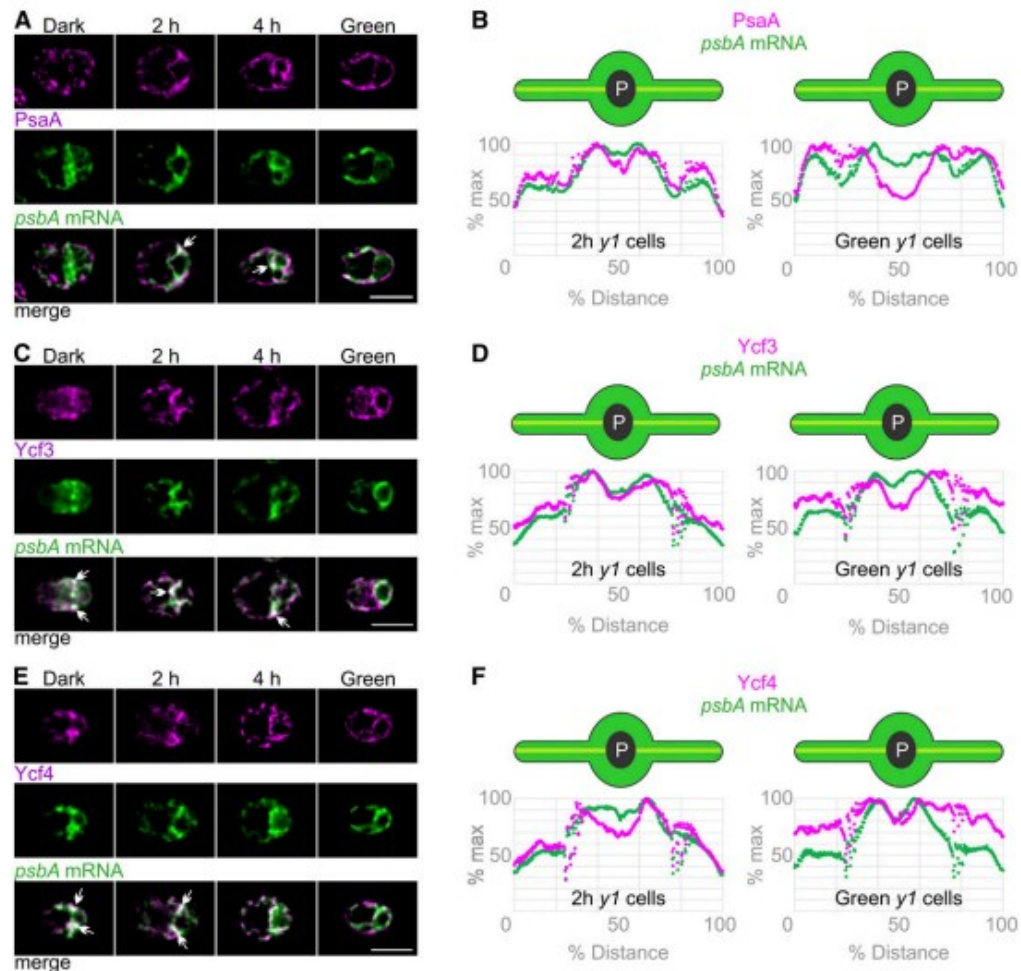


Figure 7. Localization of PSI Subunit Synthesis and Assembly to the T-Zone of Greening *y1* Cells.

(A) Overlap of the strongest signals of PSI subunit PsaA (magenta) and the *psbA* mRNA (green) in the T-zone was seen in most 2 h-*y1* cells ($n = 59$) and in approximately half of 4 h-*y1* cells ($n = 30$) but not in dark-*y1* cells ($n = 75$) or green-*y1* cells ($n = 52$). PsaA signal was enhanced in the dark-*y1* cell to allow comparisons of its distributions. Arrows indicate where the strongest signals from both channels overlap in the T-zone. Bar = 5.0 μm .

(B) The colocalization in the T-zone of 2 h-*y1* cells ($n = 73$) but not green-*y1* cells ($n = 43$) was confirmed by plots of the average signal intensities versus the chloroplast axis.

(C) Epifluorescence microscopy images show the strongest signals from Ycf3 (magenta) and the *psbA* mRNA (green) colocalized in the T-zone in most dark-*y1* cells ($n = 38$), in approximately half of 2 h-*y1* cells ($n = 84$) and 4 h-*y1* cells ($n = 136$), but not in green-*y1* cells ($n = 35$). Bar = 5.0 μm .

(D) T-zone localization of both signals in 2 h-*y1* cells ($n = 90$) but not green-*y1* cells ($n = 32$) was confirmed by plots of the average signal intensities versus position on the chloroplast axis.

(E) The strongest signals of Ycf4 (magenta) and the *psbA* mRNA (green) colocalized in the T-zone in dark-*y1* cells ($n = 40$), in 2 h-*y1* cells ($n = 55$), and in approximately half of 4 h-*y1* cells ($n = 57$) but not in green-*y1* cells ($n = 64$). Bar = 5.0 μm .

(F) T-zone localization of both signals in 2 h-*y1* cells ($n = 57$) but not green-*y1* cells ($n = 50$) was confirmed by plots of the average signal intensities.

psbA mRNA FISH signal. In green-*y1* cells, PsaA was seen throughout the chloroplast, consistent with this known distribution of thylakoids (Figure 6I). These patterns are supported by the average signal distributions along the chloroplast axis in 2 h-*y1* cells and green-*y1* cells (Figure 6J). T-zone localization of PsaA in 2 h-*y1* cells does not represent the distribution of thylakoid lamellae or stroma because it was not seen for AtpB or VIPP1

(Figures 6E–6H). Therefore, PsaA marks the T-zone as the primary location of its synthesis during *y1* greening.

This localized synthesis of PsaA in the T-zone suggests that, during greening, the newly synthesized protein migrates into the lobes where PSII is abundant in mature green-*y1* cells (Figures 6I and 6J). In support of this hypothesis, the average PsaA IF signal in 2 h-*y1* cells extended slightly farther into the lobes than did the *psbA* mRNA in the T-zone.

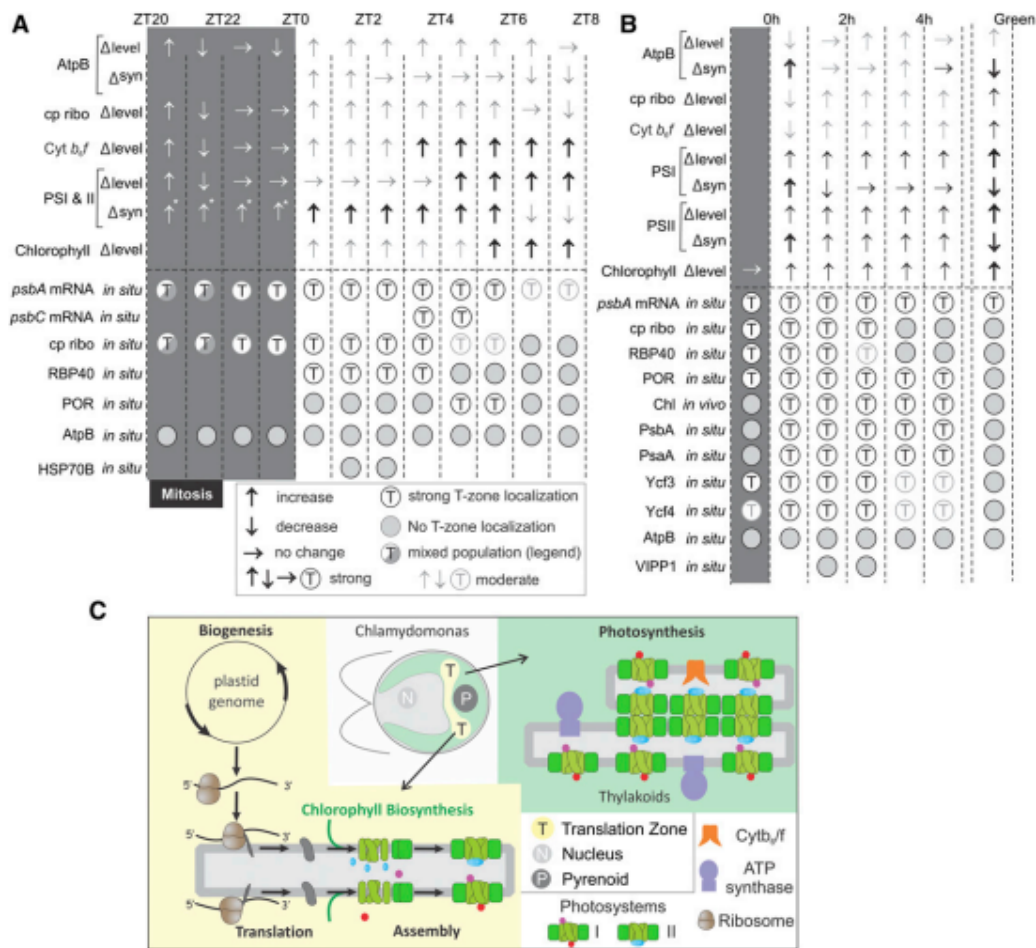


Figure 8. Summaries of the Results.

(A) For the diel cycle interval ZT20-ZT8, arrows indicate changes in steady state level (Δ level) and synthesis rate (Δ syn) of the marker proteins for the listed complexes as follows: ↑, increase; ↓, decrease; thick ↑, drastic increase; gray ↑, slight increase; →, no change. Below the broken line, for each mRNA or marker protein, T-zone localization is indicated by open circles and nonlocalization by shaded circles. Sectoring circles indicate mixed populations of premitotic and postmitotic cells showing nonlocalization or T-zone localization, respectively. Faded circles indicate weak T-zone localization. The intervals of the dark and light phases examined have shaded and white backgrounds, respectively. Absence of a circle indicates not determined. Abbreviations and marker proteins *in situ* (in parentheses) are as follows: ATP synthase (AtpB), AtpB; chloroplast ribosome (S-21), cp ribo; Cytb₆/f complex (Cytf), Cytb₆/f; PSI and PSII (PsaA and PsaB, respectively), PSI and II. Asterisks indicate that data are from Howell et al. (1977) and Lee and Herrin (2002).

(B) The results obtained with greening *y1* are summarized as described for **(A)**. Changes in protein level and synthesis rates of the marker proteins (top arrows) are presented for reference to our *in situ* results (bottom circles). Levels and synthesis rates of the markers of ATP synthase, PSI, and PSII were reported previously (Malnoë et al., 1988). **(C)** Our model shows the role of the T-zone (yellow) as a compartment in the chloroplast which is the location of photosystem subunit translation and assembly as well as chlorophyll biosynthesis and distinct from the distribution of photosynthetic thylakoid membranes throughout the chloroplast (green).

PSI Subunit Synthesis Occurs in the T-Zone of Greening *y1* Cells

To determine whether subunits of PSI also are synthesized in the T-zone, we IF stained *y1* cells for PsaA, a subunit of the PSI reaction center encoded by the plastid genome. Like PsaB, PsaA serves as a marker for the location of its own synthesis in greening *y1* cells because most of its pool is newly synthesized (Supplemental Figures 5A and 5B). The PsaA IF signal was weak

and nonlocalized in dark-*y1* cells, consistent with their trace amounts of PsaA (Figure 7A). During greening, the PsaA localized to the T-zone of 2 h-*y1* cells along with the *psbA* mRNA (Figure 7A). By 4 h of greening, the PsaA IF signal had increased in the lobes, although it still colocalized with the *psbA* mRNA in the T-zone in approximately half of these cells. Eventually, all green-*y1* cells had the PsaA IF signal throughout the chloroplast, the known distribution of PSI in thylakoid membranes (Figure 7A).

These patterns are supported by plots of the average signal intensity versus position on the chloroplast axis in 2 h-*y1* cells and green-*y1* cells (Figure 7B). These results provide evidence that the T-zone is the primary location of PSI subunit synthesis in greening *y1* cells.

As was observed for *PsbA*, the average *PsaA* IF signal in 2 h-*y1* cells extended into the lobes from the T-zone (Figure 7B). This supports the migration of the newly synthesized *PsaA* from the T-zone into the lobes during chloroplast greening.

PSI Assembly Factors Localize to the T-Zone in Greening *y1* Cells

We addressed the location where newly synthesized PSI subunits are assembled to form the PSI reaction center by characterizing the in situ distributions of two PSI-specific assembly factors. *Ycf3* and *Ycf4* interact with the newly synthesized PSI subunits and promote their assembly into the PSI reaction center, but they are not present in fully assembled and functional PSI (Nellaepalli et al., 2018). Both *Ycf3* and *Ycf4* localized to the T-zone (marked by the *psbA* mRNA FISH signal) in 2 h-*y1* cells but not in green-*y1* cells (Figures 7C to 7F). Therefore, these results provide evidence that the T-zone is the primary location of PSI assembly.

DISCUSSION

Our results reveal the T-zone as a hub for the biogenesis of PSI and PSII under developmentally relevant conditions associated with rapid chloroplast biogenesis for cellular growth or greening. Such a region where multiple pathways converge for thylakoid membrane biogenesis has been described as a "biogenesis center" (Nickelsen and Zerges, 2013; Rast et al., 2015). The T-zone is among a growing number of examples of localized translation for biogenesis and pattern formation in diverse organisms. In the cytoplasm of yeast, neurons, and developing embryos, the translation of specific mRNAs is localized to RNA granules, membrane-bound organelles, or synapses for diverse functions (Lui et al., 2014; Hughes and Simmonds, 2019; Panasenko et al., 2019). An analogous region to the T-zone of the chloroplast was recently reported in mitochondria, the other semiautonomous organelle, for the biogenesis of the respiratory electron transport chain complexes (Stoldt et al., 2018).

The T-zone under the developmentally relevant conditions examined here is slightly more anterior than the T-zone described previously in cells that were briefly shifted from dark to light to induce PSII subunit synthesis (Uniacke and Zerges, 2007). The T-zone here is adjacent to domains of the chloroplast envelope that are enriched in protein import translocons (Schottkowski et al., 2012). The cytoplasm neighboring the T-zone is enriched in cytosolic ribosomes and an mRNA encoding a subunit of the LHC of PSII (Colón-Ramos et al., 2003; Uniacke and Zerges, 2009). Invaginations of the inner envelope membrane adjacent to the T-zone were observed in cryo-electron microscopy images (Engel et al., 2015). These results suggest an intercompartmental spatial coordination in the synthesis of nuclear genome-encoded photosystem subunits in the posterior cytoplasm, protein import into the chloroplast, and

the synthesis and assembly of chloroplast genome-encoded subunits and chlorophyll in the T-zone within the chloroplast (e.g., a "thylakoid membrane biogenesis center") and analogous to an intramitochondrial "zone" and "ER membrane contact sites" with other organelles (Rast et al., 2015; Wu et al., 2018; Shimizu, 2019).

Functions of localized photosystem biogenesis to the T-zone could include any of the known roles of intracellular compartmentalization. For example, elevated local concentrations of substrates, intermediates, and biochemical factors favor forward reactions. The sequestration of substrates, intermediates, enzymes, and factors prevents deleterious side reactions, such as the aggregation of nonnative proteins or singlet oxygen production by newly synthesized chlorophyll. Finally, compartmentalization can enhance efficiency by facilitating the channeling of intermediates and spatially coordinating pathways of a network.

It is unknown how newly synthesized chlorophyll is transported from its accepted site of synthesis at the chloroplast envelope, through the stroma, to thylakoid membranes for photosystem biogenesis (Joyard et al., 2009). The colocalization of the biosynthesis of chlorophyll and chlorophyll binding apoproteins in the T-zone suggests that chlorophyll transport is unnecessary.

The ordered increase in the photosynthesis complexes suggested by our results is consistent with the programmed differentiation seen at the levels of the transcriptome and, in maize, the translome (Figures 1A and 1B; Zones et al., 2015; Chote-wutmontri and Barkan, 2016; Strenkert et al., 2019). The increase in chlorophyll levels was intermediate to the increases in the complexes that bind most of the pool of this photopigment, the photosystems and LHCII (Figure 1B).

The localization of the translation markers to the T-zone arose soon after mitosis at ZT20 in the dark phase, whereupon it was maintained until approximately ZT4 (Figures 2B, 2C, 3A to 3C, 4A, 4C, and 8). Previous reports showed that the synthesis rates of PSII subunits by chloroplastic ribosomes began to increase late in the dark phase, approximately when we observed the localization of the translation markers to the T-zone (Howell et al., 1977; Lee and Herrin, 2002). Therefore, localization of the translation markers to the T-zone after mitosis coincides with the activation of PSII subunit synthesis.

The translation markers localized to the T-zone until ZT6 (Figures 2B, 2C, and 8A). Similarly, in *y1*, the translation markers localized to the T-zone in the dark and the first 2 h of greening, but not thereafter (Figures 6A to 6D, 6I, 6J, and 8B). Therefore, in both cellular growth and greening, translation markers localized to the T-zone early but not late in these different modes of chloroplast biogenesis, even though translation rates of these subunits were sustained throughout these processes (Figure 1C; Supplemental Figures 2D, 5C, and 5D). These results support a role of the T-zone as a hub for photosystem biogenesis early in chloroplast growth and greening. Later in these processes, the redistribution of the translation markers throughout the chloroplast coincided with the preferentially elevated *PsbA* synthesis rates for PSII damage-repair cycle on stroma-exposed thylakoid membranes throughout the chloroplast (Figure 1C; Jagendorf and Michaels, 1990). Thus, *PsbA* repair synthesis on stroma-exposed thylakoid membranes,

which is believed to occur throughout the chloroplast, could have masked sustained localization of subunit synthesis in the T-zone for de novo PSII biogenesis. Alternatively, de novo photosystem biogenesis might redistribute from the T-zone to stroma thylakoids throughout the chloroplast beginning at approximately ZT4 in the diel cycle and after 2 h in the greening process of *y1*.

METHODS

Culture Conditions

The *Chlamydomonas* (*Chlamydomonas reinhardtii*) wild-type strain CC-125 (137c) was synchronized to the 12/12-h light/dark cycle by culturing in high-salt minimal (HSM) medium (Harris, 1989) with 0.5 to 1% CO₂ at a flow rate of 300 to 400 mL/min and illuminated from the four sides and below by five banks of red and blue LEDs at 250 to 280 $\mu\text{E m}^{-2} \text{s}^{-1}$ at 23°C in the day and 27°C at night, with a ramp down over the course of 1 h during the first hour of the light phase. Cultures were entrained under alternating cycles of 12 h of light/12 h of dark for 2 to 3 d to 1×10^6 to 2×10^6 cells/mL measured with a hemocytometer. Cultures were diluted with fresh HSM medium between ZT1 and ZT3 of each of the subsequent 3 d, thereby reducing the cell density to 1×10^5 to 2×10^5 cells/mL. On the final day, cultures were not diluted and samples were collected at the ZT points indicated in the text. Cells were immediately frozen at -80°C (e.g., for SDS-PAGE) or chemically fixed (i.e., for IF and FISH). ZT0 and ZT12 cells were collected ~3 min following the respective transition.

The *Chlamydomonas* mutants for *ycf3* and *ycf4* (from Yuichiro Takahashi, Okayama University), *y1*, and *psbA* (*FuD7*; CC-1168 and CC-4147, respectively; www.chlamycolection.org) were cultured in Tris-acetate-phosphate (TAP) medium (Harris, 1989) in the dark at 24°C with orbital shaking to 1×10^6 to 2×10^6 cells/mL. Light-induced chloroplast differentiation was obtained by illuminating dark-grown *y1* cultures ($\sim 30 \mu\text{E m}^{-2} \text{s}^{-1}$) for the times indicated in the text.

Immunoblot Analysis

For the immunoblots with synchronized cells, equal volumes of the culture were centrifuged (4000g, 5 min) at 4°C. For the immunoblots with *y1* cells, an equal number of cells were centrifuged at each time point. The same cell samples were used for the immunoblot analyses, although the 45-min denaturation in SDS-PAGE loading buffer was at 24°C for PsaA (to prevent it from forming large insoluble aggregates) and at 65°C for all other proteins. Proteins were resolved by SDS-PAGE (12% [w/v] acrylamide:bis-acrylamide at 29:1; Sambrook and Russell, 2001) and then were transferred to PVDF membranes (Bio-Rad) and reacted with primary and secondary antibodies (Sambrook and Russell, 2001). The primary antibodies were as follows: αPsbA (1:5000; Agrisera AS111786), αAtpB (1:5000; from André Jagendorf, Cornell University), αPsaA (1:60,000; from Kevin Redding, Arizona State University), αCytF (1:100,000), αLHCII , αCytF , and αPsbD (1:5000, 1:2000, and 1:5000, respectively; from Francis-André Wollman, Institut de Biologie Physico-Chimique, Paris), αCyl4 , $\alpha\text{S-21}$, and $\alpha\text{L-7/L-12}$ (1:6,000, 1:4,000, and 1:10,000, respectively; we have the remaining stocks of these antisera of Nicholas Gilham; Fleming et al., 1987; Randolph-Anderson et al., 1989), and αPOR (1:50,000; Katrin Philipp and Jurgen Soll, Ludwig Maximilian University, Munich). The secondary antibody was horseradish peroxidase-conjugated goat anti-rabbit IgG antibody (KPL). Signals were detected using an ECL substrate (Thermo Fisher Scientific) with an Amersham Imager 600 (GE) according to the manufacturer's protocols.

In Vivo ³⁵S-Pulse-Labeling Experiments

At each time point, a 5-mL aliquot of a culture ($\sim 1.2 \times 10^7$ cells) was centrifuged at 4000g for 2 min. Each cell pellet was resuspended in 1 mL of medium lacking sulfate (HSM-S for wild-type cells in the diel cycle and TAP-S for *y1*). When the cell pellet was fully resuspended, cycloheximide was added to 10 $\mu\text{g/mL}$. Cells were incubated for 5 min with shaking under the conditions described for each time point. Then, 90 μCi of [³⁵S]H₂SO₄ (1050–1600 Ci/mM; Perkin-Elmer) was added, and labeling was performed for 10 min. Cells were pelleted by centrifugation at 4000g for 2 min, resuspended and lysed in 200 μL of SDS-PAGE loading buffer, and incubated at room temperature for 1 h. Then, 15 μL of each sample was loaded onto a SDS-PAGE gel (12% acrylamide:bis-acrylamide at 29:1 and 8 M urea). Following electrophoresis, the gels were dried, and ³⁵S-labeled proteins were revealed with a phosphorimager (Typhoon).

FISH, IF Staining, Live-Cell Imaging, and Microscopy

The FISH and IF staining procedures and the *psbA* FISH probes were described previously by Uniacke and Zerges, (2007) and Uniacke et al., (2011). The primary antibodies and the dilutions used for IF were as follows: $\alpha\text{S-21}$ (1:1000), αRBP40 (1:1000; from Jörg Nickelsen, Ludwig Maximilian University), αHSP70B and αVIPP1 (both at 1:1000; from Michael Schroda, University of Kaiserslautern), αAtpB (1:1000), αPsbA (1:1000; Agrisera), αPsaA (1:2000), αPOR (1:1000), and αYcf3 and αYcf4 (both at 1:400). Sources of antibodies that were also used in immunoblot analyses are stated above.

Fluorescent secondary antibody used was AlexaFluor568 conjugated to goat anti-rabbit IgG (Thermo Fisher Scientific). Staining with the secondary antibody alone revealed only weak signal throughout the cells (Supplemental Figure 6). For the dual IF staining in Figure 5C, cells were first reacted with αPOR , which was subsequently indirectly IF labeled by excess AffiniPure Fab fragment donkey anti-rabbit IgG (H+L) conjugated to AlexaFluor488 (Jackson ImmunoResearch). These cells were then reacted with $\alpha\text{S-21}$, which was subsequently indirectly IF labeled by goat anti-rabbit IgG conjugated to AlexaFluor568 (Thermo Fisher Scientific). High specificities of the *psbA* FISH signal and the PsaA IF signal were demonstrated previously by Uniacke and Zerges, (2007). The IF signals from the antisera against PsaA, Ycf3, and Ycf4 were specific because they were absent in deletion mutants for the respective chloroplastic gene (Supplemental Figure 6).

Microscopy was performed with a Leica DMI6000B inverted epifluorescence microscope with a 63 \times Plan Apo objective (numerical aperture 1.4) and further magnified by a 1.6 \times tube lens. Images were acquired on a Hamamatsu Orca R2 C10600-10B camera controlled by Volocity (Improvision) software. Filters used were as follows: Texas Red (562/40 nm excitation, 624/40 nm emission) for protein labeling and GFP (472/30 nm excitation, 520/35 nm emission) for probed mRNA message *psbA*. Acquired images were taken using Z plane stacks with a spacing of 0.2 μm per section; exposure settings, gain, and excitation intensity were constant between samples. Deconvolution of IF and FISH signals was performed with AutoQuant X3 software (Bitplane) using settings for the appropriate optics, glycerol-based sample medium, and Prolong Gold Antifade (Molecular Probes). An adaptive point-spread function was applied for deconvolution of 15 iterations, using low background removal for the IF signals and medium background removal for the FISH signal from the *psbA* mRNA. The same settings were used for the acquisition and deconvolution of each IF and FISH signal in all cell images in each figure panel. However, post acquisition, the IF and FISH signals were adjusted manually to similar brightness across all images in each figure panel to allow comparisons of in situ distributions, which would have been precluded by different signal levels between time points.

Chlorophyll fluorescence was imaged by embedding cells in 3% (w/v) low-melting-point agarose (Bethesda Research Laboratories), made with

TAP medium upon a 35-mm cell culture imaging dish (Grenier Bio-one). This gel was submerged in TAP medium to prevent it from drying. Images were acquired using the same microscope, peripheral equipment, software, and settings described above and a CY5 filter cube (628/40 nm excitation, 692/40 nm emission). For time-lapse movies, dark-*y1* cells were subjected to 100 $\mu\text{mol m}^{-2} \text{s}^{-1}$ white light from a 100-W halogen bulb for the 8-h duration of the experiment. Images were captured every 10 min using a 100 \times (numerical aperture 1.3) lens on a Nikon Ti microscope fitted with a Photometrics Evolve EMCCD device. Chlorophyll fluorescence was stimulated using a 405-nm LED (Heliphor), passing through a Quad filter cube (405/485/555/640 excitation, 450/520/595/710 emission; Chroma). These images were not deconvolved.

Average Cell Signal Analysis

To determine the average distribution of fluorescent signals in cells at a specific time point, the macro was developed to operate within ImageJ (Supplemental File; Abramoff et al., 2004). The protocol is available at <https://www.protocols.io/view/cell-harvester-macro-for-fluorescence-microscopy-i-rjgd4jw>. The macro is available at <https://github.com/Zergeslab/cellHarvester>. The macro finds cells in a maximum intensity projection of the Z-stack and fits an ellipse to the outline of each. Each cell is then rotated so that its long axis lay horizontally and the brighter end of the cell (the presumed location of the T-zone) was at the right; this is verified by the user. Each cell is then scaled in X and Y so that all cells were the same size, and their fluorescence signals are normalized to their own maximum intensity so that each cell contributed equally to the final image. A mean intensity projection is then performed on all of the normalized cells, resulting in the image in Supplemental File.

TEM

Samples were collected from cultures entrained to the diurnal cycle as described above and processed as described previously, with one additional step after infiltration: embedding with Epon and polymerization at 68°C for 48 h (Elimam et al., 2016). Images were acquired on an FEI Tecnai 12 120kv transmission electron microscope using the Tecnai User Interface software and an AMTv601 CCD camera. Settings used were an aperture of 3, a spot size of 2, and variable magnifications ranging from 2900 \times to 68,000 \times .

Measurement of Chlorophyll

Chlorophyll extractions were quantified spectrophotometrically as described previously by Porra, (2002).

Accession Numbers

The fully annotated *Chlamydomonas* chloroplast genome sequence is available from GenBank (accession number BK000554) for the following genes mentioned in this study: *atpB*, *psaA*, *psbA*, *psbC*, *psbD*, *S-21/rps14* (Randolph-Anderson et al., 1989), *ycf3*, and *ycf4*. Accession numbers (Phytozome v12.1; https://phytozome.jgi.doe.gov/pz/portal.html#) for nuclear genes mentioned in this study are as follows: *HSP70B* (Cre06.g250100), *RPLL7/L12* (Cre13.g581650), *LHCB* family (*LHCBM1*, Cre01.g066917; *LHCBM2*, Cre12.g548400; and *LHCBM7*, Cre12.g548950) *PORA* (Cre01.g015350), *ABP40* (also known as RB38, Cre12.g483700), and *VIPP1* (Cre13.g583550).

Supplemental Data

Supplemental Figure 1. Cultures entrained to the 12:12 h light-dark cycle had cells that were synchronized in growth during the light phase and mitosis during the dark phase.

Supplemental Figure 2. Steady state levels and synthesis rates of marker subunits.

Supplemental Figure 3. Bright field images of the cells in the figures reveal their orientations.

Supplemental Figure 4. TEM images reveal ultrastructures of cells from time points of the diel cycle when the T-zone colocalization of translation makers was seen.

Supplemental Figure 5. Temporal patterns of protein synthesis in the chloroplast of the *y1* mutant before, during and after greening.

Supplemental Figure 6. Controls for background and signal specificities in the fluorescence microscopy images.

Supplemental Video. Live cell imaging of chlorophyll fluorescence during *y1* greening.

Supplemental File. Protocol for determining average fluorescent signal intensity along the axis of the chloroplast with the macro.

ACKNOWLEDGMENTS

All light microscopy was carried out at the Concordia Center for Microscopy and Cell Imaging. For generous gifts of antibodies, we thank Kevin Redding (α PsaA; Arizona State University); Yves Choquet and Francis-Andre Wollman (α cyf and α LHCI; IBPC, Paris); Elizabeth Harris (α AtpB, α cyL4, α S-21, and α L7/L12; Duke University); Katrin Philipp (α POR; Ludwig Maximilian University, Munich); Michael Schroda (α HSP70B and α VIPP1; University of Kaiserslautern), Jörg Nickelsen (α RBP40; Ludwig Maximilian University, Munich); and Yuichiro Takahashi (α Ycf3 and α Ycf4 as well as the *yc3* and *yc4* mutants; Okayama University). For critical reading of the article, we thank James Dhaliwal, Patrick Gulick, Ursula Oberholzer, and Aísa Piekny. For technical assistance and support, we thank Kelly Sears and Jeannie Mui and the Faculty for Electron Microscopy Research at McGill University. This work was supported by the Natural Sciences and Engineering Research Council of Canada (Discovery Grant 217566 to W.Z.).

AUTHOR CONTRIBUTIONS

Y.S., M.V.-P., and W.Z. designed the research; Y.S., M.V.-P., S.B., and Y.Z. performed the research; M.V.-P. and C.L. contributed new analytic and computational tools; Y.S., M.V.-P., S.B., and W.Z. analyzed data; Y.S., M.V.-P., and W.Z. wrote the article.

Received April 15, 2019; revised September 18, 2019; accepted October 7, 2019; published October 7, 2019.

REFERENCES

- Abramoff, M.D., Magelhaes, P.J., and Ram, S.J. (2004). Image processing with ImageJ. *Biophoton. Int.* **11**: 36–42.
- Allen, M.D., Kropat, J., and Merchant, S.S. (2008). Regulation and localization of isoforms of the aerobic oxidative cyclase in *Chlamydomonas reinhardtii*. *Photochem. Photobiol.* **84**: 1336–1342.
- Barnes, D., Cohen, A., Bruick, R.K., Kantardjiev, K., Fowler, S., Efuet, E., and Mayfield, S.P. (2004). Identification and characterization of a novel RNA binding protein that associates with the 5'-untranslated region of the chloroplast *psbA* mRNA. *Biochemistry* **43**: 8541–8550.

- Cahoon, A.B., and Timko, M.P.** (2000). *yellow-in-the-dark* mutants of *Chlamydomonas* lack the CHLL subunit of light-independent protochlorophyllide reductase. *Plant Cell* **12**: 559–568.
- Chidgey, J.W., Linhartová, M., Komenda, J., Jackson, P.J., Dickman, M.J., Canniffe, D.P., Koník, P., Piliňý, J., Hunter, C.N., and Sobotka, R.** (2014). A cyanobacterial chlorophyll synthase-HllD complex associates with the Ycf39 protein and the YidC/Alb3 insertase. *Plant Cell* **26**: 1267–1279.
- Chotewutmontri, P., and Barkan, A.** (2016). Dynamics of chloroplast translation during chloroplast differentiation in maize. *PLoS Genet.* **12**: e1006106.
- Chotewutmontri, P., and Barkan, A.** (2018). Multilevel effects of light on ribosome dynamics in chloroplasts program genome-wide and *psbA*-specific changes in translation. *PLoS Genet.* **14**: e1007555.
- Colón-Ramos, D.A., Salisbury, J.L., Sanders, M.A., Shenoy, S.M., Singer, R.H., and García-Blanco, M.A.** (2003). Asymmetric distribution of nuclear pore complexes and the cytoplasmic localization of β 2-tubulin mRNA in *Chlamydomonas reinhardtii*. *Dev. Cell* **4**: 941–952.
- Czarnecki, O., and Grimm, B.** (2012). Post-translational control of tetrapyrrole biosynthesis in plants, algae, and cyanobacteria. *J. Exp. Bot.* **63**: 1675–1687.
- de Vitry, C., Olive, J., Drapier, D., Recouvreur, M., and Wollman, F.A.** (1989). Posttranslational events leading to the assembly of photosystem II protein complex: A study using photosynthesis mutants from *Chlamydomonas reinhardtii*. *J. Cell Biol.* **109**: 991–1006.
- Elias, M., and Archibald, J.M.** (2009). Sizing up the genomic footprint of endosymbiosis. *BioEssays* **31**: 1273–1279.
- Elimam, H., Papillon, J., Kaufman, D.R., Guillemette, J., Aoudjit, L., Gross, R.W., Takano, T., and Cybulsky, A.V.** (2016). Genetic ablation of calcium-independent phospholipase A₂ γ induces glomerular injury in mice. *J. Biol. Chem.* **291**: 14468–14482.
- Engel, B.D., Schaffer, M., Kuhn Cuellar, L., Villa, E., Plietzko, J.M., and Baumeister, W.** (2015). Native architecture of the *Chlamydomonas* chloroplast revealed by in situ cryo-electron tomography. *eLife* **4**: e04889.
- Erickson, J.M., Rahire, M., and Rochaix, J.D.** (1984). *Chlamydomonas reinhardtii* gene for the 32 000 mol. wt. protein of photosystem II contains four large introns and is located entirely within the chloroplast inverted repeat. *EMBO J.* **3**: 2753–2762.
- Fleming, G.H., Boynton, J.E., and Gillham, N.W.** (1987). Cytoplasmic ribosomal proteins from *Chlamydomonas reinhardtii*: Characterization and immunological comparisons. *Mol. Gen. Genet.* **206**: 226–237.
- Freeman Rosenzweig, E.S., et al.** (2017). The eukaryotic CO₂-concentrating organelle is liquid-like and exhibits dynamic reorganization. *Cell* **171**: 148–162.e119.
- Harris, E.H.** (1989). *The Chlamydomonas Sourcebook: A Comprehensive Guide to Biology and Laboratory Use.* (San Diego, CA: Academic Press).
- Herrin, D.L., Battey, J.F., Greer, K., and Schmidt, G.W.** (1992). Regulation of chlorophyll apoprotein expression and accumulation: Requirements for carotenoids and chlorophyll. *J. Biol. Chem.* **267**: 8260–8269.
- Hooper, J.K.** (2007). Chloroplast development: Whence and whither. In *The Structure and Function of Plastids*, R.R.H.J.K. Wise, ed (Dordrecht, The Netherlands: Springer), pp. 7–55.
- Howell, S.H., Posakony, J.W., and Hill, K.R.** (1977). The cell cycle program of polypeptide labeling in *Chlamydomonas reinhardtii*. *J. Cell Biol.* **72**: 223–241.
- Hughes, S.C., and Simmonds, A.J.** (2019). *Drosophila* mRNA localization during later development: Past, present, and future. *Front. Genet.* **10**: 135.
- Idoine, A.D., Boulouis, A., Rupprecht, J., and Bock, R.** (2014). The diurnal logic of the expression of the chloroplast genome in *Chlamydomonas reinhardtii*. *PLoS One* **9**: e108760.
- Jagendorf, A.T., and Michaels, A.** (1990). Rough thylakoids: Translation on photosynthetic membranes. *Plant Sci.* **71**: 137–145.
- Jarvis, P., and López-Juez, E.** (2013). Biogenesis and homeostasis of chloroplasts and other plastids. *Nat. Rev. Mol. Cell Biol.* **14**: 787–802.
- Joyard, J., Ferro, M., Masselon, C., Seigneurin-Berny, D., Salvi, D., Garin, J., and Rolland, N.** (2009). Chloroplast proteomics and the compartmentation of plastidial isoprenoid biosynthetic pathways. *Mol. Plant* **2**: 1154–1180.
- Kannangara, C.G., Vothknecht, U.C., Hansson, M., and von Wettstein, D.** (1997). Magnesium chelatase: Association with ribosomes and mutant complementation studies identify barley subunit Xantha-G as a functional counterpart of Rhodobacter subunit BchD. *Mol. Gen. Genet.* **254**: 85–92.
- Lee, J., and Herrin, D.L.** (2002). Assessing the relative importance of light and the circadian clock in controlling chloroplast translation in *Chlamydomonas reinhardtii*. *Photosynth. Res.* **72**: 295–306.
- Legen, J., and Schmitz-Linneweber, C.** (2017). Stable membrane-association of mRNAs in etiolated, greening and mature plastids. *Int. J. Mol. Sci.* **18**: E1881.
- Liu, C., Willmund, F., Whitelegge, J.P., Hawat, S., Knapp, B., Lodha, M., and Schroda, M.** (2005). J-domain protein CDJ2 and HSP70B are a plastidic chaperone pair that interacts with vesicle-inducing protein in plastids 1. *Mol. Biol. Cell* **16**: 1165–1177.
- Lui, J., Castelli, L.M., Pizzinga, M., Simpson, C.E., Hoyle, N.P., Bailey, K.L., Campbell, S.G., and Ashe, M.P.** (2014). Granules harboring translationally active mRNAs provide a platform for P-body formation following stress. *Cell Rep.* **9**: 944–954.
- Malnoë, P., Mayfield, S.P., and Rochaix, J.D.** (1988). Comparative analysis of the biogenesis of photosystem II in the wild-type and Y-1 mutant of *Chlamydomonas reinhardtii*. *J. Cell Biol.* **106**: 609–616.
- Mattoo, A.K., and Edelman, M.** (1987). Intramembrane translocation and posttranslational palmitoylation of the chloroplast 32-kDa herbicide-binding protein. *Proc. Natl. Acad. Sci. USA* **84**: 1497–1501.
- Minagawa, J., and Takahashi, Y.** (2004). Structure, function and assembly of photosystem II and its light-harvesting proteins. *Photosynth. Res.* **82**: 241–263.
- Müller, P., Li, X.-P., and Niyogi, K.K.** (2001). Non-photochemical quenching: A response to excess light energy. *Plant Physiol.* **125**: 1558–1566.
- Nellaepalli, S., Ozawa, S.I., Kuroda, H., and Takahashi, Y.** (2018). The photosystem I assembly apparatus consisting of Ycf3-Y3IP1 and Ycf4 modules. *Nat. Commun.* **9**: 2439.
- Nelson, N., and Ben-Shem, A.** (2004). The complex architecture of oxygenic photosynthesis. *Nature Reviews Molecular Cell Biology* **5**: 971–982.
- Nickelsen, J., and Zerges, W.** (2013). Thylakoid biogenesis has joined the new era of bacterial cell biology. *Front. Plant Sci.* **4**: 458.
- Ohad, I., Siekevitz, P., and Palade, G.E.** (1967a). Biogenesis of chloroplast membranes. I. Plastid dedifferentiation in a dark-grown algal mutant (*Chlamydomonas reinhardtii*). *J. Cell Biol.* **35**: 521–552.
- Ohad, I., Siekevitz, P., and Palade, G.E.** (1967b). Biogenesis of chloroplast membranes. II. Plastid differentiation during greening of a dark-grown algal mutant (*Chlamydomonas reinhardtii*). *J. Cell Biol.* **35**: 553–584.
- Panasenko, O.O., et al.** (2019). Co-translational assembly of proteasome subunits in NOT1-containing assemblies. *Nat. Struct. Mol. Biol.* **26**: 110–120.

- Porra, R.J.** (2002). The chequered history of the development and use of simultaneous equations for the accurate determination of chlorophylls a and b. *Photosynth. Res.* **73**: 149–156.
- Randolph-Anderson, B.L., Gillham, N.W., and Boynton, J.E.** (1989). Electrophoretic and immunological comparisons of chloroplast and prokaryotic ribosomal proteins reveal that certain families of large subunit proteins are evolutionarily conserved. *J. Mol. Evol.* **29**: 68–88.
- Rast, A., Heinz, S., and Nickelsen, J.** (2015). Biogenesis of thylakoid membranes. *Biochim. Biophys. Acta* **1847**: 821–830.
- Rochaix, J.D., Dron, M., Rahire, M., and Malnoe, P.** (1984). Sequence homology between the 32K dalton and the D2 chloroplast membrane polypeptides of *Chlamydomonas reinhardtii*. *Plant Mol. Biol.* **3**: 363–370.
- Sambrook, J., and Russell, D.W.** (2001). *Molecular Cloning: A Laboratory Manual*. (Cold Spring Harbor, NY: Cold Spring Harbor Laboratory Press).
- Schottkowski, M., Peters, M., Zhan, Y., Rifai, O., Zhang, Y., and Zerges, W.** (2012). Biogenic membranes of the chloroplast in *Chlamydomonas reinhardtii*. *Proc. Natl. Acad. Sci. USA* **109**: 19286–19291.
- Schwarz, C., Elles, I., Kortmann, J., Piotrowski, M., and Nickelsen, J.** (2007). Synthesis of the D2 protein of photosystem II in *Chlamydomonas* is controlled by a high molecular mass complex containing the RNA stabilization factor Nac2 and the translational activator RBP40. *Plant Cell* **19**: 3627–3639.
- Shimizu, S.** (2019). Organelle zones in mitochondria. *J. Biochem.* **165**: 101–107.
- Solymosi, K., and Schoefs, B.** (2010). Etioplast and etio-chloroplast formation under natural conditions: The dark side of chlorophyll biosynthesis in angiosperms. *Photosynth. Res.* **105**: 143–166.
- Stoldt, S., Wenzel, D., Kehrein, K., Riedel, D., Ott, M., and Jakobs, S.** (2018). Spatial orchestration of mitochondrial translation and OXPHOS complex assembly. *Nat. Cell Biol.* **20**: 528–534.
- Strenkert, D., et al.** (2019). Multiomics resolution of molecular events during a day in the life of *Chlamydomonas*. *Proc. Natl. Acad. Sci. USA* **116**: 2374–2383.
- Sun, Y., and Zerges, W.** (2015). Translational regulation in chloroplasts for development and homeostasis. *Biochim. Biophys. Acta* **1847**: 809–820.
- Theis, J., and Schroda, M.** (2016). Revisiting the photosystem II repair cycle. *Plant Signal. Behav.* **11**: e1218587.
- Uniacke, J., Colón-Ramos, D., and Zerges, W.** (2011). FISH and immunofluorescence staining in *Chlamydomonas*. *Methods Mol. Biol.* **714**: 15–29.
- Uniacke, J., and Zerges, W.** (2007). Photosystem II assembly and repair are differentially localized in *Chlamydomonas*. *Plant Cell* **19**: 3640–3654.
- Uniacke, J., and Zerges, W.** (2009). Chloroplast protein targeting involves localized translation in *Chlamydomonas*. *Proc. Natl. Acad. Sci. USA* **106**: 1439–1444.
- van Wijk, K.J., Andersson, B., and Aro, E.M.** (1996). Kinetic resolution of the incorporation of the D1 protein into photosystem II and localization of assembly intermediates in thylakoid membranes of spinach chloroplasts. *J. Biol. Chem.* **271**: 9627–9636.
- White, R.A., and Hooper, J.K.** (1994). Biogenesis of thylakoid membranes in *Chlamydomonas reinhardtii* y1 (A kinetic study of initial greening). *Plant Physiol.* **106**: 583–590.
- Wu, H., Carvalho, P., and Voeltz, G.K.** (2018). Here, there, and everywhere: The importance of ER membrane contact sites. *Science* **361**: eaan5835.
- Zones, J.M., Blaby, I.K., Merchant, S.S., and Umen, J.G.** (2015). High-resolution profiling of a synchronized diurnal transcriptome from *Chlamydomonas reinhardtii* reveals continuous cell and metabolic differentiation. *Plant Cell* **27**: 2743–2769.
- Zoschke, R., and Barkan, A.** (2015). Genome-wide analysis of thylakoid-bound ribosomes in maize reveals principles of co-translational targeting to the thylakoid membrane. *Proc. Natl. Acad. Sci. USA* **112**: E1678–E1687.
- Zoschke, R., and Bock, R.** (2018). Chloroplast translation: Structural and functional organization, operational control, and regulation. *Plant Cell* **30**: 745–770.